ALMA MATER STUDIORUM
UNIVERSITÀ DI BOLOGNA

DOTTORATO DI RICERCA IN

SCIENZE VETERINARIE

Ciclo 38

**Settore Concorsuale:** 07/H2 - PATOLOGIA VETERINARIA E ISPEZIONE DEGLI ALIMENTI DI ORIGINE ANIMALE

**Settore Scientifico Disciplinare:** VET/03 - PATOLOGIA GENERALE E ANATOMIA PATOLOGICA VETERINARIA

# STUDY OF MORPHOLOGICAL AND MOLECULAR PARAMETERS WITH DIAGNOSTIC AND PROGNOSTIC VALUE IN CANINE NEOPLASMS

**Presentata da:** Elena Brigandì

**Coordinatore Dottorato**

Carolina Castagnetti

**Supervisore**

Giancarlo Avallone

**Co-supervisore**

Barbara Brunetti

Esame finale anno 2026

**Table of Contents**

## Abstract

Canine soft tissue sarcomas (STSs) are a heterogeneous group of mesenchymal neoplasms with overlapping histological features, historically considered as a single entity. Distinct histotypes, however, exhibit different biological behaviors, underscoring the need for detailed characterization using histology, immunohistochemistry, and molecular approaches. This study aimed to investigate three main aspects of canine STSs: (i) neoplastic cell proliferation, (ii) tumor immune microenvironment (TIME), and (iii) proteomic profiles of different STS types. Additional objectives included (iv) assessing the diagnostic utility of epithelial membrane antigen (EMA) in canine nerve sheath tumors and exploring the association of PDGFRβ expression with proliferation in intestinal leiomyosarcomas. Two studies examined neoplastic cell proliferation (i): the first confirmed the prognostic relevance of a Ki-67 cut-off of 56% in canine splenic hemangiosarcoma; the second found significant differences in the spatial distribution patterns of proliferative hotspots across different tumor types. Regarding TIME (ii), histotype-specific immune patterns were evidenced by immunohistochemistry: myxosarcomas elicited an immune response rich in M2 macrophages, B cells, and Tregs, whereas perivascular wall tumors were associated with a T-cell-rich, Treg-poor environment. The preliminary results of the proteomic profiling of canine STSs (iii), using LC-MS/MS, indicated clustering of certain histotypes (perivascular wall tumors and liposarcomas). In the additional studies (iv), EMA was widely expressed in both perivascular wall tumors and nerve sheath tumors, limiting its diagnostic utility, and PDGFRβ expression showed no statistically significant association with neoplastic cell proliferation in intestinal leiomyosarcoma, although PDGFRβ-positive cases had a higher Ki-67 labeling index. These findings increase the knowledge of the biology of canine STSs, highlighting histotype-specific differences in proliferation, immune response, and proteomic profiles, which may inform diagnosis, prognostication, and therapeutic strategies.

# Chapter 1: General Introduction

## Main characteristics of Canine Soft Tissue Tumors

**Soft Tissue Tumors** (STTs) constitute a heterogeneous group of mesenchymal neoplasms arising from soft connective tissues, including extra-skeletal, non-epithelial structures, while excluding the viscera, meninges and reticuloendothelial system (Roccabianca et al., 2020). From an embryological perspective, these tumors primarily originate from the mesoderm, with some exceptions from the neuroectoderm (Das et al., 2023; Dennis et al., 2011; Goldblum et al., 2020).

STTs are generally classified into benign and malignant. While benign STTs tend to resemble normal tissue, exhibit a limited capacity for autonomous growth, minimal local invasiveness and are associated with a low recurrence rate following conservative treatment, malignant counterparts, **Soft Tissue Sarcomas** (STSs), are locally aggressive, capable of invasive growth, recurrence and distant metastasis (Goldblum et al., 2020).

## Human Soft Tissue Sarcomas

Human STSs are rare neoplasms, accounting for less than 1.5% of all malignant tumors, with an annual incidence of 6 per 100,000 individuals (Ferrari et al., 2011; Goldblum et al., 2020; Jo and Fletcher, 2014). It is reported that in subjects under the age of 10, there is one case per 100,000 people, whereas, in adults, STSs affect approximately 18 per 100,000 people (Ferrari et al., 2011), with incidence increasing with age (Jo and Fletcher, 2014). However, certain subtypes show distinct age-related patterns, including rhabdomyosarcoma, which occurs typically in children, synovial sarcoma in young adults and liposarcomas, leiomyosarcomas, myxofibrosarcomas, and undifferentiated pleomorphic sarcomas, which are more frequent in adults (Jo and Fletcher, 2014; Kumar et al., 2020). Regarding gender, there is a male predominance with a 1.5:1 male to female ratio (Jo and

Fletcher, 2014; Kumar et al., 2020), except for alveolar sarcoma and leiomyosarcoma (Ferrari et al., 2011).

In 75% of cases, STSs originate in the lower limbs, particularly on the thighs, while in 10% of cases, they are localized in the trunk or in the retroperitoneal space (Goldblum et al., 2020; Jo and Fletcher, 2014).

The etiology of these neoplasms remains largely unknown, with factors such as radiation exposure, burns, toxins and viral agents rarely being responsible for their development (Goldblum et al., 2020). Among viral agents, human herpesvirus type 8 is of particular relevance among viral etiologies, being responsible for the development of Kaposi's sarcoma (Jo and Fletcher, 2014; Kumar et al., 2020), as well as the Epstein-Barr virus, which plays a role in the pathogenesis of smooth muscle tumors in immunodeficient patients (Goldblum et al., 2020). A minority of STSs are associated with specific genetic mutations (Kumar et al., 2020).

Several factors influence prognosis, including histotype, location, size, stage and histological grade. In general, STSs located in the skin and subcutis have a better prognosis compared to visceral or deeper lesions (Jo and Fletcher, 2014). In this context, the key prognostic factors for retroperitoneal sarcomas are the wholeness of surgical margins, the histological grade and the histotype (Jo and Fletcher, 2014).

Over the years, various grading systems have been proposed, but the most widely used is the one developed by the French Federation of Cancer Centers Sarcoma Group (FNCLCC) (Trojani et al., 1984). This system is based on parameters to which scores are assigned and the total of these scores defines the grade. These parameters include:

- The **differentiation** of neoplastic cells, defined as the similarity of the neoplastic tissue to the corresponding non-neoplastic tissue;

- The presence and the amount of **necrosis**;
- The **mitotic count (MC)**, evaluated in 10 high-power fields (HPF) (Trojani et al., 1984).

Therapeutic approaches vary depending on the stage: stage I typically requires surgical excision with wide margins, while higher stages require an increased therapeutic approach with radiotherapy and chemotherapy (Crago and Brennan, 2015; Nystrom et al., 2013).

Radiotherapy is considered standard treatment following surgical excision for high-grade STSs or those originating in deep tissues or exceeding 5 cm in diameter (Casali et al., 2018). For high-grade STSs, the choice to use chemotherapy depends on the risk of metastasis, the chemo-sensitivity of the histotype, the age of the patient and the presence of other comorbidities (Casali et al., 2018).

## Canine Soft Tissue Sarcoma

### Incidence

In contrast to humans, canine STSs represent a significant proportion of neoplasms, accounting for approximately 8-12% of malignant tumors (Das et al., 2023) and around 15-30% of all cutaneous and subcutaneous neoplasms (Dennis et al., 2011; Roccabianca et al., 2020).

The incidence of canine STSs varies and is influenced by both extrinsic and intrinsic factors, including age, sex and breed. Larger breeds, such as Dobermans, Rottweilers and Golden Retrievers, are particularly predisposed compared to smaller-sized dogs (Dobson, 2013; Grüntzig et al., 2016). Canine STSs are commonly diagnosed in both middle-aged and older dogs, with an average age of incidence around 10 years (Bray, 2016).

In dogs, STSs are most commonly located in the skin and subcutis, particularly on the limbs and trunk (Dennis et al., 2011; Roccabianca et al., 2020).

**Morphologic and Clinic characteristics**

Among the common characteristics of these neoplasms, the growth pattern is typically slow and expansive. However, in some cases, there may be more rapid and/or infiltrative growth (Liptak and Christensen, 2019). This locally expansive or infiltrative growth can extend through fascial planes and, in some histotypes, may be accompanied by the presence of satellite nodules (Avallone et al., 2014). Another key feature is the presence of an external pseudocapsule, formed by the compression of surrounding connective tissue caused by the neoplastic expansion (Dennis et al., 2011).

**Treatment**

The treatment of choice for canine STSs is surgical excision. Incomplete surgical excision margins are predictive of local recurrence, and consequently, local recurrences are more common when conservative therapies are employed (Chiti et al., 2021; Dennis et al., 2011; Kuntz et al., 1997). The risk of metastasis in STSs is considered low. However recent studies indicate that overall metastatic rates typically fall in the 10-20 % range to intermediate-grade tumors, whereas high-grade (grade III) sarcomas may metastasize in the 44 % of cases (Cardoso De Almeida Moreira et al., 2023; Ettinger et al., 2006; Selting et al., 2005). When metastases develop, they primarily spread hematogenously, affecting the liver and lungs, while lymphatic spread is less common, mainly involving regional lymph nodes (Kuntz et al., 1997) and is more frequent in myxosarcomas compared to other histotypes (Iwaki et al., 2019).

STSs larger than 5 cm in diameter tend to be less responsive to therapeutic treatments, such as chemotherapy and radiotherapy (Liptak and Christensen, 2019) and are more likely to recur (Avallone et al., 2014, 2007; Stefanello et al., 2011).

Chemotherapy is often recommended as adjunctive treatment for high-grade STSs because of their higher metastatic rate (Crownshaw et al., 2020; Ehrhart, 2005; Tierce et al., 2021).

**Histologic characteristics**

Diagnosis is often challenging, due to overlapping histological appearance among different subtypes (Das et al., 2023). The most commonly observed shared feature is the presence of spindle-shaped cells, which may aggregate into fascicular or whorled patterns (Hendrick, 2016; Roccabianca et al., 2020). Therefore, for an accurate diagnosis, it is essential to identify areas within the tumor that resemble normal tissue and to assess the expression of specific antigens through immunohistochemical techniques to determine the cellular phenotype. Immunohistochemistry allows the identification of the line of differentiation of neoplastic cells, aiding in the differentiation of tumors that share similar histological features but differ in origin and biological behavior, such as perivascular wall tumors and nerve sheath tumors (Avallone et al., 2014, 2007; Suzuki et al., 2014).

Nevertheless, even when combining immunohistochemical results with histological features, it is not always possible to precisely identify the exact histotype (Boerkamp et al., 2016; Chase et al., 2009).

**Prognostic parameters: The grading system**

In both human and veterinary medicine, STSs were historically considered as a single group because of these shared characteristics. However, there is an increasing body of evidence demonstrating that different histotypes exhibit distinct biological behavior (Canter et al., 2010; Coindre, 2006). Therefore, to better characterize the various histotypes, there has

been a significant increase in studies focusing on single STS types, such as liposarcomas (Avallone et al., 2016; Baez et al., 2004), smooth muscle tumors (Avallone et al., 2022; Pellegrino et al., 2018), perivascular wall tumors (Avallone et al., 2014, 2007), and peripheral nerve sheath tumors (Suzuki et al., 2014). When conducted on a large scale, these studies enable a more accurate characterization of different neoplasms and the evaluation of variables that may influence prognosis. Consequently, the diagnostic approach should consider specific characteristics that provide valuable information not only for diagnostic purposes but also for prognostic assessments. These parameters include histotype, histological grade, tumor size, primary site of origin, and the completeness of surgical margins (Dennis et al., 2011; Ettinger, 2003; Liptak and Christensen, 2019; Roccabianca et al., 2020).

Histotype has been considered a poor prognostic factor in canine STSs, although some studies have highlighted a significant difference in prognosis among different histotypes (Moretti and Bufalari, 2024): for instance, a 40.6% recurrence rate has been reported for myxosarcomas (Iwaki et al., 2019), while malignant peripheral nerve sheath tumors and fibrosarcomas show recurrence rates of 32% and 27%, respectively (Bray, 2016). Finally, recurrence rates vary widely in perivascular wall tumors, ranging from 9% (Bray, 2016) to 22% (Avallone et al., 2014; Stefanello et al., 2011).

The FNCLCC grading system, which was originally developed for human medicine, has been adapted for canine STSs (Kuntz et al., 1997) and remains the most widely utilized method in veterinary oncology (Roccabianca et al., 2020). The parameters employed to establish the histological grade are presented in the Table 1.1.

**Table 1.1:** Grading system for canine STSs according to the adaptation of the French grading system.

| **Tissue Differentiation** | **Score** |
|---|---|
| Sarcomas that most closely resemble normal adult mesenchymal tissue | 1 |
| Sarcomas in which the histotype can be determined, but cellular differentiation is poor | 2 |
| Undifferentiated sarcomas of unknown tissue origin | 3 |
| **Mitotic count (10 HPF, equal to 2,37mm$^2$)** | **Score** |
| 0-9 | 1 |
| 10-19 | 2 |
| ≥ 20 | 3 |
| **Tumor necrosis** | **Score** |
| No necrosis | 0 |
| ≤ 50% | 1 |
| > 50% | 2 |
| **Histologic grade** | **Total score** |
| I | ≤ 3 |
| II | 4-5 |
| III | ≥ 6 |

This system classifies tumors into three grades: Grade I (low-grade), Grade II (intermediate-grade), and Grade III (high-grade). The classification is based on the evaluation of key tumor characteristics, considering three parameters: tissue differentiation, MC and percentage of necrosis.

Regarding the first parameter, the terms 'well-differentiated' and 'poorly differentiated' are subjective, used to describe the relative maturity of the tumor compared to normal adult tissue, based on a defined set of histopathological criteria.

Generally, well-differentiated sarcomas correspond to low-grade tumors, whereas poorly differentiated sarcomas are usually high-grade neoplasms (Goldblum et al., 2020).

MC is a key parameter providing prognostic information about the tumor. It is assessed by counting the number of mitoses in multiple microscopic fields under high magnification. Recently, a standardized assessment area of 2.37 $mm^2$ has been established for MC evaluation (Meuten et al., 2016). The obtained value is then compared with a prognostic cut-off. However, determining this cut-off value remains a challenge. In veterinary medicine, the lowest mitotic threshold defining a high mitotic index in STSs is 9 mitoses per 10 high-power fields (McSporran, 2009). A higher MC correlates with an increased probability of recurrence in case of incomplete surgical margins excision, a shorter disease-free interval, a higher probability of metastasis and a reduced survival time (McSporran, 2009).

Among the indicators considered in the grading scheme, MC and the percentage of tumor necrosis emerged as the only statistically significant prognostic factors, with tumor necrosis being specifically associated with post-operative survival time (Kuntz et al., 1997; Yap et al., 2017).

Histological grading of STSs plays a critical role in predicting the risk of local recurrence and distant metastasis (Kuntz et al., 1997; Liptak and Christensen, 2019; McSporran, 2009).

Grade I is the most common grade among canine STSs, with the lowest probability of recurrence after surgical excision (McSporran, 2009). In these cases, the recurrence rate remains uncommon even if the excision margins are infiltrated (McSporran, 2009). Metastases are considered rare, but their occurrence remains a subject of debate due to the lack of standardized methods (Dennis et al., 2011). Additionally, some studies reporting metastases do not specify the grade of the primary tumor (McKnight et al., 2000), making it even more challenging to establish an accurate metastatic rate for each histologic grade.

Grade II STSs are less common than Grade I, and their recurrence rate remains low, strictly depending on the extent of surgical margins (McKnight et al., 2000). The main difference

between these two grades lies in the recurrence timing, which is shorter for Grade II STSs (McSporran, 2009). Regarding the metastatic rates, they are similar to those of Grade I and are highly variable (Dennis et al., 2011).

Grade III tumors are the least common, accounting for 7-17% of all cutaneous and subcutaneous canine STSs (Ettinger, 2003; McKnight et al., 2000). These tumors have the highest recurrence rate and the shortest disease-free interval compared to lower grades, when surgical margins are infiltrated (75%) (McSporran, 2009). Metastatic rates are also higher and highly variable, ranging from 22% to 44%, depending on the study examined (Ettinger, 2003; Kuntz et al., 1997). In a recent large cohort (Chiti et al., 2021), grade III tumors represented only 5.2% of 98 cases, yet margins status remained strongly prognostic for local recurrence. Infiltrated margins were associated with a 41% recurrence rate at 3 years compared to 7% with free margins (Chiti et al., 2021).

**Classification**

Depending on their predominant histologic features, STSs can be categorized according to their tissue differentiation, following a system that mirrors the classification established by the World Health Organization (WHO) for human sarcomas (Roccabianca et al., 2020). Accordingly, the current classification includes fibrous, adipocytic, vascular and perivascular, striated and smooth muscle, mesothelial, synovial and nerve sheath tumors (Roccabianca et al., 2020).

Predominant within this category are fibrosarcoma, myxosarcoma, liposarcoma, perivascular wall tumor (PWT), leiomyosarcoma, rhabdomyosarcoma, nerve sheath tumor (NST), hemangiosarcoma (HSA), and undifferentiated pleomorphic sarcoma (Dennis et al., 2011).

The entire tumor should be evaluated to assess the histological parameters, including exact anatomic site, depth, type of growth and tumor category and subcategory (Roccabianca et al., 2020). Further characterization requires histochemical and cytochemical stains, immunohistochemistry and immunocytochemistry, and genetic analysis for definitive diagnosis and prognosis, as many soft tissue neoplasms exhibit overlapping histologic features (Roccabianca et al., 2020) (Table 1.2).

**Table 1.2:** Distinctions among gradable canine STSs (Roccabianca et al., 2020).

| Type | Histogenesis | Histologic morphology | Histochemical & Immunohistochemistry |
|---|---|---|---|
| **Fibrosarcoma** | Fibrous tissue<br>Fibroblast, fibrocyte | Interwoven bundles, herringbone pattern, pronounced collagenous stroma | GFAP -<br>NGFR -<br>SOX-10 -<br>Olig-2 -<br>Vimentin + |
| **Myxosarcoma** | Fibrous tissue | Stellate- or spindle-shaped cells in mucinous stroma | Alcian blue + (myxoid matrix) |
| **Liposarcoma** | Fat<br>Lipoblast, lipocyte | Polygonal cells with distinctly vacuolated cytoplasm | Vimentin +<br>UCP1 +<br>S100 +/-<br>MDM2 +/- |
| **PWT** | Perivascular wall<br>Pericyte, myopericyte, smooth myocyte | Vascular growth patterns, including staghorn, placentoid, perivascular whorling, and bundles from tunica media | Calponin +<br>Pan actin +<br>SMA +/-<br>S100 -<br>NSE -<br>GFAP -<br>Myoglobin - |
| **NST** | Schwann cell, perineurial cell, neurofibroblast | Interwoven bundles, whorls around collagen bundles, Antoni A and B patterns | NSE +/-<br>S100 +/-<br>NGFR +/-<br>GFAP +/- |
| **Undifferentiated pleomorphic sarcoma** | Fibrous tissue<br>Primitive mesenchymal cells | Mixture of fibroblastic cells and karyomegalic, cytomegalic, or multinucleate histiocytoid cells in storiform patterns, with variable inflammatory infiltrate | Vimentin +<br>SMA +/-<br>Desmin +/-<br>S-100 - |
| **Leiomyosarcoma** | Smooth muscle | “Cigar-shaped” nuclei, prominent cytoplasm | SMA +<br>Desmin +<br>Calponin +<br>GFAP - |
| **Rhabdomyosarcoma** | Striated muscle | Cytoplasmic striation, “racket” and “strap” cells | Myoglobin +<br>Desmin +<br>NSE +/-<br>S-100 +/- |

*Perivascular wall tumors (PWTs)*

Perivascular wall tumors (PWTs) are the most common STSs in dogs (Dennis et al., 2011; Roccabianca et al., 2020). They originate from the non-endothelial component of the vascular wall and consist of cells phenotypically resembling pericytes, myopericytes and smooth muscle cells (Avallone et al., 2007). These tumors are most commonly found in middle-aged and older dogs, primarily affecting the limbs near the joints (Avallone et al., 2007), with less frequent occurrences on the thorax and head (Hendrick, 2017).

Macroscopically, these tumors frequently present as solitary subcutaneous masses of variable size, well-demarcated but not encapsulated. They are often located on the limbs, particularly in the proximal and distal extremities, but can also arise in other subcutaneous regions or, less frequently, at the visceral level (Hendrick, 2017). Their texture ranges from firm to elastic, largely influenced by the composition of the stromal matrix (Hendrick, 2017). On cross-section, they may appear whitish, grayish, or brownish, with possible necrotic regions or local hemorrhages (Hendrick, 2017). Furthermore, as they are considered locally invasive, they can infiltrate adjacent tissues, making surgical excision challenging and increasing the likelihood of recurrence (Stefanello et al., 2011).

The histological hallmark of PWTs is the presence of one or more of 4 perivascular patterns (Figure 1.1):

1. perivascular whorls: a proliferation of spindle-shaped cells arranged around capillaries or larger vascular structures;
2. placentoid pattern: multiple lobules with central single of multiple vessels;
3. short bundles of spindle cells radiating from vascular wall;
4. staghorn vessels: presence of thin walled branching vessels (Avallone et al., 2007).

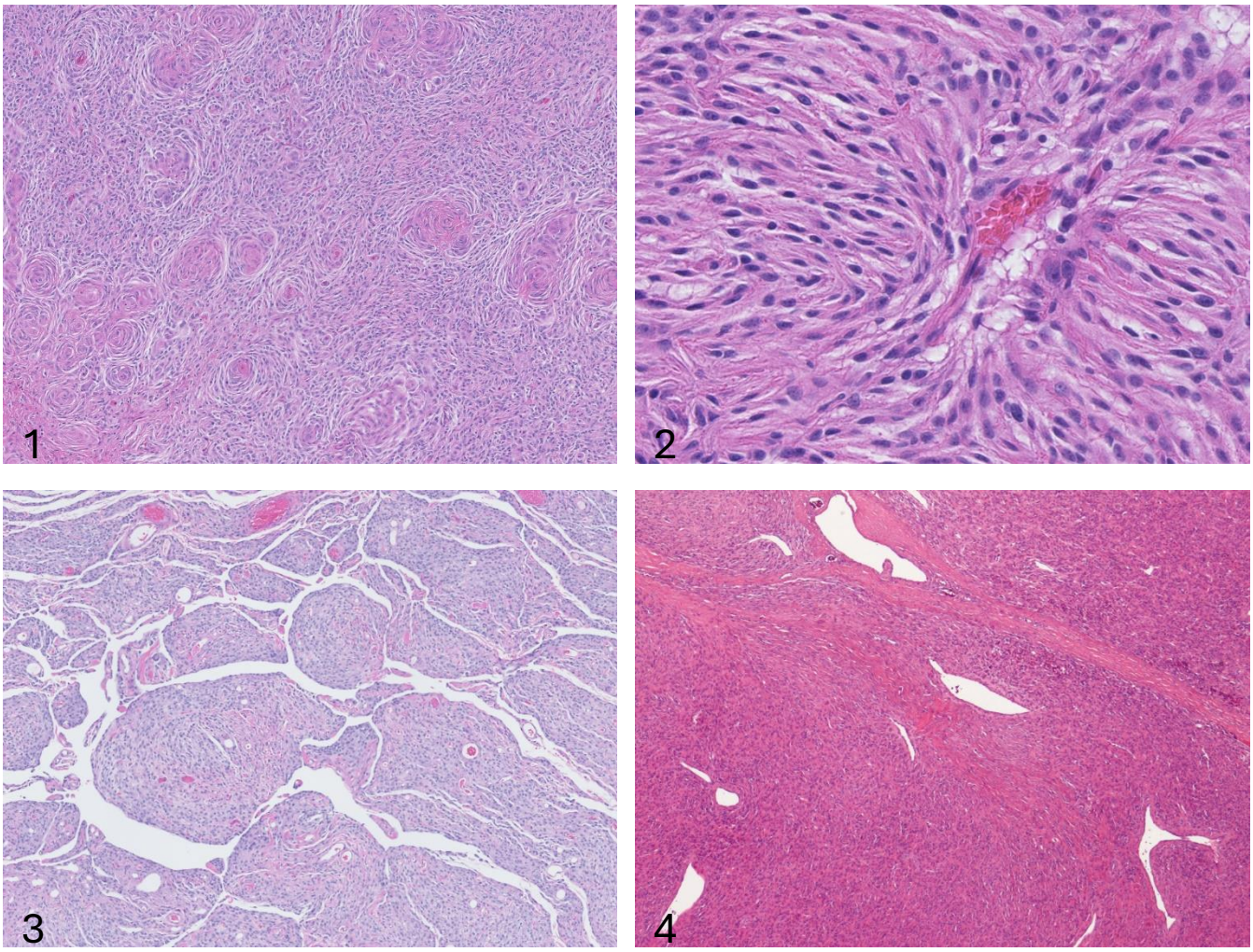


**Figure 1.1:** Typical histological patterns of PWTs: (1) perivascular whorls; (2) bundles of spindle cells radiating from a capillary wall; (3) placentoid and (4) staghorn vessels.

The stroma of these neoplasms is highly variable, ranging from dense collagen to myxoid matrix, which significantly impacts the tumor's composition and, consequently, its macroscopic appearance. Necrotic areas are observed particularly in high-grade tumors (Avallone et al., 2007).

For the histological diagnosis of different PWT subtypes, antigenic characterization of the lesion is necessary by assessing the expression of specific proteins associated with PWT through immunohistochemistry (Avallone et al., 2007).

Among the most useful immunohistochemical markers for the diagnosis of PWT are:

- Calponin: a calcium-binding protein that exerts a continuous inhibitory effect on myosin ATPase activity in smooth muscle (Avallone et al., 2007).
- Smooth muscle alpha-actin (α-SMA) and pan-actin: proteins belonging to the actin family, playing a crucial role in cytoskeletal microfilament formation and thin filament organization in muscle fibrils (Avallone et al., 2007).
- Desmin: a type III intermediate filament specific to muscle, which connects the sarcolemma, Z-disks, and nuclear membrane within sarcomeres, contributing to the maintenance and regulation of sarcomere structure (Brodehl et al., 2018).

In addition, it is also essential to assess the absence of other markers, such as myosin. A study by Avallone and colleagues demonstrated that the lack of myosin expression is due to the origin of these neoplasms from capillaries or precapillary vessel (Avallone et al., 2007). Furthermore, the application of antibodies such as NGFR and S100 is necessary to exclude other tumor types, such as NST (Suzuki et al., 2014).

The structure of the vascular wall varies among different vessel types. In capillaries the wall is thin and composed primarily of endothelial cells, pericytes and a basal membrane. In contrast, veins and large arteries possess a markedly thicker wall composed of an endothelium, a subendothelial layer, a basal membrane, a media abundant in smooth muscle cells and an adventitia containing myofibroblasts and fibroblasts. As the vessel diameter increases, subendothelial lining cells gradually evolve from pericytes in capillaries to myopericytes in pre- and post-capillary vessels, eventually differentiating into mature smooth muscle cells within arteries and large veins (Inokuchi et al., 1989; Rhodin and Fujita, 1989; Ushiwata and Ushiki, 1990).

The progressive replacement of pericytes with myopericytes and smooth muscle cells in the vascular subendothelial lining is characterized by a gradual increase in both the quantity and type of cytoplasmic contractile proteins (Frid et al., 1992; Nehls and Drenckhahn, 1991; Uranishi et al., 2001).

Accordingly, pericytes express vimentin (Metzler et al., 1992), α-smooth muscle actin (Nehls and Drenckhahn, 1991) and variably pan actin (Metzler et al., 1992), while myopericytes are characterized by the additional expression of desmin and calponin (Nehls and Drenckhahn, 1991), whereas smooth muscle cells express smoothelin and heavy caldesmon (Uranishi et al., 2001).

*Myxosarcomas*

Myxosarcomas are soft, gray-white, poorly defined masses with fibroblastic origin arising in the subcutis of the trunk or limbs and occurring from middle aged to older dogs (Roccabianca et al., 2020). These tumors are composed of an unencapsulated proliferation of stellate or spindle-shaped fibroblasts arranged in a variably abundant myxoid matrix, rich in acid mucopolysaccharides, that stains light blue with hematoxylin and eosin stain. Cellularity is low, mitotic figures are rare, nuclei tend to be small and hyperchromatic (Roccabianca et al., 2020) (Figure 1.2).

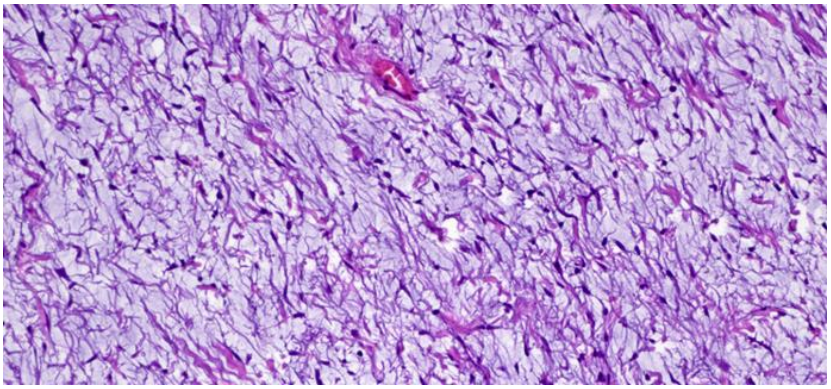

**Figure 1.2:** Histological features of myxosarcomas, showing spindle-shaped cells within abundant myxoid matrix.

The cellular features to differentiate indolent and aggressive types of this neoplasm are subjective but increased cellular density, nuclear pleomorphism, nucleolar prominence and mitotic figures warrant the diagnosis of myxosarcoma (Roccabianca et al., 2020).

When a neoplasm exhibits predominantly myxoid morphology, reaching a definitive diagnosis can be particularly challenging, as this histological feature may resemble those observed in myxoid variants of NSTs and in myxoid liposarcomas (Avallone et al., 2016; Sisó et al., 2022). In this regard, it is helpful to note that myxosarcomas consistently demonstrate immunoreactivity for vimentin, while myxoid liposarcomas can be distinguished by the presence of lipoblasts and positive lipid staining, such as with Oil Red O, myxoid variant PWTs have a perivascular pattern of growth and NST can be excluded based on immunohistochemistry for perineural markers such as NGFR, Olig2, periaxin-1 and SOX10 (Sisó et al., 2022).

Myxosarcomas exhibit an infiltrative biological behavior with poorly defined margins (Roccabianca et al., 2020). In contrast to other histotypes, myxosarcoma is more recurrent. In a study of 32 canine myxosarcomas, recurrence occurred in 13 cases (40%) and metastases were reported in 8 cases (25%), involving both regional lymph nodes and distant organs. The average time to recurrence was 1393 days in tumors with fewer than 10 mitotic figures per 10 HPF and 433 days in those with more than 10 mitotic figures per 10 HPF (Iwaki et al., 2019). Also in humans, myxosarcomas are locally aggressive tumors that have a propensity for local recurrence with a local recurrence rates ranging from 16-57% and 25-52% (Hicks et al., 2018; Sanfilippo et al., 2011).

In a study conducted by Haglund and colleagues, margin status and tumor grade have been evaluated in relationship to local recurrence: no local recurrence was noted with a margin of at least 1 cm, whereas 40% of patients had local recurrence with a less than 1 cm margin (Haglund et al., 2012). In general, the risk of local recurrence ranged from approximately

48% for low-grade tumors to 62% for high-grade tumors (Iwaki et al., 2019; Spinnato et al., 2021).

*Liposarcomas*

Liposarcomas are the most common STSs in humans, but rare in all domestic species, even if they are probably most common in dogs. Males are overrepresented in the published studies and the frequency increases with age (Avallone et al., 2016; Baez et al., 2004). The majority of cases occur in the subcutis of the axial region and proximal limbs (Avallone et al., 2016).

Most liposarcomas consist of round to polygonal cells containing lipid, arranged in sheets with minimal or no collagenous stroma (Avallone et al., 2016). Liposarcomas can be classified into well differentiated, pleomorphic, myxoid and dedifferentiated variants subtypes based on cellular morphology (Roccabianca et al., 2020).

In well-differentiated liposarcoma, the majority of cells closely resemble normal adipocytes, characterized by a single, clear lipid vacuole and a peripherally displaced nucleus. However, some cells exhibit round to oval nuclei of variable size and abundant cytoplasm containing differently sized lipid droplets (Roccabianca et al., 2020) (Figure 1.3).

Pleomorphic liposarcoma is characterized by heterogeneous cellular morphology, including the presence of large and bizarre multinucleated cells scattered throughout the tumor. Due to its rarity and overlapping features with entities such as histiocytic sarcoma and undifferentiated pleomorphic sarcoma, accurate diagnosis can be difficult. In these cases, histochemical staining, such as Oil Red O or Sudan, can be required to confirm the presence of intracellular lipid (Roccabianca et al., 2020) (Figure 1.3).

Myxoid liposarcoma is characterized by scattered round to spindle cells, lipocytes and lipoblasts dispersed within an alcian blue-positive, myxoid stroma (Roccabianca et al., 2020) (Figure 1.3).

Dedifferentiated liposarcoma contains both well-differentiated lipogenic areas and non-lipogenic regions composed of spindle cells with high proliferative activity. These areas may be adjacent or intermixed in a mosaic pattern (Roccabianca et al., 2020) (Figure 1.3).

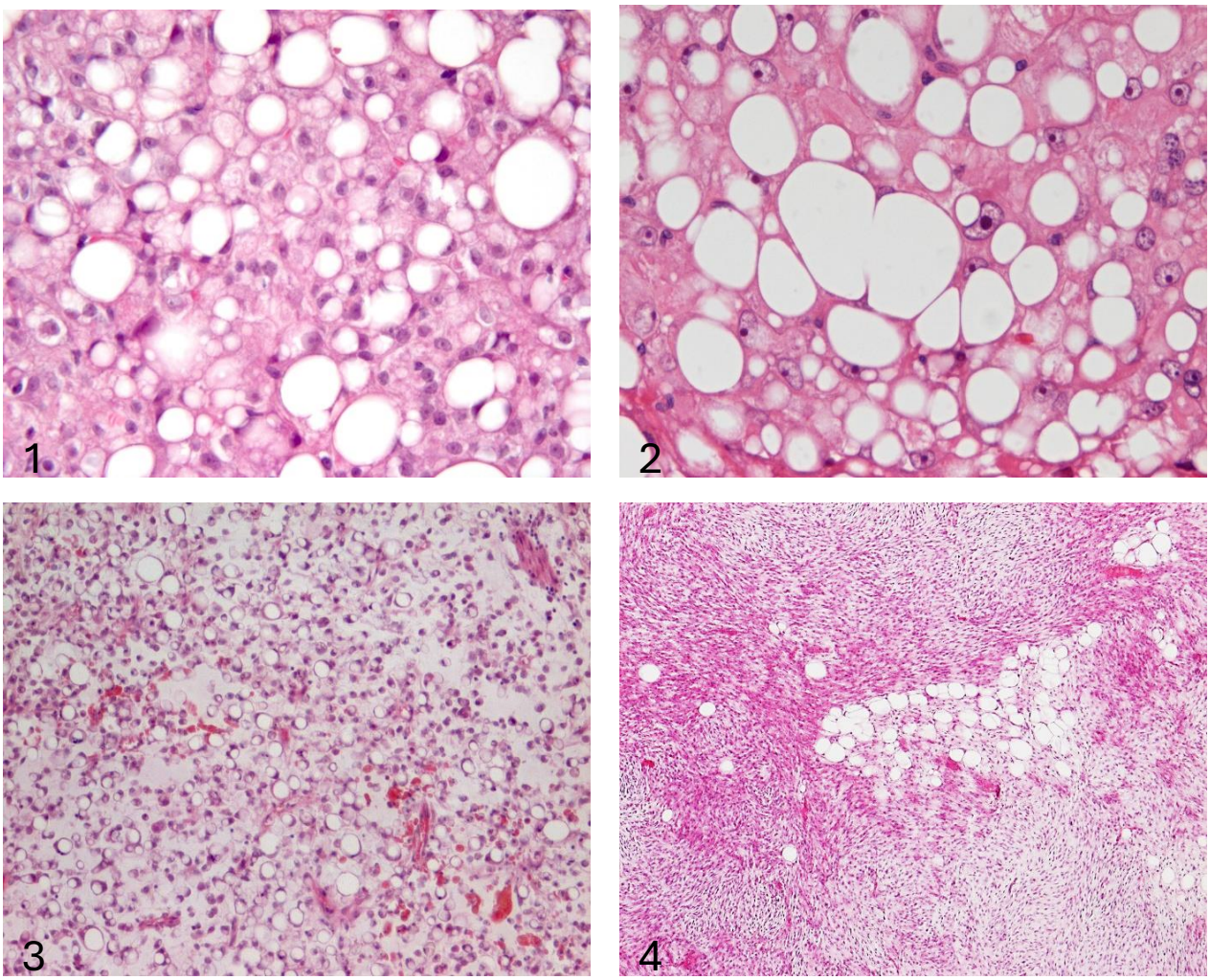


**Figure 1.3:** Histological morphology of (1) Well-differentiated liposarcoma, (2) Pleomorphic liposarcoma, (3) Myxoid liposarcoma and (4) Dedifferentiated liposarcoma.

Liposarcomas lack specific immunohistochemical markers, though canine cases have been reported as immunoreactive for *MDM2* and *CDK4* (Avallone et al., 2016). The expression of tyrosine kinase receptors and its association with Ki-67 labeling index suggest the involvement of these pathways in tumorigenesis (Avallone et al., 2017). Additionally, p53 immunolabeling and *TP53* mutations appear restricted to the myxoid variant in dogs (Avallone et al., 2020; Muscatello et al., 2024a).

*Fibrosarcomas*

Fibrosarcoma is one of the most common STSs in animals and occurs most commonly as a subcutaneous mass in dogs and less frequently as a dermal mass (Roccabianca et al., 2020). Fibrosarcomas have been classified into different variants based on histological patterns, including conventional, keloidal and myofibroblastic forms, exhibiting similar behavior.

Fibrosarcomas are infiltrative and recurrent, but metastases are uncommon. A local recurrence and metastasis rates of approximately 30% and 10% respectively have been described, and the lung is the site of metastasis most frequently reported (Bostock and Dye, 1980).

Fibrosarcomas are most common in adult and aged dogs, with a mean age of 9 years. Golden Retrievers and Doberman Pinschers are the most affected (Roccabianca et al., 2020). They can vary in size, lack a capsule, and may present as either well-circumscribed or infiltrative masses. While these tumors can arise anywhere on the body, they most commonly affect the head and limbs (Roccabianca et al., 2020).

The term "conventional" refers to the most frequently observed morphology of fibrosarcoma, distinguishing it from the other two variants (Roccabianca et al., 2020).

Conventional fibrosarcomas are composed of spindle cells embedded in collagen, arranged in interlacing fascicles or streams forming a herringbone pattern. In well-differentiated

tumors, spindle cells exhibit bland nuclei, inconspicuous nucleoli, minimal cytoplasm and abundant collagen. Poorly differentiated tumors, in contrast, show higher cellularity with larger, more vesicular nuclei, prominent nucleoli, reduced collagen, and increased mitotic activity. Ovoid, polygonal, and multinucleated giant cells may also be present, featuring large, round to oval nuclei with prominent nucleoli (Roccabianca et al., 2020).

Keloidal fibrosarcomas have a greater cellularity and less abundant hyalinized collagen fibers (Mikaelian and Gross, 2002) (Figure 1.4).

Myofibroblastic fibrosarcomas resemble conventional fibrosarcomas but immunolabel with markers of smooth muscle differentiation (Roccabianca et al., 2020).

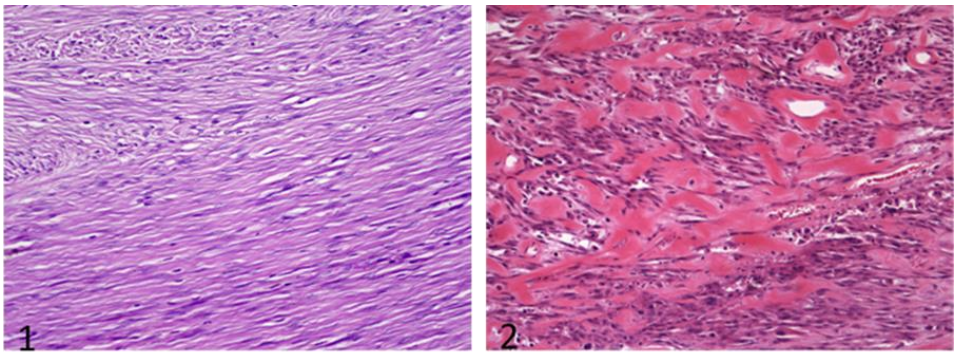


**Figure 1.4:** Histological appearance of (1) conventional fibrosarcoma and (2) keloidal fibrosarcoma.

Conventional and keloidal fibrosarcomas label only with vimentin in contrast to NSTs which typically show immunoreactivity for GFAP, NGFR, SOX-10, and Olig-2. However, IHC is of limited benefit in distinguishing between myofibroblastic fibrosarcoma and leiomyosarcoma since they both are immunoreactive for vimentin and, variably, for smooth muscle actin, calponin and desmin (Brady et al., 2022).

However, immunohistochemistry is of limited value in distinguishing myofibroblastic fibrosarcoma from leiomyosarcoma, as both entities are usually vimentin-positive and may show variable expression of smooth muscle actin, calponin, and desmin (Brady et al., 2022).

*Leiomyosarcomas*

Leiomyosarcomas are rare tumors among the skin and soft tissues reported in dogs. They develop more frequently in visceral tissues but can also originate from structures in the dermis, subcutis, blood vessels, serosal surfaces, from the retroperitoneal and pelvic cavity (Avallone et al., 2022). There is no age, breed, or sex predilection (Roccabianca et al., 2020).

When the origin of the tumor from the arrector pili muscles or vascular musculature is discernible, the prefixes pilo- and angio- are respectively used (Roccabianca et al., 2020).

Piloleiomyosarcomas arise from the arrector pili muscles and, therefore, most tumors are located on the dorsum, with fewer on the tail, limbs and muzzle (Carpenter and Hamilton, 1995; Liu and Mikaelian, 2003).

Soft tissue leiomyoma and leiomyosarcoma occur more commonly in the perigenital area in dogs (Avallone et al., 2022). Most tumors present as solitary firm nodules in the dermis or subcutis and rarely occur multiple tumors (Liu and Mikaelian, 2003).

Leiomyomas are histologically defined by well-circumscribed proliferations of monomorphic spindle-shaped cells, displaying the characteristic features of smooth muscle differentiation. These cells have abundant, brightly eosinophilic cytoplasm and oblong to bullet-shaped nuclei. Mitotic figures are rare or entirely absent. They typically show minimal stromal content, with the neoplastic cells arranged in long, interlacing fascicles. Although nuclear palisading may occasionally be observed, this feature does not support a nerve sheath origin (Avallone et al., 2022) (Figure 1.5).

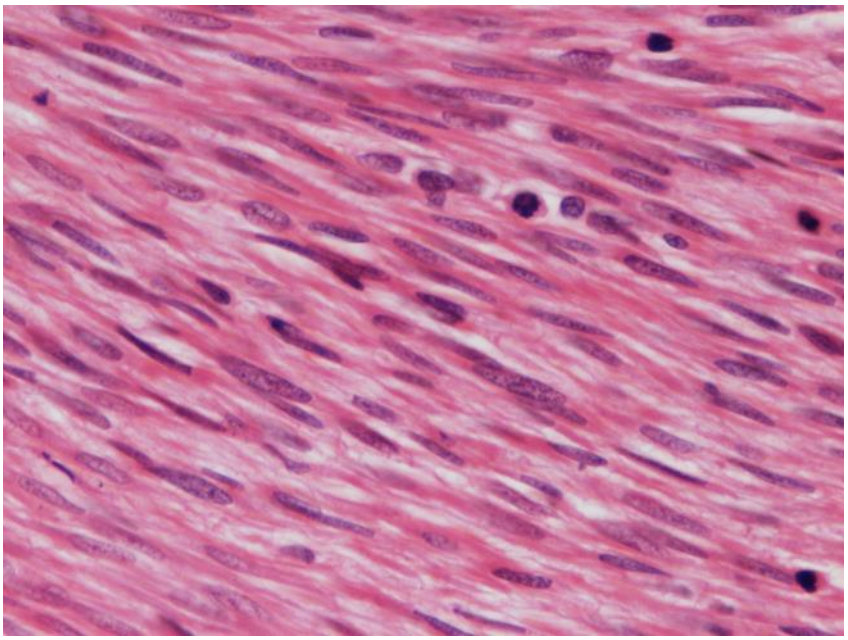

**Figure 1.5:** Histological morphology of leiomyosarcoma.

Leiomyomas and leiomyosarcomas arising in deep subcutaneous tissues exhibit histological features consistent with smooth muscle tumors. The differential diagnosis includes fibroma, myofibroblastic tumor, PWT, fibrosarcoma and malignant NST. Unlike leiomyomas, most of these neoplasms lack the abundant eosinophilic cytoplasm characteristic of smooth muscle tumors. PWTs can be distinguished by their perivascular growth pattern, while myofibroblastic tumors typically contain intercellular collagen and lymphocytes, features not seen in smooth muscle tumors (Avallone et al., 2022).

Leiomyosarcomas are typically immunoreactive for smooth muscle actin and often display desmin immunoreactivity. Smooth muscle tumors of the perigenital skin and subcutis in the dog can be immunoreactive for estrogen and/or progesterone receptors (Avallone et al., 2022) (Figure 1.6).

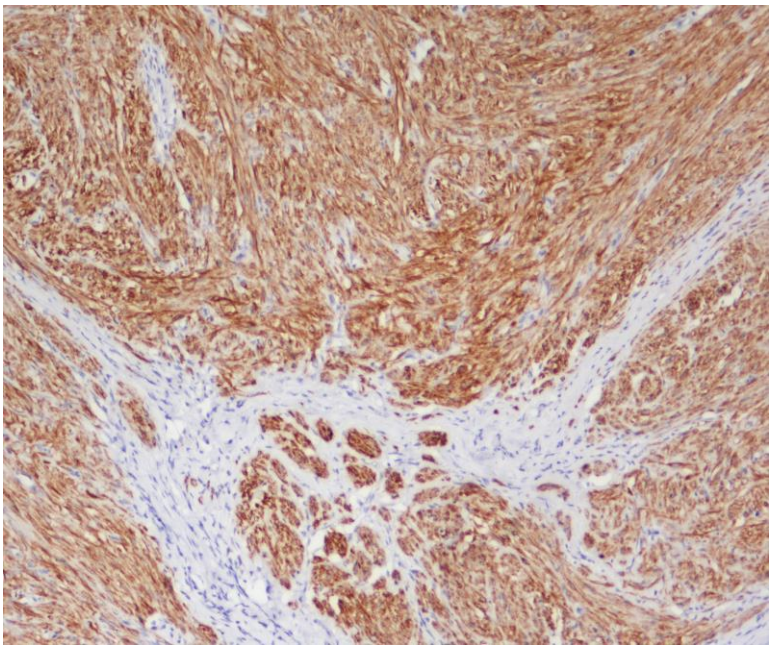

**Figure 1.6:** Immunoreactivity for desmin in a leiomyosarcomas.

*Nerve sheath tumors (NSTs)*

Nerve sheath tumors (NSTs) may arise and spread within large nerves or from small nerves in soft tissues, mostly in the dermis and subcutis (Roccabianca et al., 2020).

Benign NSTs include schwannoma (when the tumor cells are exclusively of Schwann cell origin), neurofibroma (composed of a mixture of Schwann cells, fibroblasts and perineurial cells) and perineurioma (composed of modified Schwann cells, perineurial cells). Malignant NSTs (MNSTs) may arise from any of the components of nerve sheaths (Roccabianca et al., 2020).

Middle-aged to older dogs are preferentially affected (Schulman et al., 2009) but since PWTs are sometimes misdiagnosed as NSTs, the frequency of NSTs is probably overestimated. NSTs account for 27% of all peripheral nervous system tumors in dogs (Avallone et al., 2007). NSTs are firm to soft, unencapsulated, circumscribed or infiltrative masses in the dermis or subcutis. They are usually white to gray and sometimes bulge slightly on cut surface (Roccabianca et al., 2020).

Schwannomas are well-demarcated neoplasms that typically form a single nodule, though in some cases they may present as multinodular or plexiform masses. These tumors are composed of wavy, ovoid, or spindle-shaped cells organized into bundles, whorls, and palisades, characteristic of the Antoni A pattern. In these regions, nuclear palisading and Verocay bodies can be observed (arrangements of nuclei separated by an anuclear zone). In contrast, the Antoni B pattern is characterized by lower cellularity, with tumor cells dispersed loosely within a fibrillar or mucinous stroma. The cells display elongated nuclei with small nucleoli. Occasionally, rare cells may exhibit nuclear pleomorphism, hyperchromasia, or cytoplasmic intranuclear inclusions; however, these features are not considered indicative of malignancy. (Roccabianca et al., 2020) (Figure 1.7).

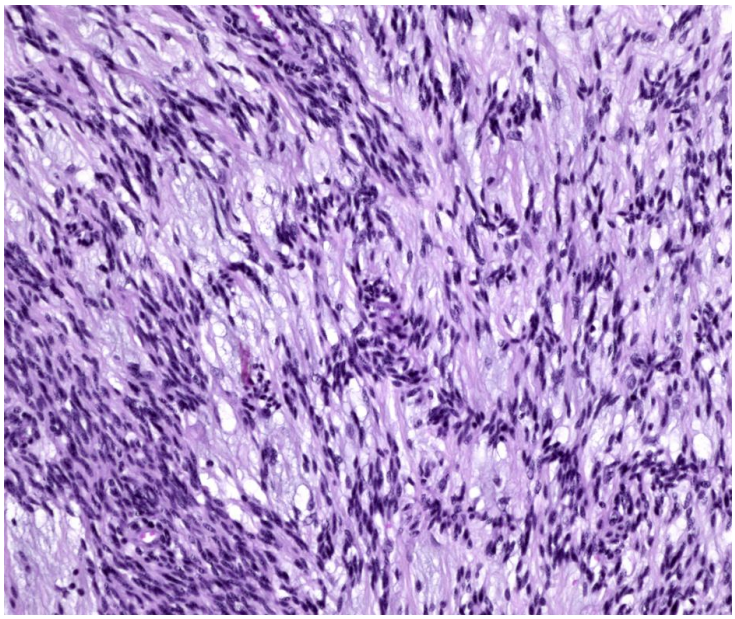

**Figure 1.7:** Verocay bodies.

Neurofibromas can have a nodular, diffuse or plexiform growth and are composed of elongated cells with small amounts of cytoplasm and wavy to tapered nuclei. The quality and quantity of extracellular matrix can vary from myxoid to collagenous and from scant to abundant respectively (Schöniger and Summers, 2009).

Perineuriomas are rare and tipically composed of spindle shaped cells forming whorls around nerve fibers creating an “onion bulb” pattern (Roccabianca et al., 2020).

The cells are densely grouped and form intersecting fascicles that in poorly differentiated cases can lack histologic features of nerve sheath origin. Nuclei are oval or oblong, with moderate pleomorphism. Neoplastic cells are often compressed at the periphery, forming a pseudocapsule. The gross appearance of this pseudocapsule often leads to inaccurate identification of margins and incomplete excisions (Roccabianca et al., 2020).

In less differentiated cases of MNST, the immunohistochemical or ultrastructural demonstration of Schwann and/or perineurial cell origin is required. Heterologous differentiation of MNST, with areas of chondroid or osseous areas, has been reported in the dog (Chijiwa et al., 2004; Mandara et al., 2013). Markers that might be used to identify cells of nerve sheath origin include S100, GFAP, NGFR, SOX10, laminin, and CNPase (Chijiwa et al., 2004; Nielsen et al., 2011) (Figure 1.8). Schwannomas and Neurofibromas have diffuse staining and scattered positivity with S100, laminin, and CNPase (Hilton and Hanemann, 2014).

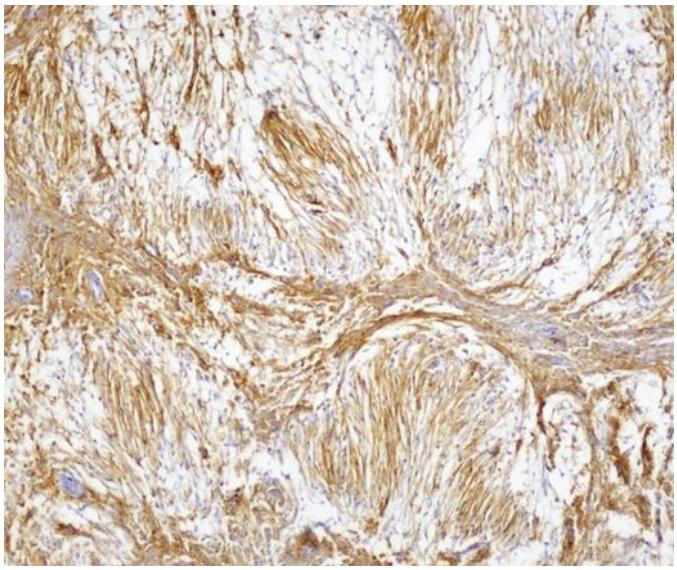

**Figure 1.8:** Immunoreactivity for NGFR in a NST.

PWT is the principal differential diagnosis for NSTs in dogs. The most effective way to distinguish between these two tumors using H&E-stained samples is by recognizing their characteristic histological features: perivascular whorls, placentoid patterns, staghorn vessels, bundles radiating from vascular walls and crown cells are diagnostic of PWTs, whereas Verocay bodies, perineurial whorls, nerve rootlet-like structures and nuclei that are wavy to tapered with dense chromatin indicate NSTs. IHC can also be useful, since some studies have found NGFR, Olig2 and SOX10 immunomarkers to be most useful to distinguish NSTs from PWTs in the dog (Chijiwa et al., 2004; Sisó et al., 2022; Suzuki et al., 2014).

*Hemangiosarcomas (HSA)*

Although not typically classified among common STSs, hemangiosarcoma (HSA) is formally part of this group, since it is a malignant neoplasm of mesenchymal origin exhibiting vascular endothelial differentiation. It occurs in several domestic animal species, with the dog being the most frequently affected (Schiffman and Breen, 2015). HSA can develop in any tissue or organ containing vascular structures (Kim et al., 2015), arising most commonly in the spleen, heart, liver, and skin (Roccabianca et al., 2020; Schiffman and Breen, 2015).

Splenic HSA occurs in 24 out of 100,000 dogs and is estimated to represent 7% of all canine malignancies (Dobson, 2013). More than half of the affected dogs die within the first year of diagnosis, and tumor-related mortality is extremely high (Antonescu, 2014).

A number of large-breed dogs, including Golden Retrievers, Labrador Retrievers, Boxers, and German Shepherds, exhibit an increased risk of developing HSA (Cohen et al., 2009; Dobson, 2013; Tamburini et al., 2009). Canine splenic HSA is a highly malignant neoplasm with a high metastatic rate and short survival time (Boston et al., 2011; Prymak et al., 1988), representing one of the most aggressive cancers in dogs (Batschinski et al., 2018; Sorenmo et al., 2004; Wendelburg et al., 2015). Hemangiosarcoma is infiltrative and aggressive, often

associated with metastases to the lymph nodes, lungs and brain. Although different histological types of hemangiosarcoma are recognizable there are no reported behavioral differences for each type (Roccabianca et al., 2020).

Pathogenesis of hemangiosarcoma is complex and multifactorial. Mutations of tumor suppressor genes including p53, Ras, and *PTEN* (phosphatase and tensin homolog) together with the dysregulation of angiogenic factors are reported in dogs (Roccabianca et al., 2020).

## References


Antonescu C. Malignant vascular tumors—an update. Modern Pathology 2014;27:S30–8.

Avallone G, Boracchi P, Stefanello D, et al. Canine Perivascular Wall Tumors: High Prognostic Impact of Site, Depth, and Completeness of Margins. Vet Pathol 2014;51:713–21.

Avallone G, Helmbold P, Caniatti M, et al. The Spectrum of Canine Cutaneous Perivascular Wall Tumors: Morphologic, Phenotypic and Clinical Characterization. Vet Pathol 2007;44:607–20.

Avallone G, Pellegrino V, Roccabianca P, et al. Tyrosine Kinase Receptor Expression in Canine Liposarcoma. Vet Pathol 2017;54:212–7.

Avallone G, Roccabianca P, Crippa L, et al. Histological Classification and Immunohistochemical Evaluation of MDM2 and CDK4 Expression in Canine Liposarcoma. Vet Pathol 2016;53:773–80.

Avallone G, Muscatello LV, Leoni A, et al. p53 Expression in Canine Liposarcoma Correlates With Myxoid Variant and Higher Proliferative Activity. Vet Pathol 2020;57:620–2.

Avallone G, Pellegrino V, Muscatello LV, et al. Canine smooth muscle tumors: A clinicopathological study. Vet Pathol 2022;59:244–55.

Baez JL, Hendrick MJ, Shofer FS, et al. Liposarcomas in dogs: 56 cases (1989–2000). Javma 2004;224:887–91.

Batschinski K, Nobre A, Vargas-Mendez E, et al. Canine visceral hemangiosarcoma treated with surgery alone or surgery and doxorubicin: 37 cases (2005-2014). Can Vet J 2018;59:967–72.

Boerkamp KM, Hellmén E, Willén H, et al. Unclassified sarcomas: a study to improve classification in a cohort of Golden Retriever dogs. J VET Diagn Invest 2016;28:623–31.

Bostock DE, Dye MT. Prognosis after Surgical Excision of Canine Fibrous Connective Tissue Sarcomas. Vet Pathol 1980;17:581–8.

Boston SE, Higginson G, Monteith G. Concurrent Splenic and Right Atrial Mass at Presentation in Dogs with HSA: A Retrospective Study. Journal of the American Animal Hospital Association 2011;47:336–41.

Brady RV, Rebhun RB, Skorupski KA, et al. Retrospective immunohistochemical investigation of suspected non-visceral leiomyosarcoma in dogs. J VET Diagn Invest 2022;34:465–73.

Bray JP. Soft tissue sarcoma in the dog – part 1: a current review. J of Small Animal Practice 2016;57:510–9.

Brodehl A, Gaertner-Rommel A, Milting H. Molecular insights into cardiomyopathies associated with desmin (DES) mutations. Biophys Rev 2018;10:983–1006.

Canter RJ, Beal S, Borys D, et al. Interaction of Histologic Subtype and Histologic Grade in Predicting Survival for Soft-Tissue Sarcomas. Journal of the American College of Surgeons 2010;210:191-198e2.

Cardoso De Almeida Moreira A, Franzoni M, Dos Anjos D, et al. Proposing Clinicopathological Staging and Mitotic Count as Prognostic Factors for Canine Soft Tissue Sarcomas. Veterinary Sciences 2023;10:327.

Carpenter JL, Hamilton TA. Angioleiomyoma of the Nasopharynx in a Dog. Vet Pathol 1995;32:721–3.

Casali PG, Abecassis N, Bauer S, et al. Soft tissue and visceral sarcomas: ESMO–EURACAN Clinical Practice Guidelines for diagnosis, treatment and follow-up. Annals of Oncology 2018;29:iv51–67.

Chase D, Bray J, Ide A, et al. Outcome following removal of canine spindle cell tumours in first opinion practice: 104 cases. J of Small Animal Practice 2009;50:568–74.

Chijiwa K, Uchida K, Tateyama S. Immunohistochemical Evaluation of Canine Peripheral Nerve Sheath Tumors and Other Soft Tissue Sarcomas. Vet Pathol 2004;41:307–18.

Chiti LE, Ferrari R, Roccabianca P, et al. Surgical Margins in Canine Cutaneous Soft-Tissue Sarcomas: A Dichotomous Classification System Does Not Accurately Predict the Risk of Local Recurrence. Animals 2021;11:2367.

Cohen SM, Storer RD, Criswell KA, et al. Hemangiosarcoma in Rodents: Mode-of-Action Evaluation and Human Relevance. Toxicological Sciences 2009;111:4–18.

Coindre J-M. Grading of Soft Tissue Sarcomas: Review and Update. Archives of Pathology & Laboratory Medicine 2006;130:1448–53.

Crago AM, Brennan MF. Principles in Management of Soft Tissue Sarcoma. Advances in Surgery 2015;49:107–22.

Crownshaw AH, McEntee MC, Nolan MW, et al. Journal of the American Veterinary Medical Association. Javma 2020;256:783–91.

Das S, Idate R, Lana SE, et al. Integrated analysis of canine soft tissue sarcomas identifies recurrent mutations in TP53, KMT genes and PDGFB fusions. Sci Rep 2023;13.

Dennis MM, McSporran KD, Bacon NJ, et al. Prognostic Factors for Cutaneous and Subcutaneous Soft Tissue Sarcomas in Dogs. Vet Pathol 2011;48:73–84.

Dobson JM. Breed-Predispositions to Cancer in Pedigree Dogs. ISRN Veterinary Science 2013;2013:1–23.

Ehrhart N. Soft-Tissue Sarcomas in Dogs: A Review. Journal of the American Animal Hospital Association 2005;41:241–6.

Ettinger SN. Principles of treatment for soft-tissue sarcomas in the dog. Clinical Techniques in Small Animal Practice 2003;18:118–22.

Ettinger SN, Scase TJ, Oberthaler KT, et al. Association of argyrophilic nucleolar organizing regions, Ki-67, and proliferating cell nuclear antigen scores with histologic grade and survival in dogs with soft tissue sarcomas: 60 cases (1996—2002). Javma 2006;228:1053–62.

Ferrari A, Sultan I, Huang TT, et al. Soft tissue sarcoma across the age spectrum: A population-based study from the surveillance epidemiology and end results database. Pediatric Blood & Cancer 2011;57:943–9.

Frid MG, Shekhonin BV, Koteliansky VE, et al. Phenotypic changes of human smooth muscle cells during development: Late expression of heavy caldesmon and calponin. Developmental Biology 1992;153:185–93.

Goldblum JR, Folpe AL, Weiss SW. Enzinger & Weiss's soft tissue tumors. Seventh edition. Philadelphia, PA: Elsevier; 2020.

Grüntzig K, Graf R, Boo G, et al. Swiss Canine Cancer Registry 1955–2008: Occurrence of the Most Common Tumour Diagnoses and Influence of Age, Breed, Body Size, Sex and Neutering Status on Tumour Development. Journal of Comparative Pathology 2016;155:156–70.

Haglund KE, Raut CP, Nascimento AF, et al. Recurrence Patterns and Survival for Patients With Intermediate- and High-Grade Myxofibrosarcoma. International Journal of Radiation Oncology*Biology*Physics 2012;82:361–7.

Hendrick M.J. Mesenchymal tumors of the skin and soft tissues. Tumors in Domestic Animals. 5th ed., John Wiley & Sons, Inc. (Wiley-Blackwell); 2017, p. 142–75.

Hendrick MJ. Mesenchymal Tumors of the Skin and Soft Tissues. Tumors in Domestic Animals. 1st ed., Wiley; 2016, p. 142–75.

Hicks JK, Henderson-Jackson E, Duggan J, et al. Identification of a novel MTAP-RAF1 fusion in a soft tissue sarcoma. Diagn Pathol 2018;13.

Hilton DA, Hanemann CO. Schwannomas and Their Pathogenesis. Brain Pathology 2014;24:205–20.

Inokuchi T, Yokoyama R, Satoh H, et al. Scanning electron microscopic study of periendothelial cells of the rat cerebral vessels revealed by a combined method of corrosion casting and KOH digestion. J Electron Microsc (Tokyo) 1989;38:201–13.

Iwaki Y, Lindley S, Smith A, et al. Canine myxosarcomas, a retrospective analysis of 32 dogs (2003–2018). BMC Vet Res 2019;15.

Jo VY, Fletcher CDM. WHO classification of soft tissue tumours: an update based on the 2013 (4th) edition. Pathology 2014;46:95–104.

Kim J-H, Graef A, Dickerson E, et al. Pathobiology of Hemangiosarcoma in Dogs: Research Advances and Future Perspectives. Veterinary Sciences 2015;2:388–405.

Kumar V, K. Abbas A, Aster JC. Robbins BASIC PATHOLOGY. 10th ed., 2020, p. 1179–226.

Kuntz CA, Dernell WS, Powers BE, et al. Prognostic factors for surgical treatment of soft-tissue sarcomas in dogs: 75 cases (1986-1996). J Am Vet Med Assoc 1997;211:1147–51.

Liptak JM, Christensen NI. Soft Tissue Sarcomas. Withrow and MacEwen's Small Animal Clinical Oncology, Elsevier; 2019, p. 404–31.

Liu SM, Mikaelian I. Cutaneous Smooth Muscle Tumors in the Dog and Cat. Vet Pathol 2003;40:685–92.

Mandara MT, Fabriani E, Pavone S, et al. Feline cutaneous nerve sheath tumours: Histological features and immunohistochemical evaluations. Research in Veterinary Science 2013;95:548–55.

McKnight JA, Mauldin GN, McEntee MC, et al. Radiation treatment for incompletely resected soft-tissue sarcomas in dogs. Javma 2000;217:205–10.

McSporran KD. Histologic Grade Predicts Recurrence for Marginally Excised Canine Subcutaneous Soft Tissue Sarcomas. Vet Pathol 2009;46:928–33.

Metzler G, Schaumburg-Lever G, Fehrenbacher B, et al. Ultrastructural localization of actin in normal human skin. Arch Dermatol Res 1992;284:242–5.

Meuten DJ, Moore FM, George JW. Mitotic Count and the Field of View Area: Time to Standardize. Vet Pathol 2016;53:7–9.

Mikaelian I, Gross TL. Keloidal Fibromas and Fibrosarcomas in the Dog. Vet Pathol 2002;39:149–53.

Moretti G, Bufalari A. Editorial: A review of canine soft tissue sarcomas: new insights in diagnostic and treatment measures. Front Vet Sci 2024;11:1454513.

Muscatello LV, De Biase D, Maloberti T, et al. Analysis of MDM2 and TP53 genes in canine liposarcoma. Sci Rep 2024;14.

Nehls V, Drenckhahn D. Heterogeneity of microvascular pericytes for smooth muscle type alpha-actin. The Journal of Cell Biology 1991;113:147–54.

Nielsen AB, Jensen HE, Leifsson PS. Immunohistochemistry for 2′,3′-Cyclic Nucleotide-3′-Phosphohydrolase in 63 Bovine Peripheral Nerve Sheath Tumors. Vet Pathol 2011;48:796–802.

Nystrom LM, Reimer NB, Reith JD, et al. Multidisciplinary Management of Soft Tissue Sarcoma. The Scientific World Journal 2013;2013.

Pellegrino V, Muscatello LV, Sarli G, et al. Canine Gastrointestinal Spindle Cell Tumors Efficiently Diagnosed by Tissue Microarray-Based Immunohistochemistry. Vet Pathol 2018;55:678–81.

Prymak C, McKee LJ, Goldschmidt MH, et al. Epidemiologic, clinical, pathologic, and prognostic characteristics of splenic hemangiosarcoma and splenic hematoma in dogs: 217 cases (1985). J Am Vet Med Assoc 1988;193:706–12.

Rhodin JA, Fujita H. Capillary growth in the mesentery of normal young rats. Intravital video and electron microscope analyses. J Submicrosc Cytol Pathol 1989;21:1–34.

Roccabianca P, Schulman FY, Avallone G, et al. Surgical Pathology of Tumors of Domestic Animals. vol. 3. 3rd ed. Kiupel M.; 2020.

Sanfilippo R, Miceli R, Grosso F, et al. Myxofibrosarcoma: Prognostic Factors and Survival in a Series of Patients Treated at a Single Institution. Ann Surg Oncol 2011;18:720–5.

Schiffman JD, Breen M. Comparative oncology: what dogs and other species can teach us about humans with cancer. Phil Trans R Soc B 2015;370:20140231.

Schöniger S, Summers BA. Localized, Plexiform, Diffuse, and Other Variants of Neurofibroma in 12 Dogs, 2 Horses, and a Chicken. Vet Pathol 2009;46:904–15.

Schulman FY, Johnson TO, Facemire PR, et al. Feline Peripheral Nerve Sheath Tumors: Histologic, Immunohistochemical, and Clinicopathologic Correlation (59 Tumors in 53 Cats). Vet Pathol 2009;46:1166–80.

Selting KA, Powers BE, Thompson LJ, et al. Outcome of dogs with high-grade soft tissue sarcomas treated with and without adjuvant doxorubicin chemotherapy: 39 cases (1996–2004). Javma 2005;227:1442–8.

Sisó S, Marco-Salazar P, Roccabianca P, et al. Nerve Fiber Immunohistochemical Panel Discriminates between Nerve Sheath and Perivascular Wall Tumors. Veterinary Sciences 2022;10:1.

Sorenmo KU, Baez JL, Clifford CA, et al. Efficacy and Toxicity of a Dose-Intensified Doxorubicin Protocol in Canine Hemangiosarcoma. J Vet Int Med 2004;18:209.

Spinnato P, Sambri A, Fujiwara T, et al. Myxofibrosarcoma: Clinical and Prognostic Value of MRI Features. CMIR 2021;17:217–24.

Stefanello D, Avallone G, Ferrari R, et al. Canine Cutaneous Perivascular Wall Tumors at First Presentation: Clinical Behavior and Prognostic Factors in 55 Cases. Veterinary Internal Medicne 2011;25:1398–405.

Suzuki S, Uchida K, Nakayama H. The Effects of Tumor Location on Diagnostic Criteria for Canine Malignant Peripheral Nerve Sheath Tumors (MPNSTs) and the Markers for Distinction Between Canine MPNSTs and Canine Perivascular Wall Tumors. Vet Pathol 2014;51:722–36.

Tamburini BA, Trapp S, Phang TL, et al. Gene Expression Profiles of Sporadic Canine Hemangiosarcoma Are Uniquely Associated with Breed. PLoS ONE 2009;4:e5549.

Tierce R, Martin T, Hughes KL, et al. Response of Canine Soft Tissue Sarcoma to Stereotactic Body Radiotherapy. Radiation Research 2021;196.

Trojani M, Contesso G, Coindre JM, et al. Soft-tissue sarcomas of adults; study of pathological prognostic variables and definition of a histopathological grading system. Intl Journal of Cancer 1984;33:37–42.

Uranishi R, Baev NI, Kim JH, et al. Vascular Smooth Muscle Cell Differentiation in Human Cerebral Vascular Malformations. Neurosurgery 2001;49:671–80.

Ushiwata I, Ushiki T. Cytoarchitecture of the smooth muscles and pericytes of rat cerebral blood vessels: A scanning electron microscopic study. Journal of Neurosurgery 1990;73:82–90.

Wendelburg KM, Price LL, Burgess KE, et al. Survival time of dogs with splenic hemangiosarcoma treated by splenectomy with or without adjuvant chemotherapy: 208 cases (2001–2012). Javma 2015;247:393–403.

Yap FW, Rasotto R, Priestnall SL, et al. Intra- and inter-observer agreement in histological assessment of canine soft tissue sarcoma. Vet Comparative Oncology 2017;15:1553–7.

## General objectives

Given the biological diversity of canine STSs, this research aims to deepen our understanding of these tumors by integrating histological, immunohistochemical, and molecular data. The PhD project has been designed around three main research areas:

- **Proliferation** of neoplastic cells, which encompassed two studies: one aimed at defining prognostic thresholds of Ki-67 labeling index in splenic hemangiosarcoma and the other examining the spatial distribution of proliferative hotspots across different tumor types.
- **Tumor Immune Microenviroment**, which focused on characterizing two key cellular populations, tumor-infiltrating lymphocytes (TILs) and tumor-associated macrophages (TAMs) in canine STSs.
- **Proteomic profiling**, which involved a comprehensive analysis of different STSs histotypes, through Liquid Chromatography and Tandem Mass Spectrometry (LC-MS/MS).

Further studies were conducted, exploring the diagnostic utility of epithelial membrane antigen (EMA) in the differential diagnosis between nerve sheath tumors (NSTs) and perivascular wall tumors (PWTs), and the expression of platelet-derived growth factor receptor beta (PDGFR$\beta$) in canine intestinal leiomyosarcomas investigating potential associations with tumor proliferation.

## Chapter 2: Proliferation

### *Chapter overview*

*Regulation and Dysregulation of the Cell Cycle*

Cell proliferation is a fundamental process essential for the growth and maintenance of tissues, regulated by the cell cycle, an orchestrated sequence of events that ensures accurate cell duplication and division.

The cell cycle is divided into distinct phases (G1, S, G2, and M) and is regulated by activators and inhibitors, which are responsible for the correct progression of the process.

Cells in a quiescent state reside in the G0 phase and require stimulation by growth factors to enter the G1 phase (Assoian and Zhu, 1997). At this stage, progression through the G1 phase is regulated primarily by Cyclins D and E (Ciemerych et al., 2002). In early G1, the formation of Cyclin D-cyclin-dependent Kinase (CDK) 4/6 complexes is crucial for cell cycle progression, followed by the activation of Cyclin E-CDK2 complexes during mid-to-late G1 (Vermeulen et al., 2003).

The first checkpoint occurs at the G1/S transition, aiming to prevent the replication of damaged or incomplete DNA. This phase is regulated by the retinoblastoma (*RB*) gene family, which encodes for Rb/p105, Rb2/p107 and Rb2/p130, characterized by a highly conserved binding region, known as the pocket domain, which serves to mediate interactions with oncoproteins (Dyson, 1998). Of these, the retinoblastoma protein (pRB) is regulated by phosphorylation. In quiescent cells, pRB is hypophosphorylated and tightly bound to E2F transcription factors, keeping them in an inactive state (Adams and Kaelin, 1995). In response to mitogenic signals, the formation of the Cyclin D-CDK4/6 complex leads to the phosphorylation of pRB, resulting in its inactivation and the subsequent release of E2F transcription factors. E2F transcription factors activate the expression of genes

required for S phase entry. At this point, the Cyclin E-CDK2 complex forms, promoting the cell's progression toward the S phase. The maintenance of pRB in a hyperphosphorylated state throughout the remainder of the cell cycle is ensured by the activity of the Cyclin A-CDK2 complex (Dick and Rubin, 2013).

The S phase is regulated by Cyclin A-CDK2, which can control the timing of mitosis and E2F phosphorylation (De Boer et al., 2008). In addition, Cyclin A plays a key role in the G2 phase by forming a complex with CDK1, which initiates the molecular events required for entry into mitosis (Vermeulen et al., 2003).

The second checkpoint occurs at the G2/M transition, preventing cells with damaged or incompletely replicated DNA from entering mitosis. This checkpoint ensures that the Cyclin B-CDK1 complex is only activated when the cell is fully prepared for mitosis. If DNA damage is detected, signaling pathways halt cell cycle progression to allow time for DNA repair or, if damage is irreparable, cause apoptosis (Vermeulen et al., 2003).

In the M phase, cyclin A-CDK1 and Cyclin B-CDK1 complexes promote mitosis. Towards the end of M phase, the anaphase promoting complex (APC) causes ubiquitination and destruction of Cyclin A and Cyclin B, that leads to termination of M phase (De Boer et al., 2008).

Cell cycle progression is also modulated by inhibitors of CDKs, which prevent CDK activation. Currently, two distinct families of CDK inhibitors are recognized: the INK4 family and the Cip/Kip family, each targeting specific stages of the cell cycle.

The first family, the INK4, includes $p15^{INK4b}$, $p16^{INK4a}$, $p18^{INK4c}$ and $p19^{INK4d}$. They specifically inhibit the interaction and binding of CDK4/6 with Cyclin D during the G1 phase (Ventura and Giordano, 2019). The most important CDK inhibitor, $p16^{INK4a}$, regulates the cell cycle negatively by binding to CDK4 and CDK6, either individually or as part of the Cyclin D-

CDK4/6 complex. This inhibition prevents RB phosphorylation, leading to cell cycle arrest in the G1 phase (Vidal and Koff, 2000).

The Cip/Kip family includes p21 (Cip1), p27 (Cip2), p57 (Kip2), which can block the cell cycle by binding CDKs. Among these, p21 inhibits the CDK4/6-Cyclin D and CDK2-Cyclin E complexes, thereby blocking the cell cycle at the G1-S and G2-M transitions, respectively (Vermeulen et al., 2003).

In cooperation with CDK inhibitors, p53 ensures that only cells with intact DNA proceed to replication, acting as a tumor suppressor protein and playing a key role in preventing mutations and the development of neoplasms. When DNA damage occurs, p53 is upregulated, leading to the induction of p21 expression (Chen, 2016).

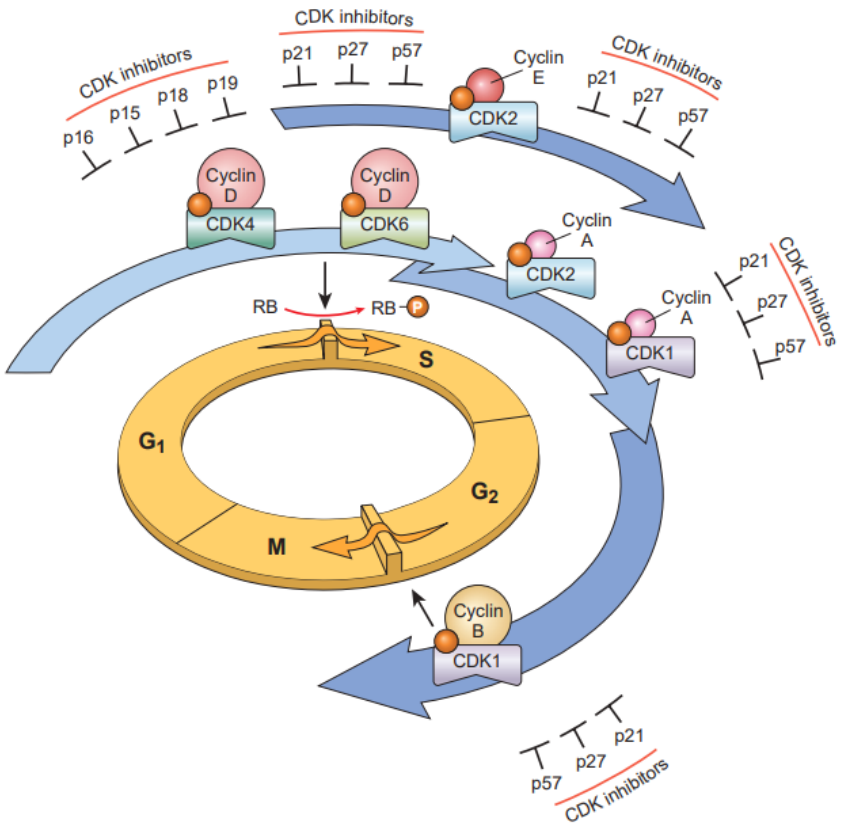


**Figure 2.1:** The main regulatory proteins of the cell cycle (Kumar et al., 2020).

In cancer, the genetic regulation of cell division is fundamentally disrupted, leading to uncontrolled cell proliferation. Mutations mainly occur in two classes of genes: proto-oncogenes and tumor suppressor genes. In normal cells, the products of proto-oncogenes act at different levels along the pathways that stimulate cell proliferation. Mutated versions of proto-oncogenes or oncogenes can contribute to tumor development and growth (Vermeulen et al., 2003) (Figure 2.2).

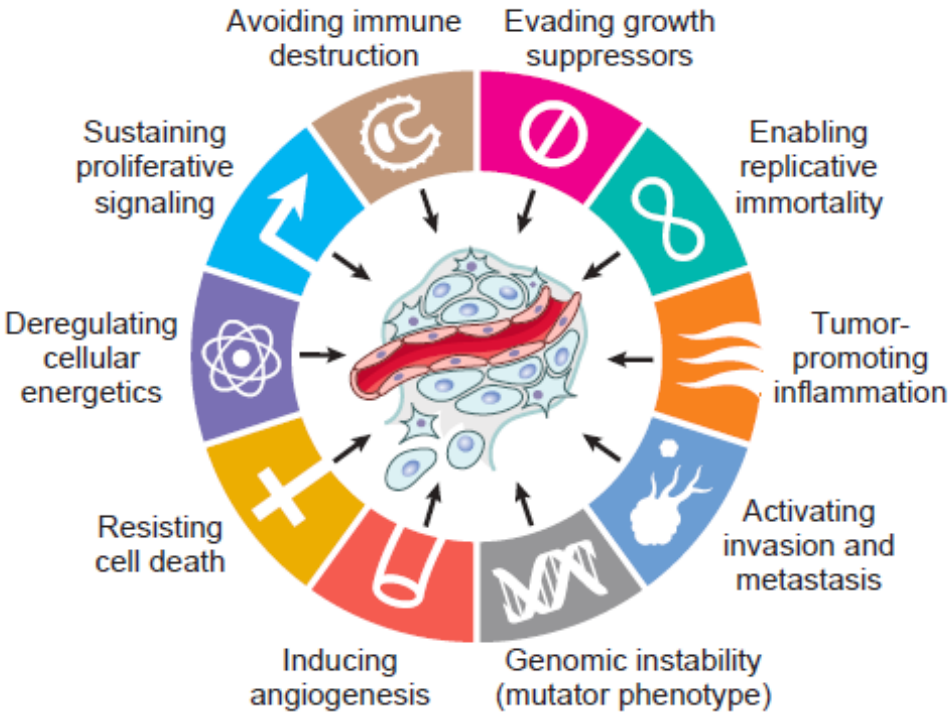


**Figure 2.2:** Main properties acquired by cancer cells as a consequence of mutations in critical genes (Hanahan and Weinberg, 2011).

Cancer cells can maintain continuous proliferative signaling through several mechanisms. One way is by producing their own growth factor ligands and by expressing the corresponding receptors, allowing for autocrine stimulation. Alternatively, cancer cells can stimulate nearby normal cells in the tumor-associated stroma to release growth factors,

indirectly supporting tumor growth (Bhowmick et al., 2004; Cheng et al., 2008). In addition, receptor signaling may also become deregulated through an increased presence of receptor proteins on the surface of cancer cells, making them overly responsive even to minimal amounts of growth factor ligands. Similarly, structural modifications in the receptors can lead to their activation in the absence of ligand binding, resulting on a continuous signaling (Hanahan and Weinberg, 2011).

Cancer cells are able to overcome mechanisms that normally inhibit cell proliferation. Many of these inhibitory pathways are based on tumor suppressor genes. Two classic examples of tumor suppressors are the proteins encoded by the *RB* and *TP53* genes. As mentioned before, these proteins play a central role in two complementary cellular pathways that determine whether a cell continues to divide or enters senescence and undergoes programmed cell death (Hanahan and Weinberg, 2011). The loss or inactivation of tumor suppressor genes like *RB* further contributes to uncontrolled proliferation by disabling critical cell cycle checkpoints, particularly the G1/S transition (Manning and Dyson, 2012). At the same time, the inactivation of the other key tumor suppressor, p53, destabilizes the cell's ability to respond to DNA damage or internal stress by blocking cell cycle arrest, senescence and apoptosis, removing crucial safeguards that prevent malignant transformation (Joerger and Fersht, 2016).

*Assessment of proliferative activity of neoplastic cells*

As cell cycle dysregulation plays a central role in cancer development, the proliferation rate of neoplastic cells is essential to assess tumor progression. It is considered an indication of the biological behavior of the neoplasm in many tumor types and its assessment has become essential (Almalki, 2023; Glaviano et al., 2025; Tan et al., 2020). Among the most commonly used systems to evaluate proliferative activity are **mitotic count** (MC) and **Ki-67** immunohistochemistry assessment.

Ki-67 is a nuclear protein expressed during all active phases of the cell cycle (G1, S, G2 and M), but is absent in resting cells (G0) (Hooghe et al., 2008; Li et al., 2015; Shirendeb et al., 2009). In later phases of mitosis (during anaphase and telophase), it occurs a decrease in Ki-67 levels (Modlin et al., 2008). Expression of the Ki-67 protein (pKi-67) is associated with tumor aggressiveness and proliferative cell activity in malignant tumors (Brown and Gatter, 2002; Klöppel et al., 2004). The prognostic value of pKi-67 has been investigated in a number of studies as a potential reliable marker in this field, such as in cancers of the breast, soft tissue, lung, prostate, cervix and central nervous system in human (Ciancio et al., 2012; Ishihara et al., 2013; Josefsson et al., 2012; Sorbye et al., 2012, 2011).

In parallel, the MC reflects the number of cells actually undergoing mitosis (specifically in M phase) and serves as a key parameter in evaluating the tumor proliferative rate (Khan et al., 2013; Sinicrope et al., 1999; Van Diest, 2004; Zhang and Liu, 2020).

Specifically, mitotic activity is a highly relevant measure for the growth of tumor proliferation (Sledge et al., 2016) and is thus generally expected to correlate with a more aggressive biological behavior and less favorable patient outcomes for various malignant tumor types (Bertram et al., 2024a, 2024b).

In fact, MC is an important part of histological grading of tumors such as canine mast cell tumors (Kiupel et al., 2011; Patnaik et al., 1984), canine mammary tumors (Peña et al., 2013), canine melanoma (Spangler and Kass, 2006), and canine STSs (Kuntz et al., 1997; McSporran, 2009).

Quantification of mitotic figures is a standard tool for tumor prognostication in veterinary pathology due to its high practicability and assumed high prognostic value (Donovan et al., 2021; Meuten et al., 2021).

Descriptions of the measuring methods of mitotic activity in oncologic research must be adequately detailed such that others can reliably and accurately reproduce the methods and data can be compared (Meuten et al., 2018).

A major challenge in this standardization lies in the limited reproducibility, primarily due to the lack of clearly defined and reproducible assessment methods (Bonert and Tate, 2017; Ellis and Whitehead, 1981; Meuten et al., 2016). As a result, the evaluation of several parameters, including MC, often relies on subjective approaches, which consistent comparisons across studies (Meuten et al., 2021).

Recent guidelines have defined key aspects of the MC, including the region of interest (ROI) within the tumor section, the size of the ROI in $mm^2$, the spatial arrangement of the fields of view within the ROI, and the morphologic criteria for the identification of mitotic figures (Donovan et al., 2021; Meuten et al., 2021).

**References**

Adams PD, Kaelin WG. Transcriptional control by E2F. Seminars in Cancer Biology 1995;6:99–108.

Almalki SG. The pathophysiology of the cell cycle in cancer and treatment strategies using various cell cycle checkpoint inhibitors. Pathology - Research and Practice 2023;251:154854.

Assoian RK, Zhu X. Cell anchorage and the cytoskeleton as partners in growth factor dependent cell cycle progression. Current Opinion in Cell Biology 1997;9:93–8.

Bertram CA, Donovan TA, Bartel A. Mitotic activity: A systematic literature review of the assessment methodology and prognostic value in canine tumors. Vet Pathol 2024;61:752–64.

Bertram CA, Donovan TA, Bartel A. Mitotic activity: A systematic literature review of the assessment methodology and prognostic value in feline tumors. Vet Pathol 2024;61:743–51.

Bhowmick NA, Neilson EG, Moses HL. Stromal fibroblasts in cancer initiation and progression. Nature 2004;432:332–7.

Bonert M, Tate AJ. Mitotic counts in breast cancer should be standardized with a uniform sample area. BioMed Eng OnLine 2017;16.

Brown DC, Gatter KC. Ki-67 protein: the immaculate deception? Histopathology 2002;40:2–11.

Chen J. The Cell-Cycle Arrest and Apoptotic Functions of p53 in Tumor Initiation and Progression. Cold Spring Harb Perspect Med 2016;6:a026104.

Cheng N, Chytil A, Shyr Y, et al. Transforming Growth Factor-β Signaling–Deficient Fibroblasts Enhance Hepatocyte Growth Factor Signaling in Mammary Carcinoma Cells to Promote Scattering and Invasion. Molecular Cancer Research 2008;6:1521–33.

Ciancio N, Galasso MG, Campisi R, et al. Prognostic value of p53 and Ki-67 expression in fiberoptic bronchial biopsies of patients with non small cell lung cancer. Multidiscip Respir Med 2012;7.

Ciemerych MA, Kenney AM, Sicinska E, et al. Development of mice expressing a single D-type cyclin. Genes Dev 2002;16:3277–89.

De Boer L, Oakes V, Beamish H, et al. Cyclin A/cdk2 coordinates centrosomal and nuclear mitotic events. Oncogene 2008;27:4261–8.

Dick FA, Rubin SM. Molecular mechanisms underlying RB protein function. Nat Rev Mol Cell Biol 2013;14:297–306.

Donovan TA, Moore FM, Bertram CA, et al. Mitotic Figures—Normal, Atypical, and Imposters: A Guide to Identification. Vet Pathol 2021;58:243–57.

Dyson N. The regulation of E2F by pRB-family proteins. Genes Dev 1998;12:2245–62.

Ellis PSJ, Whitehead R. Mitosis counting—A need for reappraisal. Human Pathology 1981;12:3–4.

Glaviano A, Singh SK, Lee EHC, et al. Cell cycle dysregulation in cancer. Pharmacological Reviews 2025;77:100030.

Hanahan D, Weinberg RA. Hallmarks of Cancer: The Next Generation. Cell 2011;144:646–74.

Hooghe B, Hulpiau P, Van Roy F, et al. ConTra: a promoter alignment analysis tool for identification of transcription factor binding sites across species. Nucleic Acids Research 2008;36:W128–32.

Ishihara M, Mukai H, Nagai S, et al. Retrospective Analysis of Risk Factors for Central Nervous System Metastases in Operable Breast Cancer: Effects of Biologic Subtype and Ki-67 Overexpression on Survival. Oncology 2013;84:135–40.

Joerger AC, Fersht AR. The p53 Pathway: Origins, Inactivation in Cancer, and Emerging Therapeutic Approaches. Annu Rev Biochem 2016;85:375–404.

Josefsson A, Wikström P, Egevad L, et al. Low endoglin vascular density and Ki-67 index in Gleason score 6 tumours may identify prostate cancer patients suitable for surveillance. Scandinavian Journal of Urology and Nephrology 2012;46:247–57.

Khan MS, Luong TV, Watkins J, et al. A comparison of Ki-67 and mitotic count as prognostic markers for metastatic pancreatic and midgut neuroendocrine neoplasms. Br J Cancer 2013;108:1838–45.

Kiupel M, Webster JD, Bailey KL, et al. Proposal of a 2-Tier Histologic Grading System for Canine Cutaneous Mast Cell Tumors to More Accurately Predict Biological Behavior. Vet Pathol 2011;48:147–55.

Klöppel G, Perren A, Heitz PU. The Gastroenteropancreatic Neuroendocrine Cell System and Its Tumors: The WHO Classification. Annals of the New York Academy of Sciences 2004;1014:13–27.

Kumar V, K. Abbas A, Aster JC. Robbins BASIC PATHOLOGY. 10th ed., 2020, p. 1179–226.

Kuntz CA, Dernell WS, Powers BE, et al. Prognostic factors for surgical treatment of soft-tissue sarcomas in dogs: 75 cases (1986-1996). J Am Vet Med Assoc 1997;211:1147–51.

Li LT, Jiang G, Chen Q, et al. Ki-67 is a promising molecular target in the diagnosis of cancer (Review). Molecular Medicine Reports 2015;11:1566–72.

Manning AL, Dyson NJ. RB: mitotic implications of a tumour suppressor. Nat Rev Cancer 2012;12:220–6.

McSporran KD. Histologic Grade Predicts Recurrence for Marginally Excised Canine Subcutaneous Soft Tissue Sarcomas. Vet Pathol 2009;46:928–33.

Meuten DJ, Moore FM, George JW. Mitotic Count and the Field of View Area: Time to Standardize. Vet Pathol 2016;53:7–9.

Meuten D, Munday JS, Hauck M. Time to Standardize? Time to Validate? Vet Pathol 2018;55:195–9.

Meuten DJ, Moore FM, Donovan TA, et al. International Guidelines for Veterinary Tumor Pathology: A Call to Action. Vet Pathol 2021;58:766–94.

Modlin IM, Moss SF, Chung DC, et al. Priorities for Improving the Management of Gastroenteropancreatic Neuroendocrine Tumors. JNCI: Journal of the National Cancer Institute 2008;100:1282–9.

Patnaik AK, Ehler WJ, MacEwen EG. Canine Cutaneous Mast Cell Tumor: Morphologic Grading and Survival Time in 83 Dogs. Vet Pathol 1984;21:469–74.

Peña L, Andrés PJD, Clemente M, et al. Prognostic Value of Histological Grading in Noninflammatory Canine Mammary Carcinomas in a Prospective Study With Two-Year

Follow-Up: Relationship With Clinical and Histological Characteristics. Vet Pathol 2013;50:94–105.

Shirendeb U, Hishikawa Y, Moriyama S, et al. Human Papillomavirus Infection and Its Possible Correlation with p63 Expression in Cervical Cancer in Japan, Mongolia, and Myanmar. Acta Histochem Cytochem 2009;42:181–90.

Sinicrope FA, Hart J, Hsu HA, et al. Apoptotic and mitotic indices predict survival rates in lymph node-negative colon carcinomas. Clin Cancer Res 1999;5:1793–804.

Sledge DG, Webster J, Kiupel M. Canine cutaneous mast cell tumors: A combined clinical and pathologic approach to diagnosis, prognosis, and treatment selection. The Veterinary Journal 2016;215:43–54.

Sorbye SW, Kilvaer TK, Valkov A, et al. Prognostic Impact of Jab1, p16, p21, p62, Ki-67 and Skp2 in Soft Tissue Sarcomas. PLoS ONE 2012;7:e47068.

Sorbye SW, Kilvaer T, Valkov A, et al. Prognostic Impact of Lymphocytes in Soft Tissue Sarcomas. PLoS ONE 2011;6:e14611.

Spangler WL, Kass PH. The Histologic and Epidemiologic Bases for Prognostic Considerations in Canine Melanocytic Neoplasia. Vet Pathol 2006;43:136–49.

Tan P, Ellis I, Allison K, et al. WHO Classification of Tumours: : Breast Tumours. vol. 2. 5th ed. International Agency for Research on Cancer (IARC).; 2020.

Van Diest PJ. Prognostic value of proliferation in invasive breast cancer: a review. Journal of Clinical Pathology 2004;57:675–81.

Ventura E, Giordano A. Cell Cycle. Reference Module in Life Sciences, Elsevier; 2019.

Vermeulen K, Van Bockstaele DR, Berneman ZN. The cell cycle: a review of regulation, deregulation and therapeutic targets in cancer. Cell Proliferation 2003;36:131–49.

Vidal A, Koff A. Cell-cycle inhibitors: three families united by a common cause. Gene 2000;247:1–15.

Zhang H, Liu Q. Prognostic Indicators for Gastrointestinal Stromal Tumors: A Review. Translational Oncology 2020;13:100812.

## *Experimental Part*

To further explore the diagnostic and prognostic relevance of proliferative markers in veterinary oncology, the following section presents two studies focused on Ki-67 expression and mitotic count in canine tumors.

These studies not only highlight the prognostic significance of these parameters but also address key methodological considerations, such as assessment techniques and spatial distribution of proliferative activity, thus contributing to a more standardized, reproducible and clinically meaningful application in diagnostic pathology.

Specifically, the first study evaluates the prognostic value of Ki-67 expression and mitotic count in canine splenic hemangiosarcoma, proposing a diagnostic cut-off value with clinical relevance. The second study addresses methodological challenges by analyzing the spatial distribution of proliferative hotspots across various canine tumor types, offering guidance for optimized and standardized mitotic count assessment.

Collectively, these studies seek to advance our understanding of tumor proliferation and aim to enhance the accuracy and reproducibility of proliferation-based prognostic evaluation in veterinary oncology.

**Prognostic impact of Ki-67 in canine splenic hemangiosarcoma: A preliminary study**

Brigandì E, Valenti P, Bacci B, Brunetti B, Avallone G.

Vet Pathol. 2024 Jul;61(4):534-540. doi: 10.1177/03009858231225507.

Epub 2024 Jan 12. PMID: 38214328.

## Abstract

Canine splenic hemangiosarcoma has a high metastatic rate and short survival time. Currently, the main prognostic parameters are tumor stage and therapy, while data on histologic parameters, such as grade and Ki-67 expression, are scarce. The aims of this study were to compare two methods of assessment of Ki-67, verify their prognostic impact, and define a threshold value based on survival. Thirty-one cases of histologically diagnosed canine splenic hemangiosarcoma, which were treated with splenectomy and had full staging and follow-up information, were collected. Three were stage I, 17 stage II, and 11 stage III. The mean mitotic count (MC) was 23.9 (standard deviation [SD]: 22.1) and the median was 15 (range, 1-93). Immunohistochemistry for Ki-67 was performed, the Ki-67 labeling index (Ki-67LI) was assessed as a percentage of positive neoplastic nuclei per ≥ 500 cell, and the Ki-67 count (KI-67C) was defined as the average number of positive nuclei using a 1 $cm^2$ optical grid performed in 5, 40X fields. The mean Ki-67LI and Ki-67C were 56.4% (SD: 38.7) and 27.2 (SD: 12.9) and medians were 51% (range, 8.2-55.2) and 26 (range, 5.5-148), respectively. Using a cut-off of 56% and 9, respectively, Kaplan-Meier survival curves showed an association of overall survival with Ki-67LI and MC. In addition to clinical stage, Ki-67LI maintained its prognostic value on multivariate analysis, supporting the role of Ki-67LI as an independent prognostic parameter. Based on these results, we propose a diagnostically applicable cut-off value of 56% for Ki-67LI as a prognostic parameter for canine splenic hemangiosarcoma.

## Introduction

Hemangiosarcoma (HSA) is a malignant neoplasm that has vascular endothelial differentiation. It occurs in several domestic animal species, with the dog being the most frequently affected (Schiffman and Breen, 2015). HSA can develop in any tissue or organ containing vascular structures (Kim et al., 2015), and in the dog it arises most commonly in the spleen, heart, liver, and skin (Roccabianca et al., 2020; Schiffman and Breen, 2015).

Splenic HSA arises in 24 out of 100,000 dogs and is estimated to represent 7% of all canine malignancies (Dobson, 2013). More than half of the affected dogs die within the first year of diagnosis, and tumor-related mortality is extremely high (Antonescu, 2014). Several breeds, including Golden retriever, Labrador retriever, Boxer, German shepherd, and other large-breed dogs, have an increased incidence of HSAs (Cohen et al., 2009; Dobson, 2013; Tamburini et al., 2009). Canine splenic HSA is a highly malignant neoplasm with a high metastatic rate and short survival time (Boston et al., 2011; Prymak et al., 1988), representing one of the most aggressive cancers in dogs (Batschinski et al., 2018; Sorenmo et al., 2004; Wendelburg et al., 2015).

Clinically, splenic HSA can be categorized by a 3-stage classification scheme. Stage I refers to tumors confined to the spleen and less than 5 cm in diameter with no regional lymph node involvement and no evidence of distant metastasis, stage II refers to ruptured splenic tumors or tumors greater than 5 cm in diameter with or without regional lymph node involvement, and stage III refers to tumors with distant metastases (Mullin et al., 2020).

Currently, tumor stage and therapy are the only reliable prognostic parameters for splenic HSA in dogs. Dogs with stage II and III HSA have a shorter median survival time (MST) compared with those with stage I (Kim et al., 2015; Matsuyama et al., 2017; Pintar et al., 2003; Sorenmo et al., 2004). Batschinski et al observed a significant difference in the MST based on therapy, with values of 66 days for surgery alone and 274 days for surgery followed

by chemotherapy. Histological parameters of canine splenic HSA with a clear prognostic impact are lacking. Mitotic count (MC) and overall survival have been associated with canine splenic HSA treated with surgery and chemotherapy (Moore et al., 2017), and a histologic grading system for canine HSA originating from any site was first proposed in 1996 (Ogilvie et al., 1996), but this grading system provided inconsistent results and has never been widely applied (Moore et al., 2017; Ogilvie et al., 1996).

Ki-67 is a nuclear protein widely used for the evaluation of cell proliferation, expressed only in proliferating cells and in all active phases of the cell cycle, including early division. Increased Ki-67 is generally associated with high-grade tumors and a poorer prognosis (Rozolen et al., 2021; Sierra Matiz et al., 2018; Smedley et al., 2022). Despite its importance in veterinary oncology, only one study assessed the Ki-67 labeling index (Ki-67LI) in 47 canine splenic HSA and found no association with the metastatic status (Rozolen et al., 2021). In contrast, an association was identified between Ki-67LI and tumor stage, with tumor stages II and III showing a higher Ki-67LI when compared with stage I. A longer survival time was associated with a lower Ki-67LI (Rozolen et al., 2021). Nevertheless, a prognostically significant cut-off value for Ki-67LI has not been identified (Rozolen et al., 2021).

The **aims** of this study were as follows:

- To compare the assessment of Ki-67 immunohistochemical reactivity using 2 different methods: Ki-67 count (Ki-67C) using an optical grid and Ki-67LI assessed in ≥ 500 cells;
- To verify the prognostic impact of Ki-67 expression in canine splenic HSA;
- To define a prognostically relevant Ki-67 cut-off value for splenic HSA.

Two different methods for the assessment of Ki-67 were chosen to compare the results with a previously investigated HSA case series (Rozolen et al., 2021), as well as with data available for other canine tumors (Sierra Matiz et al., 2018; Smedley et al., 2022).

## Materials & Methods

### *Case Selection*

Canine splenic HSA cases were retrospectively collected from the cases of a veterinary oncological referral practice, over a period of 7 years (2015-2022) based on the following inclusion criteria: (1) histologic diagnosis of splenic hemangiosarcoma, (2) treatment with splenectomy, (3) staged at the time of presentation or referral, (4) available formalin-fixed paraffin-embedded tissue, and (5) available tumor-related survival time (from the day of surgery until tumor-related death).

### *Staging, Treatment, and Follow-up*

Staging tests included hematology (complete blood count), biochemistry, coagulation profile (prothrombin time, activated partial thromboplastin clotting time, and fibrinogen), urinalysis, and diagnostic imaging.

The diagnostic tests and imaging modality performed at the time of staging were at the discretion of the clinician. Imaging techniques included abdominal ultrasonography combined with 3-view thoracic radiographs and echocardiography or total body contrast-enhanced computed tomography. Cases subsequently underwent adjuvant treatment with anthracyclines or metronomic chemotherapy-based protocols. Dogs were usually restaged at the time of the fourth or fifth anthracyclines treatment or at the end of the protocol and then every 2 to 3 months if no signs of disease progression were identified earlier. Dogs receiving metronomic chemotherapy were usually restaged every 2 to 3 months. Procedures performed at the time of follow-up visits included hematology, biochemistry, and urinalysis

with 3-view thoracic radiographs and abdominal ultrasound or total body computed tomography depending on the managing clinician and owners' preference. For each dog, data collected included breed, age, sex, date of the diagnosis, date of death, disease-free time, and overall survival. Follow-up in the majority of the cases was based on recheck at the hospital. Follow-up information not available in the medical record was obtained through telephone calls to the referring veterinarians and/or the owners.

*Histologic Evaluation*

All hematoxylin and eosin-stained slides available were reviewed to select blocks containing neoplastic tissue with the highest cellularity and lowest amount of necrosis, hemorrhage, inflammation, and extramedullary hematopoiesis.

MC was assessed simultaneously by 2 experienced board-certified pathologists at a multiheaded microscope, selecting the areas with the highest cellularity and proliferative activity and by counting 10 consecutive high-power fields, equating to the standard area of 2.37 $mm^2$ (Meuten et al., 2016).

*Immunohistochemistry*

Serial sections of 3 to 4 μm were obtained from selected paraffin blocks, air dried, dewaxed, and rehydrated. Endogenous peroxidase was blocked by immersion in 3% $H_2O_2$ in methanol for 30 minutes. Heat-induced antigen retrieval was used (pH 6.0 citrate buffer, in a microwave oven at 750 W for 4 cycles of 5 minutes each).

After cooling, sections were preincubated with blocking solution (10% normal goat serum with phosphate-buffered saline) for 30 minutes. Anti-Ki-67 primary antibody (mouse monoclonal, clone MIB-1, dilution 1:400, Dako, Glostrup, Denmark) was applied and incubated at 4°C overnight.

Sections were then incubated for 30 minutes at room temperature with anti-mouse biotin-conjugated secondary antibody (dilution 1:200, Dako, Glostrup, Denmark). The reaction was amplified by the avidin-biotin method (ABC kit elite; Vector, Burlingame, CA) and visualized by incubating with 3,30-diaminobenzidine for 2 minutes. Harris' hematoxylin was used as counterstaining. Finally, the sections were dehydrated and cover slipped. Sections of canine small intestine were used as positive control. Negative controls included slides incubated with a nonspecific antibody or the omission of the primary antibody.

*Immunohistochemistry Evaluation*

Measurements of Ki-67-positive cells (Figure 2.3) were performed in areas with the highest proliferation (selected by scanning the entire section at low magnification) using 2 distinct methods, by 2 distinct operators (one for each method):

- Ki-67LI was defined as the percentage of Ki-67-positive cells out of at least 500 neoplastic cells for each case, as previously reported (Smedley et al., 2022). Cells were counted using the manual counting tool of ImageJ 1.48 analysis software on digital pictures taken at 40X. For each case, 5 nonoverlapping, consecutive images were taken in the areas of highest proliferation. The total number of neoplastic cells in the images that were evaluated when the number of cells counted reached 500 was included to avoid subjectivity.
- Ki-67C was defined as the average number of positive cells in a 1 $cm^2$ optical grid performed in 5 high-power fields (40X), as previously reported for other canine tumors (Sierra Matiz et al., 2018; Smedley et al., 2022). The total area assessed (equating the 5 grids) was 0.3125 $mm^2$.

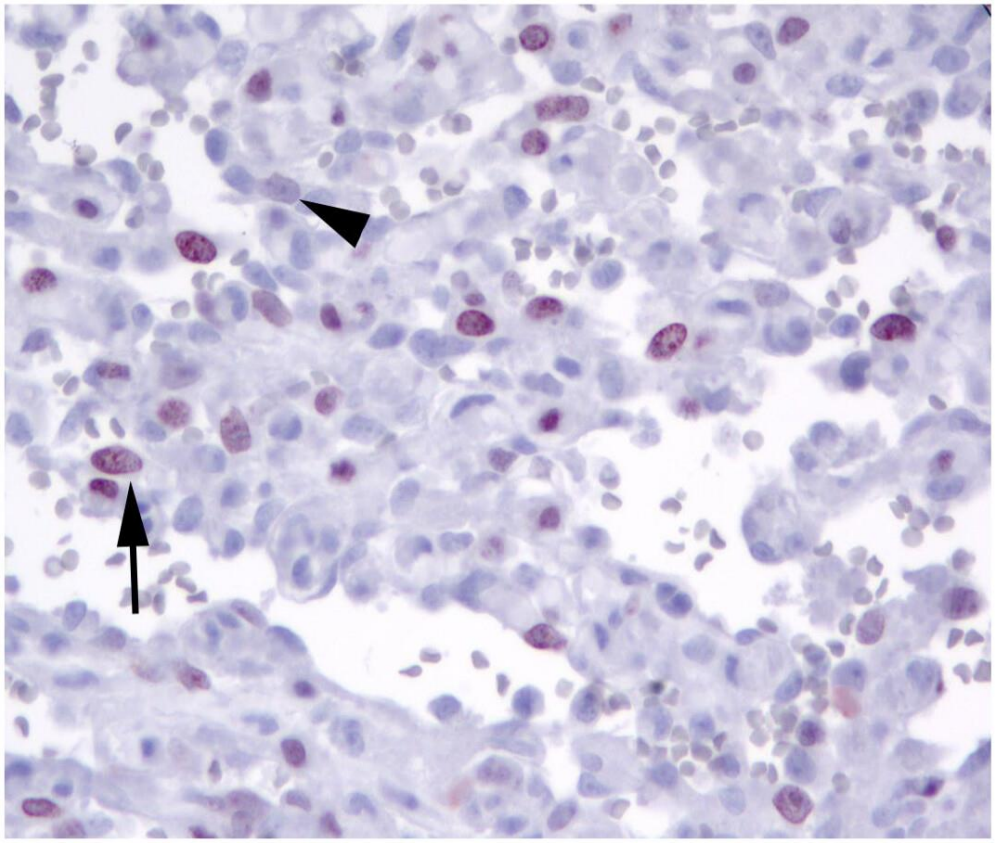

**Figure 2.3:** Splenic hemangiosarcoma, Ki-67 immunohistochemistry. Neoplastic cells have variable expression of Ki-67. Only cells with clearly visible nuclear labeling were considered positive (arrow), while cells with questionable labeling (arrowhead) were considered negative.

*Statistical Analysis*

For continuous variables, mean, median, standard deviation (SD), and range were identified. To quantify the linear correlation among continuous variables, Pearson's correlation coefficient was used. Optimal cut-off values for MC, Ki-67LI, and Ki-67C were determined by receiver-operating characteristic curves. For each variable, the sensitivity-specificity threshold was the value closer to the top-left corner.

Tumor-related survival was defined as the time from the date of diagnosis to death due to HSA. Cases were censored if the dog was alive at the end of the study, had been lost to

follow-up, or died due to causes unrelated to HSA. Survival probabilities and MSTs were estimated with the Kaplan-Meier product-limit estimated and were compared among groups by log-rank tests. The Cox proportional hazard model was used for the univariate analysis of the continuous variables (Ki-67LI, Ki-67C, and MC) and for the multivariate analysis; variables were included in the multivariate analysis only if they were significant at univariate analysis. Since the study population included only 3 stage I cases, stage I and II cases were grouped for all analyses including the clinical stage. For each test, differences were considered significant when $P \leq .05$. Statistical analysis was performed using R (version 4.1.2 for Windows, Vienna, Austria).

**Results**

A total of 31 splenic HSAs in 31 dogs were included in the study. Ten dogs were crossbreeds, 6 were retrievers, 5 were boxer dogs, 4 were German shepherd dogs, and 1 dog represented each of the following breeds: Akita Inu, beagle, bulldog, Cocker Spaniel, Siberian husky, and pinscher. Sixteen dogs were female and 15 were male. Ages were available in 25 out of 31 cases and ranged between 6 and 14 years (mean = 10.5, median = 10, SD = 2.64).

At the time of diagnosis, 3 of 31 dogs were stage I (10%), 17 of 31 were stage II (55%), and 11 of 31 were stage III (36%). Twelve out of 31 tumors (39%) were metastatic at the time of diagnosis. Of these, 8 metastasized to the liver (67%), 1 to the regional lymph node (8%), 1 to the retroperitoneum (8%), and 2 dogs had multiorgan metastases to liver, kidneys, lungs, muscle, and/or subcutaneous tissue (17%). Metastases were confirmed histologically.

All cases underwent splenectomy, and 21 of 31 received adjuvant chemotherapy (68%). Twenty-one dogs out of 31 died due to tumor-related causes (68%). Seven cases were censored: 3 died for causes unrelated to hemangiosarcoma (10%), 3 were still alive at the end of the study, and 1 was lost to follow-up. MC, Ki-67LI, and Ki-67C descriptive statistics are reported in Table 2.1.

**Table 2.1:** Descriptive statistics for Ki-67LI (labeling index), Ki-67C (count with optical grid), and MC (mitotic count).

| | **Ki-67LI (%)** | **Ki-67C** | **MC** |
|---|---|---|---|
| **Mean** | 56.41 | 27.17 | 23.90 |
| **Median** | 51.4 | 26 | 15 |
| **Standard deviation** | 38.70 | 12.89 | 22.15 |
| **Range** | 8.2–55.2 | 5.5–148 | 1–93 |

A statistically significant correlation was observed between Ki-67C and Ki-67LI ($p$ = .00344, Pearson's correlation coefficient = 0.509, 95% confidence interval (CI) = 0.189–0.732), but not between Ki-67LI and MC ($p$ = .121, Pearson's correlation coefficient = 0.284, 95% CI = 0.0778–0.58) or Ki-67C and MC ($p$ = .066, Pearson's correlation coefficient = 0.334, 95% CI = 0.0228–0.616).

To determine optimal cut-off value for Ki-67C, Ki-67LI, and MC, analyses of the corresponding receiver-operating characteristics curves were performed comparing the variables with survival at 2, 4, and 6 months; results are reported in Table 2.2. The highest area under the curve value was obtained at 6-month survival for all the tested variables, and the cut-offs selected based on the best combination of specificity and sensitivity were 9 for MC, 24 for Ki-67C, and 56% for Ki-67LI.

**Table 2.2:** Area under the curve (AUC) assessed by receiver-operating characteristic (ROC) curve analysis.

| **Survival** | **Ki-67LI (%)** | **Ki-67C** | **MC** |
|---|---|---|---|
| **2 months** | | | |
| AUC (95% CI) | 0.526 (0.304–0.748) | 0.561 (0.353–0.77) | 0.539 (0.331–0.748) |
| Cut-off (sp, se) | 56.6 (0.684, 0.583) | 16.7 (0.315, 0.916) | 11 (0.473, 0.833) |
| **4 months** | | | |
| AUC (95% CI) | 0.672 (0.467–0.877) | 0.473 (0.251–0.694) | 0.618 (0.381–0.855) |
| Cut-off (sp, se) | 38.0 (0.571, 0.823) | 34.5 (0.357, 0.823) | 10 (0.571, 0.882) |
| **6 months** | | | |
| AUC (95% CI) | 0.754 (0.533–0.975) | 0.7 (0.441–0.959) | 0.804 (0.574–1) |
| Cut-off (sp, se) | **56.6 (1.0, 0.5)** | **24.4 (0.8, 0.615)** | **9 (0.8, 0.84)** |

Abbreviation: Ki-67C, count with optical grid; Ki-67LI, labeling index; AUC, area under the curve; MC, mitotic count.

For each variable, AUC with 95% confidence interval (CI), and optimal cut-off value with specificity (sp) and sensitivity (se) are reported. Cut-off values with the best combinations of sensitivity and specificity values are in bold.

These cut-off values were used to assess differences in survival times using Kaplan-Meier survival curves. Cases with Ki-67LI above 56% had significantly shorter survival compared with those that had lower Ki-67LI ($p$ = .00721, log-rank test). Cases with MC above 9 had significantly shorter survival compared with those that had lower MC ($p$ = .00281, log-rank test). Kaplan-Meier curves (Figure 2.4) showed no statistically significant relation between Ki-67C and survival ($p$ = .293, log-rank test). Results are reported in Table 2.3.

**Table 2.3:** Survival analysis of MC (mitotic count), Ki-67C (count with optical grid), Ki-67LI (labeling index), clinical stage, and treatment (log-rank test).

| Variable | No. of Cases | MST (95% CI) (days) | P Value |
|---|---|---|---|
| **MC** | | | **.003** |
| < 9 | 8 | 220.0 (50–NA) | |
| ≥ 9 | 23 | 67.5 (42–133) | |
| **Ki-67C** | | | **.293** |
| < 24 | 13 | 173 (45–220) | |
| ≥ 24 | 18 | 115 (42–162) | |
| **Ki-67LI** | | | **.007** |
| < 56% | 18 | 173 (50–220) | |
| ≥ 56% | 13 | 60 (42–117) | |
| **Clinical Stage** | | | **.003** |
| I | 3 | 173.0 (173–NA) | |
| II | 17 | 137.5 (71–188) | |
| III | 11 | 45.0 (17–64) | |
| **Clinical Stage[a]** | | | **.002** |
| H | 11 | 45 (17–64) | |
| L | 20 | 162 (72–188) | |
| **Treatment** | | | **.106** |
| Surgery | 10 | 45 (14–142) | |
| Surgery + chemotherapy | 21 | 162 (64–188) | |

Abbreviations: MST, median survival time; CI, confidence interval; NA, not applicable.

(a) L = stage I + stage II; H = stage III.

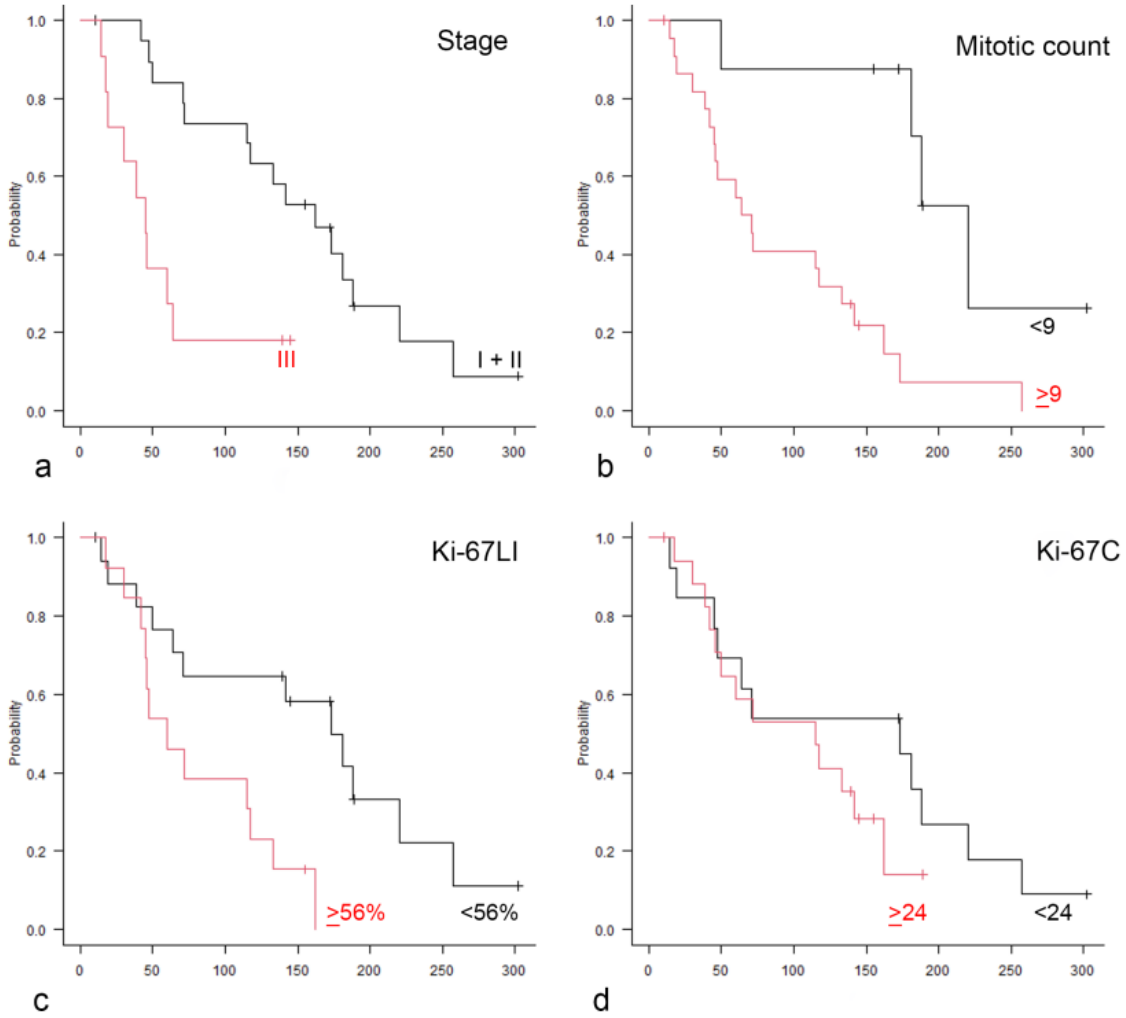


**Figure 2.4:** Kaplan-Meier curves comparing the survival probability of dogs with splenic hemangiosarcoma. X-axis represents overall survival expressed in days. (a) Red line, high-stage cases (stage III); black line, low-stage cases (stage I and II). (b) Red line, cases with mitotic counts higher than or equal to 9; black line, cases with mitotic counts lower than 9. (c) Red line, cases with Ki-67 labeling index (Ki-67LI) higher than or equal to 56%; black line, Ki-67LI lower than 56%. (d) Red line, cases with Ki-67 grid count (Ki-67C) higher than or equal to 24; black line, Ki-67C lower than 24.

In addition to receiver-operating characteristic curve analyses, Ki-67C, Ki-67LI, and MC were analyzed as continuous variables in univariate Cox proportional hazards models, which did not show statistically significant relations with the survival times (Table 2.4).

**Table 2.4:** Univariate Cox proportional hazard analysis for Ki-67LI (labeling index), Ki-67C (count with optical grid), and MC (mitotic count).

| Variable | Hazard Ratio | 95% CI | P Value |
|---|---|---|---|
| KI-67LI (%) | 1.009 | 0.9994–1.019 | .067 |
| KI-67C | 1.009 | 0.9761–1.043 | .600 |
| MC | 1.006 | 0.9896–1.023 | .466 |

Abbreviation: CI, confidence interval.

The clinical variables, stage and type of treatment, were included in the survival analysis. Stage I and stage II cases were grouped together (low stage) and compared with stage III (high stage) because of the low number of stage I HSAs. Dogs with high-stage tumors had a significantly shorter MST than dogs with low-stage tumors (MST = 45 days, 95% CI = 17–64 and 162 days, 95% CI = 72–188, respectively). Cases undergoing surgery and chemotherapy had a longer MST (145 days, 95% CI = 64–181) compared with dogs that were treated with surgery alone (MST = 45 days, 95% CI = 14–142), excluding dogs that were still alive or died for causes unrelated to the disease.

To analyze the impact of Ki-67LI on survival, a multivariate analysis was performed using the Cox proportional hazard regression model that included variables that were significant at univariate analysis: Ki-67LI, MC, clinical stage (low vs high), and treatment type (surgery vs surgery and chemotherapy). Of these, Ki-67LI and clinical stage remained significant on multivariate analysis. Specifically, Ki-67LI at its optimal cut-off value represented an

independent prognostic variable (hazard ratio = 4.1380, 95% CI = 1.49–11.48, $p$ = .006351). In addition, high-stage (stage III) cases had a larger instantaneous death risk than low-stage (stage I/II) cases, and clinical stage also represented an independent prognostic factor (hazard ratio = 5.38, 95% CI = 1.75–16.53, $p$ = .003). By contrast, treatment type and MC were not statistically significant in the multivariate analysis. Results are summarized in Table 2.5.

**Table 2.5:** Multivariate Cox proportional hazard regression model for variables Ki-67LI (labeling index), MC (mitotic count), stage, and treatment.

| Variable | Hazard Ratio | 95% CI | P Value |
|---|---|---|---|
| Ki-67LI ≥56% | 4.1900 | 1.5100–11.630 | .006 |
| MC ≥9 | 0.9968 | 0.9755–1.018 | .767 |
| Stage (high/low) | 5.1100 | 1.7660–14.790 | .003 |
| Treatment | 0.5769 | 0.2237–1.488 | .268 |

Abbreviation: CI, confidence interval.

## Discussion

Canine HSA is one of the most aggressive cancers in dogs (Batschinski et al., 2018; Sorenmo et al., 2004; Wendelburg et al., 2015), and tumor stage and therapy are the only reliable prognostic parameters reported thus far (Kim et al., 2015; Matsuyama et al., 2017; Pintar et al., 2003; Sorenmo et al., 2004), while histological features with a clear prognostic impact are lacking.

A histologic grading system for canine HSA (originating from any site) was first proposed in 1996 (Ogilvie et al., 1996). This grading system takes into account the differentiation of tumor cells, cellular pleomorphism, percentage of necrosis, and MC (number/10 high-

powered fields) (Moore et al., 2017). The prognostic significance of this grading scheme was suggested by univariate but not by multivariate analysis, and therefore, it has not been widely applied (Avallone et al., 2021). To the best of our knowledge, only one study in the literature evaluated Ki-67 expression in canine splenic HSA, showing a correlation of Ki-67LI with overall survival; however, prognostically relevant threshold values for Ki-67 were not provided (Rozolen et al., 2021). Therefore, the main aims of our study were to evaluate the prognostic impact of Ki-67 expression assessed by 2 different methods and to define a Ki-67 cut-off that could be of prognostic relevance.

Metastases occurred in approximately one third of cases, with the liver being the most common site of metastases, as reported in the literature (Clendaniel et al., 2014; Göritz et al., 2013). In our study, the stage at diagnosis had a statistically significant correlation with tumor-related survival, representing one of the most important prognostic factors, in agreement with the literature (Batschinski et al., 2018; Masyr et al., 2021; Moore et al., 2017; Sorenmo et al., 2004; Wendelburg et al., 2015).

All cases in this study underwent splenectomy and 21 received adjuvant chemotherapy, including different chemotherapy protocols. Taking all cases into consideration, therapy was not associated with tumor-related survival. Nevertheless, as 2 out of 3 stage I cases were still alive at the end of the study, one of which was a small tumor treated with surgery alone, we hypothesize these cases may have produced a confounding effect. Indeed, by removing them from the analysis, the 2 treatment modalities were associated with survival. The cases with stage II or III HSA that underwent surgery followed by chemotherapy had a longer survival time than those treated with surgery alone, as demonstrated in previous studies (Faulhaber et al., 2021; Treggiari et al., 2020).

For the first time in this study, 2 different methods of assessment of Ki-67-positive cells were performed and compared. As expected, there was a statistically significant correlation

between Ki-67C and Ki-67LI, indicating a linear relationship between these 2 continuous variables, but a correlation between MC and Ki-67LI or Ki-67C was not found.

The prognostic value of MC, Ki-67LI, and Ki-67C was assessed with the Kaplan-Meier survival curve and log-rank test using the cut-off derived from the receiver-operating characteristic curve analysis. This approach allowed demonstration of an association of tumor-related survival with Ki-67LI and MC using the cut-off of 56% and 9, respectively. Ki-67LI was also confirmed as an independent prognostic parameter on multivariate analysis, together with treatment and clinical stage. These results further support the previously reported prognostic impact of Ki-67 expression in canine splenic HAS (Rozolen et al., 2021) and provide a cut-off value of potential use in everyday diagnostic activity.

In summary, in this study, the prognostic role of Ki-67LI was demonstrated for canine splenic HSAs, providing a counting technique and a statistically valid cut-off value of practical use in a diagnostic setting. Further studies on larger caseloads may be useful to confirm and/or refine these results and to investigate the prognostic value of Ki-67.

**References**

Antonescu C. Malignant vascular tumors—an update. Modern Pathology 2014;27:S30–8.

Avallone G, Rasotto R, Chambers JK, et al. Review of Histological Grading Systems in Veterinary Medicine. Vet Pathol 2021;58:809–28.

Batschinski K, Nobre A, Vargas-Mendez E, et al. Canine visceral hemangiosarcoma treated with surgery alone or surgery and doxorubicin: 37 cases (2005-2014). Can Vet J 2018;59:967–72.

Boston SE, Higginson G, Monteith G. Concurrent Splenic and Right Atrial Mass at Presentation in Dogs with HSA: A Retrospective Study. Journal of the American Animal Hospital Association 2011;47:336–41.

Clendaniel DC, Sivacolundhu RK, Sorenmo KU, et al. Association Between Macroscopic Appearance of Liver Lesions and Liver Histology in Dogs With Splenic Hemangiosarcoma: 79 Cases (2004–2009). Journal of the American Animal Hospital Association 2014;50:e6–10.

Cohen SM, Storer RD, Criswell KA, et al. Hemangiosarcoma in Rodents: Mode-of-Action Evaluation and Human Relevance. Toxicological Sciences 2009;111:4–18.

Dobson JM. Breed-Predispositions to Cancer in Pedigree Dogs. ISRN Veterinary Science 2013;2013:1–23.

Faulhaber EA, Janik E, Thamm DH. Adjuvant carboplatin for treatment of splenic hemangiosarcoma in dogs: Retrospective evaluation of 18 cases (2011-2016) and comparison with doxorubicin-based chemotherapy. Veterinary Internal Medicne 2021;35:1929–34.

Göritz M, Müller K, Krastel D, et al. Canine Splenic Haemangiosarcoma: Influence of Metastases, Chemotherapy and Growth Pattern on Post-splenectomy Survival and Expression of Angiogenic Factors. Journal of Comparative Pathology 2013;149:30–9.

Kim J-H, Graef A, Dickerson E, et al. Pathobiology of Hemangiosarcoma in Dogs: Research Advances and Future Perspectives. Veterinary Sciences 2015;2:388–405.

Masyr AR, Rendahl AK, Winter AL, et al. Retrospective evaluation of thrombocytopenia and tumor stage as prognostic indicators in dogs with splenic hemangiosarcoma. Javma 2021;258:630–7.

Matsuyama A, Poirier VJ, Mantovani F, et al. Adjuvant Doxorubicin with or without Metronomic Cyclophosphamide for Canine Splenic Hemangiosarcoma. Journal of the American Animal Hospital Association 2017;53:304–12.

Meuten DJ, Moore FM, George JW. Mitotic Count and the Field of View Area: Time to Standardize. Vet Pathol 2016;53:7–9.

Moore AS, Rassnick KM, Frimberger AE. Evaluation of clinical and histologic factors associated with survival time in dogs with stage II splenic hemangiosarcoma treated by splenectomy and adjuvant chemotherapy: 30 cases (2011–2014). Javma 2017;251:559–65.

Mullin C, Clifford CA, Liptak JM. Miscellaneous tumors. Withrow and MacEwen's Small Animal Clinical Oncology, 2020, p. 773–8.

Ogilvie GK, Powers BE, Mallinckrodt CH, et al. Surgery and Doxorubicin in Dogs With Hemangiosarcoma. Veterinary Internal Medicne 1996;10:379–84.

Pintar J, Breitschwerdt EB, Hardie EM, et al. Acute Nontraumatic Hemoabdomen in the Dog: A Retrospective Analysis of 39 Cases (1987–2001). Journal of the American Animal Hospital Association 2003;39:518–22.

Prymak C, McKee LJ, Goldschmidt MH, et al. Epidemiologic, clinical, pathologic, and prognostic characteristics of splenic hemangiosarcoma and splenic hematoma in dogs: 217 cases (1985). J Am Vet Med Assoc 1988;193:706–12.

Roccabianca P, Schulman FY, Avallone G, et al. Surgical Pathology of Tumors of Domestic Animals. vol. 3. 3rd ed. Kiupel M.; 2020.

Rozolen JM, Teodoro TGW, Sobral RA, et al. Investigation of Prognostic Value of Claudin-5, PSMA, and Ki-67 Expression in Canine Splenic Hemangiosarcoma. Animals 2021;11:2406.

Schiffman JD, Breen M. Comparative oncology: what dogs and other species can teach us about humans with cancer. Phil Trans R Soc B 2015;370:20140231.

Sierra Matiz OR, Santilli J, Anai LA, et al. Prognostic significance of Ki-67 and its correlation with mitotic index in dogs with diffuse large B-cell lymphoma treated with 19-week CHOP-based protocol. J VET Diagn Invest 2018;30:263–7.

Smedley RC, Sebastian K, Kiupel M. Diagnosis and Prognosis of Canine Melanocytic Neoplasms. Veterinary Sciences 2022;9:175.

Sorenmo KU, Baez JL, Clifford CA, et al. Efficacy and Toxicity of a Dose-Intensified Doxorubicin Protocol in Canine Hemangiosarcoma. J Vet Int Med 2004;18:209.

Tamburini BA, Trapp S, Phang TL, et al. Gene Expression Profiles of Sporadic Canine Hemangiosarcoma Are Uniquely Associated with Breed. PLoS ONE 2009;4:e5549.

Treggiari E, Borrego JF, Gramer I, et al. Retrospective comparison of first-line adjuvant anthracycline vs metronomic-based chemotherapy protocols in the treatment of stage I and II canine splenic haemangiosarcoma. Vet Comparative Oncology 2020;18:43–51.

Wendelburg KM, Price LL, Burgess KE, et al. Survival time of dogs with splenic hemangiosarcoma treated by splenectomy with or without adjuvant chemotherapy: 208 cases (2001–2012). Javma 2015;247:393–403.

**Analysis of Ki-67 Density Maps Reveals Variation of Spatial Proliferation Patterns in Different Canine Neoplasms**

Brigandì E, Bacci B, Brunetti B, Rigillo A, Roccabianca P, Bellini G, Chiappelli C, Avallone G

Vet Comp Oncol. 2025 Sep 2. doi: 10.1111/vco.70019.

Epub ahead of print. PMID: 40897397.

## Abstract

Mitotic count (MC) is a well-established prognostic factor in many canine malignancies. While standardisation efforts have improved inter-pathologist agreement regarding the morphology of mitotic figures and the size of the counting area, the selection of the tumour region for MC assessment remains to be standardised. This study aimed to evaluate the spatial distribution of the most proliferative areas in selected canine tumour types, using Ki-67 immunohistochemistry, to identify optimal candidate regions for MC assessment. Tumour types analysed included melanomas, cutaneous mast cell tumours (cMCT), canine mammary carcinomas (CMC) and soft tissue sarcomas (STS). Using image analysis, Ki-67 density maps were generated from digital slides and classified according to their distribution pattern (focal/multifocal or diffuse) and location within the tumour (central, peripheral or scattered). A total of 202 cases were included: 43 melanomas, 30 cMCTs, 42 CMCs and 87 cSTSs. The vast majority of tumours (92.6%) exhibited a multifocal hotspot distribution. Peripheral hotspot localisation was predominant in 55% of cases, particularly in cMCTs (73.3%) and melanomas (76.7%). In contrast, cSTSs more frequently showed a scattered hotspot pattern (60.9%) ($x^2 = 41.9$; $p < 0.001$). CMCs had a higher proportion of centrally located hotspots (16.7%). These findings suggest that pathologists should focus on peripheral tumour regions when assessing MC in cMCTs and melanomas. Both central and peripheral regions should be considered in CMCs, while a more extensive, comprehensive

evaluation may be required in STSs. The observed association between tumour histotype and proliferation pattern likely reflects inherent biological differences among the tumour types studied.

**Introduction**

Mitotic count (MC) is one of the most commonly used prognostic factors in veterinary tumour pathology. The association between a high number of mitotic figures (MF) and the aggressive behaviour of several neoplasms is widely acknowledged (Avallone et al., 2021; Elston et al., 2009; Horta et al., 2018; Meuten et al., 2016; Romansik et al., 2007; Schott et al., 2018; Vascellari et al., 2013). In veterinary medicine, MC is also included in the histological grading systems of canine mast cell tumours (cMCT) (Kiupel et al., 2011; Patnaik et al., 1984), mammary carcinomas (Mills et al., 2015; Peña et al., 2013), canine melanomas (Spangler and Kass, 2006), and canine soft tissue sarcomas (cSTS) (Kuntz et al., 1997; McSporran, 2009). The importance of standardising histological parameters such as MC has become increasingly apparent (Meuten et al., 2018). A major challenge in this standardisation lies in the limited reproducibility, primarily due to the lack of clearly defined and reproducible assessment methods (Bonert and Tate, 2017; Ellis and Whitehead, 1981; Meuten et al., 2016). As a result, the evaluation of several parameters, including mitotic count (MC), often relies on subjective approaches, which hinders consistent comparisons across studies (Meuten et al., 2021). Considerable efforts are underway to address these limitations, with proposed guidelines and protocols outlining best practices for measuring specific histological parameters across various tumour types (https://vcgp.org/guidelines-and-protocols/) (Meuten et al., 2021). In the context of MC assessment, standardisation should address the following key elements:

1) The histologic morphology of MF: Only figures from prometaphase to telophase should be counted, focusing on chromosomal aggregates lacking a nuclear membrane (Meuten et al., 2021).
2) The size of the counting area: MC should be assessed in a total field area of 2.37 $mm^2$, which varies depending on the field number of the ocular and the magnification of the objective lens (Ellis and Whitehead, 1981; Meuten et al., 2016).
3) The selection of tumour regions for MC assessment: counting should be performed in areas exhibiting the highest proliferative activity (Bertram et al., 2020; Stålhammar et al., 2018; Van Diest et al., 1992; Wei et al., 2019).

In many tumour types, the MC is evaluated in regions of maximal mitotic density within tumours (Al-Janabi et al., 2013; Baak et al., 2009; Meuten et al., 2016; Meyer et al., 2009; Veta et al., 2015). However, identifying these regions is not straightforward, and there are no clear indications regarding the choice of site with higher proliferative activity across different tumour types. Some studies suggest that the tumour periphery is the preferred site for MC assessment, as it often represents the invasive front and may exhibit higher proliferative activity (Bertram et al., 2020; Meuten et al., 2016). Additionally, tissue fixation is typically more effective at the tumour edges (Baak et al., 2009; Bertram et al., 2020; Meuten et al., 2016). A study on human breast carcinoma reported that the tumour periphery contained a higher density of Ki-67-positive hotspots, and the proportion of Ki-67-positive nuclei in these regions correlated with patient prognosis (Gudlaugsson et al., 2012). However, other studies in human breast carcinoma have found that assessing Ki-67 hotspots – regardless of their location within the tumour – yields stronger prognostic value than location-based assessment alone (Stålhammar et al., 2018). In veterinary medicine, Bertram and colleagues demonstrated that in cMCT, the MC varied significantly across different tumour regions. Notably, pathologists were often unable to accurately identify the

area with the highest MC when evaluating whole-slide images (Bertram et al., 2020). Although MC has long been a mainstay of tumour assessment, until recently, there has been no standardisation of any element of this parameter in veterinary pathology. Performing the MC is considered laborious and is characterised by inter-pathologist variation (Bertram et al., 2018; Meyer et al., 2005; Tsuda et al., 2000). Standardising methods should increase reproducibility, decrease subjectivity and improve the predictability of this commonly used prognostic marker. Automated image analysis systems represent promising tools for selecting the area with the highest mitotic activity within large tumour sections more accurately (Bertram et al., 2020). The **aim** of this study is to evaluate the spatial distribution of the most proliferative regions in different canine tumour types, in order to identify the most appropriate areas for MC assessment, with the aid of image analysis software.

## Materials & Methods

*Case Selection*

Tumour types for which the MC is considered a prognostic parameter or is integrated in the grading system were included. Cutaneous cMCT, canine mammary carcinomas (CMC), oral and cutaneous canine melanomas (malignant melanomas) and canine soft tissue sarcomas (cSTS) were selected from the archives of three institutions. Complex and mixed canine mammary carcinomas were excluded to avoid the confounding effect of myoepithelial or mesenchymal cell proliferation. cSTS cases with a specific diagnosis were enrolled, including perivascular wall tumours, myxosarcomas, fibrosarcomas, liposarcomas and leiomyosarcomas. cSTS diagnoses were performed by two board-certified pathologists experienced in the diagnosis of cSTS and were based on histological features according to the most recent classification system (Roccabianca et al., 2020) and, when necessary, with the application of the appropriate immunohistochemical protocols. Cases with uncertain diagnoses were not included. Only cases with recognisable tissue orientation and with at

least half of a transversal section of the neoplasm available for immunohistochemistry were included. The diagnoses were confirmed by re-assessment of the original hematoxylin and eosin-stained sections by two board-certified pathologists.

*Immunohistochemical Labelling*

All cases underwent immunohistochemistry for Ki-67. Section 3 to 4 µm thick were obtained from selected paraffin blocks to assess at least half of the transversal section of the neoplasm. Pigmented melanomas underwent de-pigmentation before immunohistochemical staining by incubation for 27 min in potassium permanganate (0.25 g/100 mL; Merck, Germany), followed by rinsing in distilled water and immersion for 20–30 s – depending on the required level of depigmentation – in oxalic acid (5 g/100 mL; DDK Italia, Italy). Sections were air-dried, dewaxed and rehydrated. Endogenous peroxidase was blocked by immersion in 3% $H_2O_2$ in methanol for 30 min. Heat-induced antigen retrieval was used (pH 6.0 citrate buffer, in a pressure cooker at 110°C for 20 min). After cooling, sections were preincubated with a blocking solution (10% normal goat serum with phosphate-buffered saline) for 30 min. Anti-Ki-67 primary antibody (mouse monoclonal, clone MIB-1, dilution 1:1500, Dako, Glostrup, Denmark) was applied and incubated overnight at 4°C. Sections were then incubated for 30 min at room temperature with anti-mouse biotin-conjugated secondary antibody (dilution 1:200, Dako, Glostrup, Denmark). The reaction was amplified by the avidin-biotin method (ABC kit elite; Vector, Burlingame, CA) and visualised by incubating with 3,30-diaminobenzidine for 2 min. Harris' hematoxylin was used as counterstaining. Finally, the sections were dehydrated and cover-slipped. Sections of the canine small intestine were used as a positive control. Negative controls included slides incubated with a non-specific antibody or the omission of the primary antibody.

*Immunohistochemical Evaluation and Image Analysis*

The immunohistochemical slides were scanned using Grundium Ocus 20 (Tampere, Finland) at 20X magnification (0.25 µm/pixel) to obtain a whole slide image (WSI). The digital images were analysed using the open-source DIA software QuPath v0.5.0.3. Analysis was performed starting with manual selection of the tumour section area (Figure 2.5A) and positive cell detection tool (Analyse → Cell analysis → Positive cell detection) (Figure 2.5B). Neoplastic tissue was selected while non-neoplastic tissue adjacent to or entrapped within the neoplasm, necrotic areas, granulation tissue and clearly recognisable inflammatory aggregates were avoided. Afterward, a density map was created to define areas of higher proliferation and demonstrate their predominant distribution within the section (Figure 2.5C). For each image, the selection parameters were adjusted iteratively to find the optimal combination, resulting in an accurate selection of Ki-67-positive cells (Figure 2.5D,E).

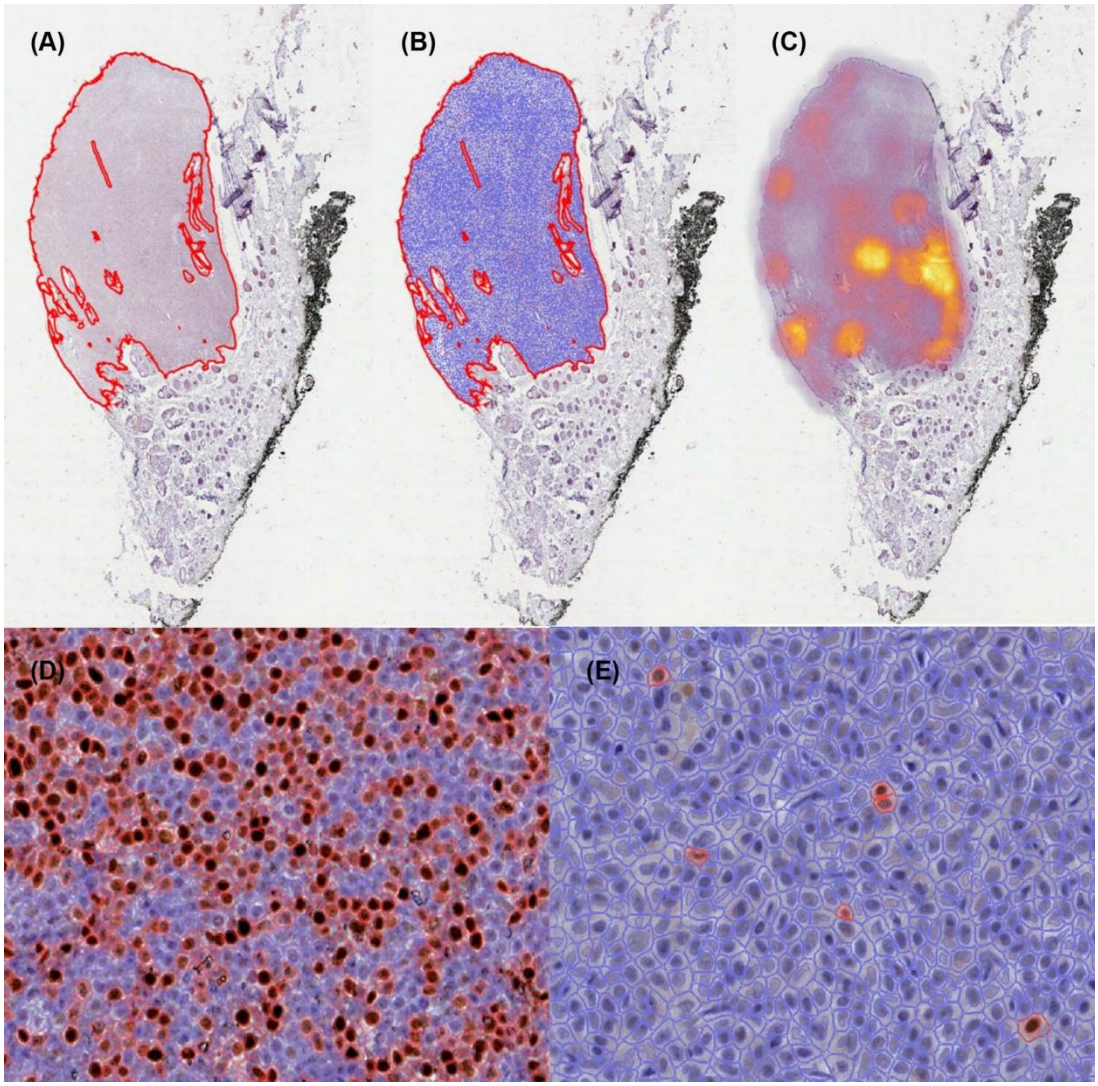


**Figure 2.5:** Examples of image analysis on whole slide image of Ki-67 immunohistochemistry. (A) Selection of the region of interest (ROI) (red line): Non-neoplastic tissue, holes and artefacts are excluded; (B) Positive cell detection performed on the ROI: In blue are negative cells, in red are positive cells; (C) Density maps showing the regions of the tumour with higher positive cell density (yellow shade); (D) Positive cell detection in a canine mast cell tumour with high proliferative activity, and (E) in a canine soft tissue sarcoma with low proliferative activity. In blue are negative cells, in red are positive cells.

Each density map was subsequently subjected to visual analysis by experienced pathologists to categorise it into a specific group, classified based on:

- Hotspots distribution: focal/multifocal (one or multiple hot spots were visible) or diffuse (relatively uniform positive cell density within the tumour).
- Hotspot location: central (at the centre of the neoplasm), peripheral (at the external regions of the neoplasm) or scattered (when both at central and peripheral regions of the neoplasm).

Examples of the most common spatial arrangements of Ki-67 hot spots are depicted in Figure 2.6.

The dataset explores the relationships between two diagnostic variables and the host spots' spatial arrangements. The first diagnostic variable, “Diagnosis 1”, identifies broad tumour categories, including CMC, cSTS, melanoma and cMCT. The second diagnostic variable, “Diagnosis 2,” provides a more detailed classification and was applied to soft tissue sarcomas (including perivascular wall tumours, myxosarcomas, fibrosarcomas, liposarcomas and leiomyosarcomas) and melanomas (oral or cutaneous). The analysis was performed using the chi-square test to assess the association between distribution and location (alone and in combination) with diagnosis 1 and diagnosis 2 (when available). This test was chosen to compare the observed frequencies with the expected ones under the null hypothesis, determining statistical significance. A Kruskal-Wallis one-way analysis of variance was used to assess the association of distribution and location of hot spots with MC and Ki-67 labelling index (expressed as number of positive cells/$mm^2$). Post hoc pairwise analysis was performed with the Dwass-Steel-Critchlow-Fligner test. Results were considered significant for $p$-values < 0.05. Statistical analyses were performed using Jamovi (version 2.4.12.0).

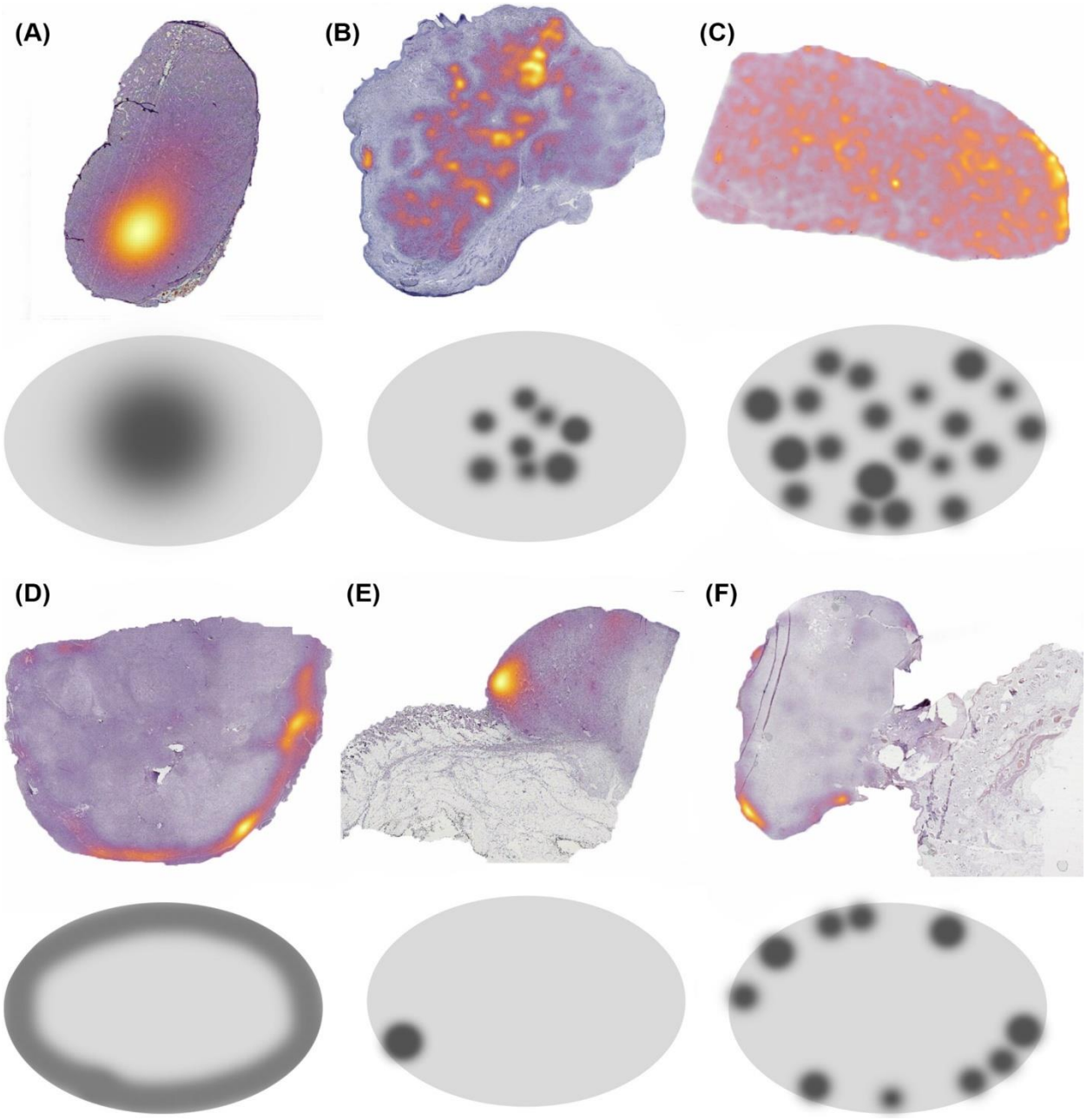


**Figure 2.6:** Examples of the most frequent patterns of density maps and corresponding example pictograms. (A) Central diffuse pattern in a canine mammary carcinoma; (B) Central multifocal pattern in a canine mammary carcinoma; (C) Scattered multifocal pattern in a canine liposarcoma; (D) Peripheral diffuse pattern in a canine perivascular wall tumour; (E) Peripheral focal pattern in a cutaneous mast cell tumour; (F) Peripheral multifocal pattern in a canine cutaneous melanoma.

## Results

A total of 202 cases were collected: 43 melanomas (22 oral and 21 cutaneous), 30 cMCT (21 low grade and 9 high grade), 42 CMC (14 grade 1, 20 grade 2 and 8 grade 3), and 87 STS (49 grade 1, 32 grade 2 and 9 grade 3). STS included 22 perivascular wall tumours, 15 myxosarcomas, 16 leiomyosarcomas, 22 liposarcomas and 12 fibrosarcomas. Hot spot distribution was diffused in 10 cases (5%), focal in 5 (2.5%) and multifocal in 187 (92.6%), and was associated with diagnosis 1 (chi-square = 25.5; $p < 0.001$). Specifically, distribution was diffuse in 2/30 (6.7%) cMCT, 5/42 (11.9%) CMC, 2/43 (4.7%) melanomas and 1/87 (1.1%) cSTS; focal in 4/30 (13.3%) cMCT, 1/42 (2.4%) CMC, 0/43 melanomas and 0/87 cSTS; and multifocal in 24/30 (80%) cMCT, 36/42 (85.7%) CMC, 41/43 (95.3%) melanomas and 86/87 (98.9%) cSTS (Figure 2.7A).

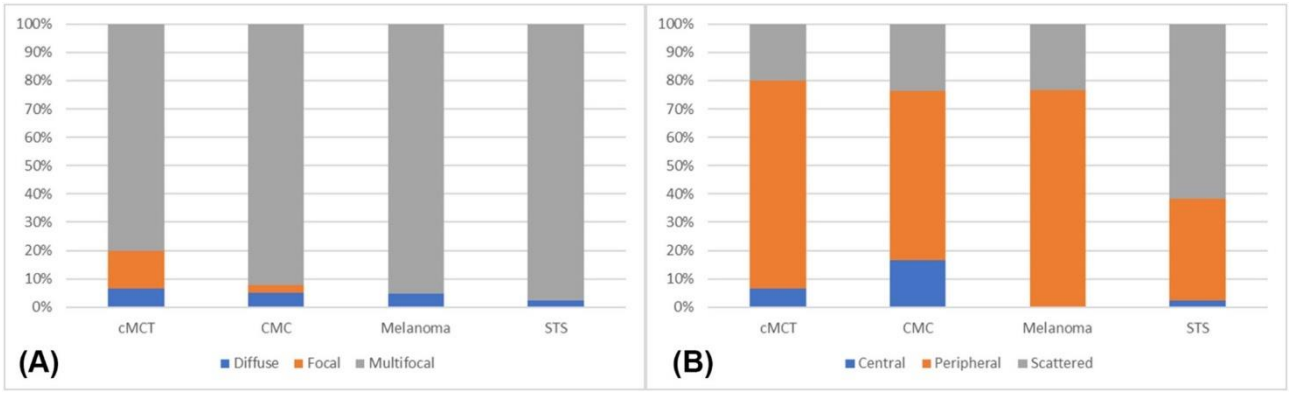


**Figure 2.7**: Bar plots depicting the percentage of cases presenting (A) diffuse, focal or multifocal distribution and (B) central, peripheral and scattered location. Mast cell tumours have a higher percentage of focal distribution and soft tissue sarcomas have a higher percentage of scattered location. cMCT: cutaneous mast cell tumours; CMC: canine mammary carcinoma; STS: soft tissue sarcoma.

The hot spot location was central in 12 cases (5.9%), peripheral in 111 (55%) and scattered in 79 (39.1%), and was associated with diagnosis 1 (chi-square = 41.9; $p < 0.001$). Specifically, the location was central in 2/30 (6.7%) cMCT, 7/42 (16.7%) CMC, 0/43 melanomas, and 3/87 cSTS; peripheral in 22/30 (73.3%) cMCT, 25/42 (59.5%) CMC, 33/43 (76.7%) melanomas, and 31/87 (35.6%) cSTS; and scattered in 6/30 (20%) cMCT, 10/42 (23.8%) CMC, 10/43 (23.3%) melanomas and 53/87 (60.9%) cSTS (Figure 2.7B). Considering the hot spot patterns derived from the combination of distribution and location, the peripheral-multifocal pattern was found in 100/202 cases (49.5%), scattered multifocal in 79/202 (39.1%), central multifocal in 8/202 (4.0%), peripheral diffuse in 6/202 (3.0%), peripheral focal in 5/202 (2.5%), and central diffuse in 4/202 (2.0%), correlating with diagnosis 1 (chi-square test, $p < 0.001$). Specifically, in cMCT the pattern was peripheral multifocal in 17/30 (56.7%), scattered multifocal in 6/30 (20.0%), peripheral focal in 4/30 (13.3%), central diffuse in 1/30 (3.3%), central multifocal in 1/30 (3.3%) and peripheral diffuse in 1/30 (3.3%). In CMC, it was peripheral multifocal in 21/42 (50.0%), scattered multifocal in 10/42 (23.8%), central multifocal in 5/42 (11.9%), peripheral diffuse in 3/42 (7.1%), central diffuse in 2/42 (4.8%) and peripheral focal in 1/42 (2.4%). In melanomas, the patterns were peripheral multifocal in 31/43 (72.1%), scattered multifocal in 10/43 (23.3%), peripheral diffuse in 2/43 (4.7%) and no cases were recorded for the other patterns. In STS, the pattern was as follows: scattered multifocal in 53/87(60.9%), peripheral multifocal in 31/87 (35.6%), central multifocal in 2/87 (2.3%), central diffuse in 1/87 (1.1%) and no cases were observed for the remaining patterns. No statically significant association of the host spot distribution, location and combined pattern with diagnosis 2 (STS histotype and cutaneous versus oral melanoma) was found. In 10 out of 21 cases of cutaneous melanoma and 13 out of 22 cases of oral melanoma, we were able to assign a third pattern based on the superficial or deep localisation of the hotspots. It was visually observed that, in 7 out of 10 (70%) cutaneous melanomas, the hotspots were located on the superficial side, while in

8 out of 13 (62%) cases of oral melanomas, the hotspots were found on the deep side of the neoplasm. Similarly, in 10 MCTs cases, 5 had superficial hotspots and 5 had deep hotspots. Finally, in CMC, the localization of the third pattern was assigned in 10 cases, and in 4 of these, the distribution mirrored the lobular arrangement of the carcinoma. A statistically significant association was found between the Ki-67 labelling index and both location and distribution, being higher in cases with scattered location compared with peripheral ($W = 3.33$, $p = 0.49$), and in cases with multifocal distribution compared with a diffuse one ($W = 4.66$, $p = 0.003$).

**Discussion**

MC is one of the most commonly used histological prognostic factors in veterinary tumour pathology (Meuten et al., 2016). However, the current method of MC assessment presents significant limitations due to intra-tumoral variability and observer subjectivity. Considerable efforts have been dedicated to overcoming these limitations, resulting in the establishment of a standard area for MC and the morphology of mitotic figures. Nevertheless, there are no guidelines on selecting the tumour region where the count should be performed (Meuten et al., 2016). These limitations compromise the reliability of MC as a prognostic factor. The introduction of computer-assisted diagnosis systems offers promising solutions to address the current challenges of MC (Bertram et al., 2018). Nevertheless, until most laboratories have entirely switched to digital microscopy (Bertram et al., 2018), this approach will not be widely applied. Furthermore, a limited number of prognostic studies on canine tumours have used digital microscopy and associated the digital counts with outcome (Bertram et al., 2023; Wei et al., 2019). This study aimed to investigate the regional distribution of proliferative hotspots for different canine tumour types, providing guidelines for pathologists when assessing the MC, following the general rule that MC should be evaluated in areas of highest proliferation (Avallone et al., 2021). The multifocal distribution was the predominant location

of hot spots for all tumour types included in the study. In STS and melanoma, multifocality was observed in all cases except for one and two cases, respectively. In contrast, a diffuse or focal distribution was found in more than 10% of CMC and cMCT cases, respectively.

We interpreted the multifocality as a consequence of tumour heterogeneity, further confirming the need for more clearly defined indications for selecting the tumour region for MC assessment. This heterogeneity, together with other factors, may be at the root of the low inter-pathologist agreement on MC results. The significant number of CMC with a diffuse distribution may indicate a lower heterogeneity of this tumour type, which may be derived from the inclusion of simple carcinoma only. Regarding the hot spot location, the peripheral one was the most common in all tumour types examined, except for STS. In the past, it has been postulated that the peripheral portion of the tumour, representing the invasive front, was the most proliferative (Baak et al., 2009; Bertram et al., 2020; Meuten et al., 2016). This appears to be especially true in cMCT and canine melanoma, in which the peripheral distribution represented approximately 75% of the cases. This suggests that, in these tumour types, pathologists should focus mainly on the periphery when assessing the MC. Interestingly, despite the higher frequency of the peripheral pattern, CMC included a large number of cases characterised by central hotspots. This result may indicate that, when a low MC is found, or when mitotic figures are difficult to find at the periphery of a CMC, it could be useful to assess the tumour centre. Anyway, this indication cannot be extrapolated to all CMC types, as only simple carcinomas were included in this study. Furthermore, the central proliferation in CMC could represent a biologically distinct variant. On the other hand, in cSTS, Ki-67 scattered distribution was the most frequent, followed by the peripheral one, in both cases associated with a multifocal distribution. This data indicates a high intra-tumoral heterogeneity of proliferative activity of cSTS cells and suggests that sections should be carefully scrutinised for the detection of regions with high mitotic activity

(Roccabianca et al., 2020). Furthermore, the different spatial distribution of Ki-67 hotspots may also partially reflect tumour biology. In melanomas and cMCT, proliferative activity is concentrated at the tumour edges, suggesting that these areas are the most representative of accurate mitotic diagnosis. Peripheral proliferation in these tumours can be indicative of active margins, which may contribute to greater infiltrative potential. In cSTS, the predominant scattered proliferation could reflect a less focused distribution, potentially associated with their less aggressive tumour behaviour. This hypothesis should be confirmed by assessing the spatial distribution of hotspots in a caseload with available clinical follow-ups. Furthermore, the Ki-67 labelling index was significantly higher in cases with a multifocal distribution compared with those with a diffuse pattern, and to a lesser extent, in cases with a scattered location compared with a peripheral one. This may suggest that while a baseline proliferative activity is uniformly present throughout the tumour, peaks of proliferative activity occur in areas where more aggressive neoplastic cell clones undergo selection. Finally, in some cases, a low correspondence was observed between MC and the Ki-67 labelling index. A low MC in tumours with a high Ki-67 index is likely due to the count being performed in an area that did not correspond to the most proliferative region. Conversely, a high MC in tumours with a low Ki-67 index may result from the count being carried out in a localised hotspot within a tumour otherwise characterized by few proliferative foci and an overall low proliferation rate, considering that the Ki-67 index was calculated across the entire section. Both scenarios highlight the need for more detailed guidelines to standardise the selection of tumour regions for MC assessment. One limitation of this study is the use of an anti-Ki-67 antibody, which detects cells at any phase of the cell cycle except for G0, thus labelling not only cells in mitosis but also those in G1, G2, and S phase (Sun and Kaufman, 2018). As a consequence, it is likely that there is no exact correspondence between Ki-67 hotspots and mitotic figure hotspots. Nevertheless, we chose to use this marker since these results can also be applied to the selection of regions for assessing the

Ki-67 labelling index. This additional prognostic parameter is often required by oncologists for canine melanoma and cMCT, necessitating the identification of highly proliferative regions (Freytag et al., 2021; Smedley et al., 2022). A second limitation is the exclusion of complex and mixed mammary tumours. This was opted for because the separation of the myoepithelial and non-epithelial components would have required a different and more complex image analysis protocol. Finally, we selected cases having a small diameter, so we could examine at least half of a transversal section. This criterion might have introduced a bias related to a possible different distribution of proliferative hotspots in larger lesions. Further studies are advisable to confirm our results, to expand the caseload to other tumour types, including subcutaneous cMCT and other mammary tumour types, and compare the distribution patterns with the biological behaviour of the tumours. In conclusion, the peripheral proliferation observed in melanomas and cMCT, as well as the scattered pattern typical of cSTS, represents distinctive features that may assist in selecting hotspots and could have significant diagnostic and prognostic implications. The association between histological diagnosis and the pattern of proliferation found in this study likely reflects the biological differences among the tumour types studied. A better understanding of proliferative hotspot distribution can contribute to a more targeted prognostic stratification in canine tumours.

## References


Al-Janabi S, Van Slooten H-J, Visser M, et al. Evaluation of Mitotic Activity Index in Breast Cancer Using Whole Slide Digital Images. PLoS ONE 2013;8:e82576.

Avallone G, Rasotto R, Chambers JK, et al. Review of Histological Grading Systems in Veterinary Medicine. Vet Pathol 2021;58:809–28.

Baak JPA, Gudlaugsson E, Skaland I, et al. Proliferation is the strongest prognosticator in node-negative breast cancer: significance, error sources, alternatives and comparison with molecular prognostic markers. Breast Cancer Res Treat 2009;115:241–54.

Bertram CA, Aubreville M, Gurtner C, et al. Computerized Calculation of Mitotic Count Distribution in Canine Cutaneous Mast Cell Tumor Sections: Mitotic Count Is Area Dependent. Vet Pathol 2020;57:214–26.

Bertram CA, Bartel A, Donovan TA, et al. Atypical Mitotic Figures Are Prognostically Meaningful for Canine Cutaneous Mast Cell Tumors. Veterinary Sciences 2023;11:5.

Bertram CA, Gurtner C, Dettwiler M, et al. Validation of Digital Microscopy Compared With Light Microscopy for the Diagnosis of Canine Cutaneous Tumors. Vet Pathol 2018;55:490–500.

Bonert M, Tate AJ. Mitotic counts in breast cancer should be standardized with a uniform sample area. BioMed Eng OnLine 2017;16.

Ellis PSJ, Whitehead R. Mitosis counting—A need for reappraisal. Human Pathology 1981;12:3–4.

Elston LB, Sueiro FAR, Cavalcanti JN, et al. Letter to the Editor: The Importance of the Mitotic Index as a Prognostic Factor for Survival of Canine Cutaneous Mast Cell Tumors: A Validation Study. Vet Pathol 2009;46:362–4.

Freytag JO, Queiroz MR, Govoni VM, et al. Prognostic value of immunohistochemical markers in canine cutaneous mast cell tumours: A systematic review and meta-analysis. Vet Comparative Oncology 2021;19:529–40.

Gudlaugsson E, Skaland I, Janssen EAM, et al. Comparison of the effect of different techniques for measurement of Ki-67 proliferation on reproducibility and prognosis prediction accuracy in breast cancer. Histopathology 2012;61:1134–44.

Horta RS, Lavalle GE, Monteiro LN, et al. Assessment of Canine Mast Cell Tumor Mortality Risk Based on Clinical, Histologic, Immunohistochemical, and Molecular Features. Vet Pathol 2018;55:212–23.

Kiupel M, Webster JD, Bailey KL, et al. Proposal of a 2-Tier Histologic Grading System for Canine Cutaneous Mast Cell Tumors to More Accurately Predict Biological Behavior. Vet Pathol 2011;48:147–55.

Kuntz CA, Dernell WS, Powers BE, et al. Prognostic factors for surgical treatment of soft-tissue sarcomas in dogs: 75 cases (1986-1996). J Am Vet Med Assoc 1997;211:1147–51.

McSporran KD. Histologic Grade Predicts Recurrence for Marginally Excised Canine Subcutaneous Soft Tissue Sarcomas. Vet Pathol 2009;46:928–33.

Meuten DJ, Moore FM, George JW. Mitotic Count and the Field of View Area: Time to Standardize. Vet Pathol 2016;53:7–9.

Meuten D, Munday JS, Hauck M. Time to Standardize? Time to Validate? Vet Pathol 2018;55:195–9.

Meuten DJ, Moore FM, Donovan TA, et al. International Guidelines for Veterinary Tumor Pathology: A Call to Action. Vet Pathol 2021;58:766–94.

Meyer JS, Alvarez C, Milikowski C, et al. Breast carcinoma malignancy grading by Bloom–Richardson system vs proliferation index: reproducibility of grade and advantages of proliferation index. Modern Pathology 2005;18:1067–78.

Meyer JS, Cosatto E, Graf HP. Mitotic Index of Invasive Breast Carcinoma. Archives of Pathology & Laboratory Medicine 2009;133:1826–33.

Mills SW, Musil KM, Davies JL, et al. Prognostic Value of Histologic Grading for Feline Mammary Carcinoma: A Retrospective Survival Analysis. Vet Pathol 2015;52:238–49.

Patnaik AK, Ehler WJ, MacEwen EG. Canine Cutaneous Mast Cell Tumor: Morphologic Grading and Survival Time in 83 Dogs. Vet Pathol 1984;21:469–74.

Peña L, Andrés PJD, Clemente M, et al. Prognostic Value of Histological Grading in Noninflammatory Canine Mammary Carcinomas in a Prospective Study With Two-Year Follow-Up: Relationship With Clinical and Histological Characteristics. Vet Pathol 2013;50:94–105.

Roccabianca P, Schulman FY, Avallone G, et al. Surgical Pathology of Tumors of Domestic Animals. vol. 3. 3rd ed. Kiupel M.; 2020.

Romansik EM, Reilly CM, Kass PH, et al. Mitotic Index Is Predictive for Survival for Canine Cutaneous Mast Cell Tumors. Vet Pathol 2007;44:335–41.

Schott CR, Tatiersky LJ, Foster RA, et al. Histologic Grade Does Not Predict Outcome in Dogs with Appendicular Osteosarcoma Receiving the Standard of Care. Vet Pathol 2018;55:202–11.

Smedley RC, Sebastian K, Kiupel M. Diagnosis and Prognosis of Canine Melanocytic Neoplasms. Veterinary Sciences 2022;9:175.

Spangler WL, Kass PH. The Histologic and Epidemiologic Bases for Prognostic Considerations in Canine Melanocytic Neoplasia. Vet Pathol 2006;43:136–49.

Stålhammar G, Robertson S, Wedlund L, et al. Digital image analysis of Ki-67 in hot spots is superior to both manual Ki-67 and mitotic counts in breast cancer. Histopathology 2018;72:974–89.

Sun X, Kaufman PD. Ki-67: more than a proliferation marker. Chromosoma 2018;127:175–86.

Tsuda H, Akiyama F, Kurosumi M, et al. Evaluation of the Interobserver Agreement in the Number of Mitotic Figures Breast Carcinoma as Simulation of Quality Monitoring in the Japan National Surgical Adjuvant Study of Breast Cancer (NSAS-BC) Protocol. Japanese Journal of Cancer Research 2000;91:451–7.

Van Diest PJ, Baak JPA, Matze-Cok P, et al. Reproducibility of mitosis counting in 2,469 breast cancer specimens: Results from the Multicenter Morphometric Mammary Carcinoma Project. Human Pathology 1992;23:603–7.

Vascellari M, Giantin M, Capello K, et al. Expression of Ki-67, BCL-2, and COX-2 in Canine Cutaneous Mast Cell Tumors: Association With Grading and Prognosis. Vet Pathol 2013;50:110–21.

Veta M, Van Diest PJ, Willems SM, et al. Assessment of algorithms for mitosis detection in breast cancer histopathology images. Medical Image Analysis 2015;20:237–48.

Wei B-R, Halsey CH, Hoover SB, et al. Agreement in Histological Assessment of Mitotic Activity Between Microscopy and Digital Whole Slide Images Informs Conversion for Clinical Diagnosis. Academic Pathology 2019;6:2374289519859841.

## Chapter 3: Tumor Immune Microenvironment

### *Chapter Overview*

*Tumor Immune Microenvironment and Its Impact on Tumor Progression*

The interaction between cancer and tumor immune microenvironment (TIME), which includes tumor-infiltrating lymphocytes (TILs), tumor-associated macrophages (TAMs), dendritic cells, myeloid-derived suppressor cells and natural killer (NK) cells, is crucial for the control of the development and progression of malignant tumors (Cortiana et al., 2025; Jumaniyazova et al., 2023). This interaction influences tumor progression and response to treatment (Cortiana et al., 2025).

This aligns with the widely accepted concept of immunosurveillance, which suggests that the immune system continuously identifies and eliminates cancerous cells by recognizing tumor-specific neoantigens arising from somatic mutations (Dunn et al., 2004). Therefore, the capacity of cancer cells to evade immune-mediated elimination is now recognized as a fundamental step in the progression of tumors to a clinically detectable stage (Hanahan and Weinberg, 2011).

In general, tumor-immune interactions can be classified into three main phenotypic categories:

- **immune-excluded tumors**, where the TIME is shielded from immune cell infiltration by altered stromal factors, vascularization and constitution of the extracellular matrix;
- **immune desert tumors**, where the absence of pro-inflammatory factors and the avoidance of antigen presentation by tumor cells reduce the visibility of cancer to the surveillant immune system;

- **inflamed tumors**, where infiltrates of immune effector cells within the TIME exhibit evidence of an exhausted activatory state that is influenced by tumor and stromal factors (Kerrison et al., 2022a).

Over the last decade, it has become increasingly clear that immune cells in the TIME play a critical role in controlling or promoting tumor growth (Anderson and Simon, 2020; Tang et al., 2021).

Basically, it can be stated that immune cells fall into two categories: *adaptive immune cells* and *innate immune cells*.

Adaptive immunity is activated by exposure to specific antigens and uses an immunological memory to evaluate the risk and improve immune responses. T-cells and B-cells belong to the adaptive immune response. Innate immunity is a non-specific defense mechanism that comes into play within hours of a foreign antigen entering the body. Cells that carry out an innate immune response include macrophages, neutrophils and dendritic cells (Anderson and Simon, 2020).

More specifically, CD8+ cytotoxic T-cells, T-helper 1 cells producing interferon-γ (IFN-γ), NK cells are generally associated with favorable responses **(anti-tumoral)**, along with macrophages polarized to an M1 phenotype and dendritic cells showing a DC1 phenotype. Immunosuppressive effects **(pro-tumoral)** are seen with T-helper 2 cells, M2 macrophages, DC2 dendritic cells, myeloid-derived suppressor cells and FoxP3+ regulatory T-cells (Treg) producing Interleukin-10 (IL-10) and Transforming growth factor beta (TGF-β) (Lee and Margolin, 2012). Furthermore, B-cells and plasma cells can adopt either effector or regulatory phenotypes and consequently can carry a pro- or anti-tumoral function depending on contextual factors in TIME. For example, the presence of tertiary lymphoid structures

(TLS) in TIME is correlated with better prognosis in many solid tumors (Dieu-Nosjean et al., 2014; Yuen et al., 2016).

The amount, localization and phenotypes of TILs are not only predictive of response to immunotherapy but also key modulators of clinical disease progression (Bruno, 2020).

STSs comprise a diverse group of neoplasms traditionally considered poorly immunogenic, often described as “immunogenically cold” (Kerrison et al., 2022a). However, recent studies in human medicine are changing this notion, showing that certain STS subtypes exhibit significant immune cell infiltration and genetic profiles indicative of an active antitumor immune response (Dancsok et al., 2019).

A poor clinical outcome has been associated with immunosuppressive elements within the STS immune microenvironment, suggesting that immune evasion may contribute to a more aggressive sarcoma phenotype (Dancsok et al., 2019; Lee et al., 2008; Smolle et al., 2021).

In particular, STS immune microenvironment is often characterized by an immune-suppressive landscape, with low CD8+ T-cell infiltration and an abundance of Tregs and CD206+ macrophages, which produce immunosuppressive cytokines such as IL-10 and TGF-β (Liu et al., 2021).

Continuous exposure of T-cells to tumor antigens leads to exhaustion, reducing their cytotoxic abilities and proliferation, and expressing multiple inhibitory receptors such as Programmed Cell Death Protein 1 (PD-1), T-cell immunoglobulin and mucin-domain containing-3 (TIM-3) and Lymphocyte-activation gene 3 (LAG-3) (Ando et al., 2020). Inhibitory T-cell immune checkpoint receptors like PD-1, when interacting with the Programmed death-ligand 1 (PD-L1), inhibit T-cell function, predicting responses to immune checkpoint inhibitors (ICIs) (Anastasiou et al., 2023). Tregs produce immunosuppressive cytokines such as IL-10 and TGF-β, express coinhibitory molecules including Cytotoxic T-

Lymphocyte Associated Protein 4 (CTLA-4), PD-1 and PD-L1, capture Interleukin-2 (IL-2), inhibiting T-cell responses and promoting tumor immune escape (Ando et al., 2020).

Targeting molecules such as CTLA-4 and PD-1, have revolutionized cancer treatment across multiple malignancies, including melanoma, lung cancer and lymphomas (Kerrison et al., 2022a). However, the effectiveness of such therapies varies significantly depending on the characteristics of the TIME.

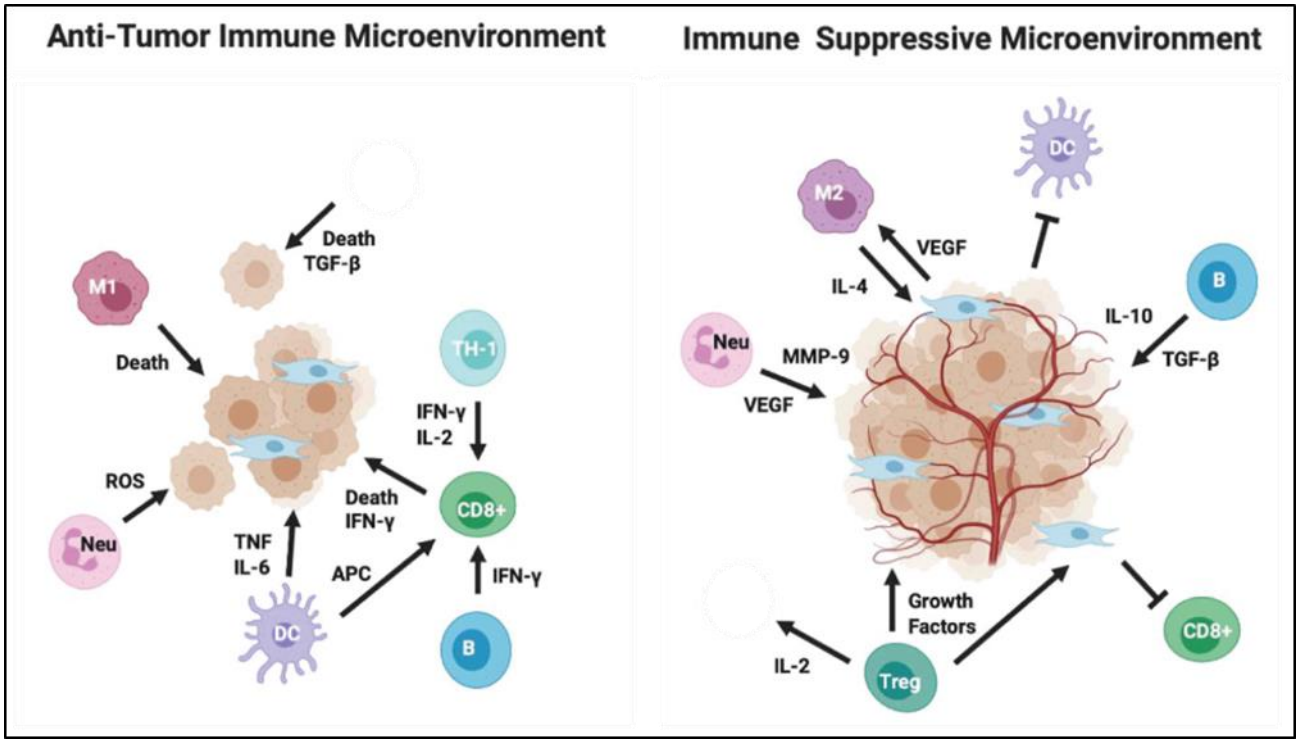


**Figure 3.1:** The role of immune cells in the TIME is to either suppress tumor formation (anti-tumor microenvironment) or promote tumorigenesis (immunosuppressive microenvironment) (Anderson and Simon, 2020).

### *Tumor infiltrating lymphocytes (TILs)*

#### T-cells

Several distinct populations of T-cells influence tumor progression:

- **Cytotoxic T-cells CD8+** detect abnormal tumor antigens expressed on cancer cells and target tumor cells for destruction. The presence of cytotoxic T-cells in the TIME is often associated with positive prognosis in cancer patients. Aside from killing tumor cells, cytotoxic T-cells also suppress angiogenesis through the secretion of IFN-γ (Anderson and Simon, 2020).
- **CD4+ T-cells** differentiate into a variety of subtypes and thus coordinate a wide range of immune responses within the context of the TIME.
    - **T helper 1 (Th-1)** cells are proinflammatory CD4+ T-cells that support CD8+ cells through the secretion of IL-2 and IFN-γ (Anderson and Simon, 2020). Increased levels of Th-1 cells within the TIME are related with positive outcomes in many types of solid neoplasms (Maggi et al., 2024) and specifically in colorectal tumors (Galon et al., 2006).
    - **Regulatory T-cells (Tregs) FoxP3+** are normally required to suppress inflammatory responses and control autoimmunity. In the context of the TIME, Tregs are widely present and facilitate tumor growth and progression by suppressing antitumor immune activity. For example, Tregs secrete IL-2 which modulates NK cell homeostasis and function. Additionally, Tregs cells directly support the survival of cancer cells through the secretion of growth factors, and indirectly through interaction with fibroblasts and endothelial cells (Anderson and Simon, 2020). FoxP3+ TILs infiltration has been associated with a reduced overall survival (OS) in most human cancers, including breast, hepatocellular, gastric, ovarian, cervical and cholangiocarcinoma (Brummel et

al., 2023; Cao et al., 2020; Chen et al., 2022; deLeeuw et al., 2012; Eschweiler et al., 2021; Hwang et al., 2012).

CD3+ TIL infiltration was associated with increased progression-free survival and OS across malignancies (Borst et al., 2018). In fact, high CD3+ TIL infiltration has proven highly reliable in follow-up studies and has been associated with an improved OS in almost all cancer types, including melanoma and breast, colorectal, gastric, hepatocellular, and head and neck cancer (Al-Shibli et al., 2008; Dieu-Nosjean et al., 2014; Erdag et al., 2012; Germain et al., 2014; Hernández-Prieto et al., 2015; Ladányi et al., 2011; Lund and Randall, 2010).

Apart from the frequently used parameters of presence and density of TILs, recent studies also show that the location of TILs and their spatial organization may carry additional prognostic value, showing that a high CD3+ TIL infiltrate in the invasive tumor margin had a positive correlation with OS and disease-free survival in patients with colorectal cancer (Mei et al., 2014). Conversely, a high CD3+ TIL infiltrate in the tumor center or tumor stroma had no association with OS (Mei et al., 2014).

While certain STS subtypes exhibit minimal immune infiltration, others have shown variability in both the quantity and composition of infiltrating immune cells (Tazzari et al., 2021). Notably, STS subtypes characterized by single-gene translocations typically harbor few TILs, whereas those associated with greater genomic complexity show wider variability in TILs density (Dancsok et al., 2019).

Immunohistochemical and gene expression studies provide convincing evidence that a subset of genomically complex STS cases, crossing various histological subtypes, exhibit an inflamed (immune hot) TIME, which has been associated with more favorable outcomes. This association underscores the biologically and clinically relevant role of host immunity in

defining sarcoma disease phenotype (Petitprez et al., 2020; Sautès-Fridman et al., 2019; Thorsson et al., 2018).

In human medicine, infiltrating T-cells are CD3+, with a majority of cytotoxic CD8+ T-cells, alongside a mixed population of CD4+ helper T-cells and FoxP3+ Tregs (Jumaniyazova et al., 2023) and vary according to histological subtype. For example, leiomyosarcomas and myxofibrosarcomas exhibit significantly higher TIL counts compared to synovial sarcomas (Hemminger and Iwenofu, 2013). Moreover, specific STS subtypes, such as alveolar sarcomas, rhabdomyosarcomas and highly mutagenic sarcomas, are notably enriched in CD3+ T-cell (Nakajima and Raz, 2021; Pollack et al., 2017; Smolle et al., 2021). The number of CD4+ TIL counts may exceed those of CD8+ in differentiated and dedifferentiated retroperitoneal liposarcoma (Tseng et al., 2015); additionally, CD8+ T-cells in these tumors are often exhausted and express PD-1, which makes them less effective in fighting the tumor (Tseng et al., 2015).

In fact, most T-cells within a tumor exhibit signs of activatory exhaustion, a state associated with chronic exposure to immunogenic tumor related antigens in the absence of co-stimulatory signals and the presence of suppressive cell-cell and cytokine interactions (Jiang et al., 2015). Exhausted T-cells have decreased cytotoxic potential and are characterized by high surface expression levels of inhibitory immune checkpoint receptors such as PD-1 (Jumaniyazova et al., 2023).

The prognostic significance of T-cell infiltration in STS remains a subject of debate. Some data suggest a beneficial influence of lymphocyte infiltration, particularly with CD4+ T-cells (Boxberg et al., 2018; Fujii et al., 2014; Judge et al., 2020). Other studies, however, demonstrate a negative prognostic value of TIL counts (Conley et al., 2018) or a lack of significant association (Blay et al., 2021; Lawrence et al., 2013).

In a study by Smolle and colleagues (Smolle et al., 2021), high FoxP3+ cell levels were significantly associated with improved OS via univariate analysis. These observations are consistent with the molecular data of Bae and colleagues (Bae et al., 2020) demonstrating strong intratumoral expression of FoxP3 and other immune-associated genes in patients with relatively mild courses of STS. However, Tregs were the only TIL phenotype of independent negative prognostic significance for local recurrence (Smolle et al., 2021), which indicates a strong local effect of Tregs, thereby suppressing the activity of TILs and thus mitigating the antitumor immune responses. Other studies, however, revealed no significant associations of Treg counts with the prognosis in STSs (Tseng et al., 2015).

**B-cells**

B-cells are specialized immune cells responsible for antibody production, antigen presentation and secretion of cytokines. Typically, B-cells concentrate at the margin of tumors and are commonly found in lymph nodes in close proximity to the TIME (Anderson and Simon, 2020). Compared to T-cells, the TIME has relatively few infiltrating B-cells; however, recent studies have demonstrated that the presence and function of B-cells are important during tumorigenesis. As mentioned before, tumor infiltrating B-cells are important in the formation of TLS, which are ectopic lymphoid structures formed within the TIME (Anderson and Simon, 2020). TLS allow close association between T and B-cells and are a positive prognostic marker in breast cancer, melanoma and ovarian cancer (Anderson and Simon, 2020; Kasikova et al., 2024). The anti-tumorigenic roles of B-cells, include antigen-presentation to T-cells, anti-tumor antibody production and secretion of cytokines that promote cytotoxic immune responses (e.g. IFN-γ) (Sun and Liu, 2024). Alternatively, B cells can exert pro-tumoral effects, and their presence within the TIME may be associated with poor outcomes in bladder cancer, prostate cancer, and renal cell carcinoma (Anderson and Simon, 2020). Regulatory B-cells promote tumor aggression through production of cytokines

(e.g. IL-10 and TGF-β) that promote immune suppressive phenotypes in macrophages, neutrophils and cytotoxic T-cells (Downs-Canner et al., 2022).

In STSs, B-cells have been implicated in antitumor responses (Sharonov et al., 2020), but their presence varies; for example, in differentiated and dedifferentiated retroperitoneal liposarcomas, these cells are scarce (Tseng et al., 2015). For STSs with broad resection margins, high counts of B-cells can be prognostically favorable (Sorbye et al., 2011); in some cases, the cells can be nonuniformly distributed across the tumor, with entire regions being B-cell deprived (Tsagozis et al., 2019).

Petitprez and colleagues (Petitprez et al., 2020) analyzed in an integrative manner the influence of B-cells infiltration on survival and immunotherapy response in STS, thereby confirming the positive prognostic value of this parameter, including the PD-1 inhibition sensitivity.

A positive correlation between B-cell marker expression and response to immunotherapy in STS was also revealed by Helmink and colleagues (Helmink et al., 2020). Nyström and colleagues (Nyström et al., 2023) identified CD20+ B-cells in 14% of STSs, including high-grade leiomyosarcomas, liposarcomas and synovial sarcomas. The CD20+ infiltration rates positively correlated with survival without clear association with other prognostic factors. A recently identified subset of regulatory B-cells was implicated in confronting inflammation and autoimmune diseases (Gray and Gray, 2010). High CD20+ lymphocyte counts, often correlating with CD8+ infiltration (Petitprez et al., 2020), also appear to be favorable prognostic indicators (Boxberg et al., 2018).

**Natural Killer (NK) Cells**

NK cells check the blood stream and search for out virally infected host cells or tumor cells. Functionally, NK cells can be broken down into two classes; they either directly participate

in cell-mediated killing of tumor cells or they secrete inflammatory cytokines. NK cells are highly efficient at killing tumor cells within the circulation and can participate in blocking metastasis, but are less efficient at killing within the TIME (Anderson and Simon, 2020).

***Tumor infiltrating macrophages (TAMs)***

Tumor-associated macrophages (TAMs), which are an essential component of the TIME, play decisive roles in tumor-associated inflammation (Borst et al., 2018; Mantovani et al., 2017; Noy and Pollard, 2014).

Macrophages are a critical component of the innate immune system that modulate immune responses through pathogen phagocytosis and antigen presentation. In addition, macrophages are critical in damage healing and tissue repair.

Under the influence of TIME, TAMs polarize as either anti-oncogenic M1s or pro-oncogenic M2s (Malfitano et al., 2020). M1 macrophages present antigens (Allavena et al., 2008), produce interleukins (IL-12 and IL-23) (Verreck et al., 2004) and activate T-cell type I responses (Allavena et al., 2008), acting as potent effector cells defending the body from pathogens and tumor cells. On the other side, M2 macrophages exhibit poor antigen-presenting capacity, suppress inflammatory responses and Th1 adaptive immunity, and promote angiogenesis and tissue remodeling (Allavena et al., 2008; Bouhlel et al., 2007).

While both classes of macrophages can be found within tumors, TIME promotes the M2 phenotype through hypoxia and the secretion of cytokines such as Interleukin-4 (IL-4), thus supporting tumor growth and progression (Anderson and Simon, 2020). Typically, high macrophage infiltration is associated with poor patient prognosis in many types of cancer, such as breast cancer, lung cancer and gastric cancer (Zhang et al., 2016).

Macrophage polarization is induced by cytokines and chemokines produced by other immune cells (Bouhlel et al., 2007). Myeloid cells, which are the most prominent immune

population within sarcomas and some epithelial tumors, differentiate into TAMs. Although these cells may initially exhibit antitumor properties, the TIME gradually shifts them toward immunosuppressive phenotypes that support tumor progression (Cheng et al., 2021). Consequently, TAMs promote angiogenesis and release metabolites that fuel emerging therapy resistance mechanisms (El-Kenawi et al., 2021).

In general, high expression of CD204+ macrophages has frequently been correlated with poor prognosis in various types of cancers (Chen et al., 2024; Hirayama et al., 2012; Komohara et al., 2008; Ohtaki et al., 2010). CD204 (also known as class A scavenger receptor) is a widely used marker to identify M2 macrophages, the subpopulation of TAMs linked to immunosuppressive functions, promotion of tumor growth, and negative modulation of the antitumor response (Hirayama et al., 2012).

In STSs**,** the presence of M2 macrophages, has been associated with poor prognosis in non-gynecological leiomyosarcomas (Lee et al., 2008). In myxoid liposarcomas, the total count of TAMs correlates with poor outcomes, as high levels of TAM-produced heparin-binding EGF-like growth factor (HB-EGF) activate the EGFR-PI3K/Akt pathway in tumor cells, thereby increasing cellular plasticity and promoting chemoresistance (Nabeshima et al., 2015).

Several studies emphasize the correlation of cellular composition of the infiltrate with the prognosis. STSs characterized by high counts of CD8+ T-cells, along with positive markers for M1 macrophages and plasma cells, have been associated with better outcomes (Boxberg et al., 2018; Deng et al., 2020; Gu et al., 2020; Hu et al., 2020; Judge et al., 2020).

High numbers of M0 and M2 TAMs within TIME correlate with reduced CD8+ T-cell presence and more aggressive clinical progression (Dufresne et al., 2020; Zhu and Hou, 2020).

Overall, the quantitative prevalence of TAMs over TILs in STSs has been associated with increased risks of metastasis (Salah et al., 2017).

*Tumor Immune Microenvironment in Veterinary Medicine*

In recent years, the study of the TIME in canine neoplasms has gained increased attention, reflecting its established and confirmed relevance in human medicine. Even though the research is still in its early stage, emerging studies can already state that the composition and spatial distribution of immune cells within canine tumors can have significant implications for prognosis and therapeutic strategies.

The introduction of immunotherapies has revolutionized the field, promising numerous advantages as in humans (Bai et al., 2021) also in dogs (Von Rueden and Fan, 2021). Among the most successful immunotherapies in humans are those that aim to block the interaction between PD-1, a suppressive immunoreceptor expressed in exhausted T-cells, and its ligands PD-L1 and PD-L2 (Pardoll, 2012). Several attempts, ended to develop similar therapies for canine melanoma, have produced reports of decreased tumour size, prolonged survival times, and complete remission (Igase et al., 2022; Maekawa et al., 2017; Stevenson et al., 2023).

Although TILs, TAMs, and PD-1/PD-L1 axis expression have been investigated in several canine tumor types (Muscatello et al., 2024b), such as mast cell tumors (Bardales et al., 2025; Costa et al., 2022), mammary carcinoma (Muscatello et al., 2022) and osteosarcomas (Razmara et al., 2021), data focusing specifically on canine STSs are still scarce.

As mentioned human STSs have long been considered immune deserts and thought to be poor candidates for immune therapies, however, this belief is increasingly changing (Petitprez et al., 2020; Sharma et al., 2017; Sousa et al., 2021).

*Histological Assessment of TILs according to Salgado: Limitations and Adaptations in STSs*

The histological evaluation system for TILs proposed by Salgado and colleagues in 2015 is widely recognized in oncology practice, particularly for breast carcinoma. Based on this system, TILs evaluation is performed in the peri- and intra-tumoral stroma, and in the intraepithelial region, where lymphocytes are present among the neoplastic epithelial cells. The evaluation focuses on the percentage of stromal area occupied by lymphocytes, excluding granulocytes and necrotic areas. A lymphocytic infiltration exceeding 50-60% is often indicative of a "lymphocyte-predominant breast cancer" (LPBC), that does not represent a specific diagnosis but rather a description of the local immune status, which in many studies is associated with a better prognosis and response to immunotherapies (Salgado et al., 2015).

The Salgado scoring system has also been applied in veterinary pathology. In particular, Muscatello and colleagues have adapted this approach to evaluate TILs in canine mammary carcinoma. They demonstrated that a standardized semiquantitative scoring of TILs can provide relevant prognostic data in dogs, highlighting that infiltration by stromal TILs and invasive front TILs is associated with increased tumor malignancy. These results suggest that the evaluation of TILs rearranged on the basis of the Salgado's system, may represent a useful tool for prognostic stratification and for exploring the immunological landscape of canine tumors (Muscatello et al., 2022).

However, the applicability of the Salgado system to STSs is limited due to the high cellular heterogeneity and complex nature of the TIME in these tumors. Unlike epithelial tumors, this morphological quantification of TILs, fails to capture the diversity of immune cell populations and their spatial distribution, which are essential to understand sarcoma biology (Dancsok et al., 2019; Petitprez et al., 2020). Moreover, STSs often exhibit cold or immune-desert phenotypes, with significant involvement of immunosuppressive cells such as M2

macrophages and myeloid-derived suppressor cells, components that are not accounted for in this system (Pollack et al., 2017).

Consequently, immunohistochemical analysis is essential to accurately identify and quantify specific immune cell phenotypes within the STSs TIME (Dancsok et al., 2019; Stevenson et al., 2023).

In this context, several studies have applied immunohistochemistry to better classify the immune infiltration in STSs. In one of these studies, Dancsok and colleagues performed a large-scale analysis of different STSs subtypes in human, assessing the density and composition of tumor-infiltrating immune cells, using a panel of markers including CD4, CD8, CD56, FoxP3, PD-1, LAG-3, TIM-3 and PD-L1. They found that genomically complex, non-translocation-associated STSs exhibited significantly higher levels of immune infiltrates (particularly $CD8^+$ T-cells) than translocation-driven types. Notably, while PD-1 and CD56 expression correlated with worse overall survival, the emerging checkpoints LAG-3 and TIM-3 were frequently expressed across most sarcoma subtypes and often co-expressed with PD-L1, suggesting potential therapeutic targets (Dancsok et al., 2019).

Although no universally and fully accepted classification exists, Petitprez and colleagues developed a novel STS classification based on tumor microenvironment composition in large patient cohorts (Petitprez et al., 2020), using the Microenvironment T-cell Populations (MCP) counter method, a gene-expression-based TIME deconvolution tool (Becht et al., 2016). An immune-based classification of STS was developed from this analysis and tumors were assigned to one of five sarcoma immune classes (SICs), labelled A, B, C, D and E, with highly distinct profiles (Petitprez et al., 2020). SIC A, the “immune desert,” showed the lowest expression of immune-related gene signatures and low vascularization. SIC C, the “vascularized” subtype, was marked by high expression of endothelial cell-related genes. SIC E, the “immune-high/TLS-high” subtype, displayed the highest expression of genes

associated with immune cell populations, including T-cells, CD8+ T-cells, NK cells, and cytotoxic lymphocytes. A key feature of SIC E was the strong expression of the B-cell lineage signature. SIC B and SIC D showed heterogeneous profiles but were generally immune-low and immune-high, respectively (Petitprez et al., 2020).

To conclude, while the morphological assessment of TILs according to Salgado provides a useful reference, the complexity of the immune microenvironment in sarcomas requires more specific approaches, such as immunohistochemistry and immune-based classifications. The genomic aspects, which contribute to these differences in immune response, will be discussed in greater detail in the next section.

## References


Al-Shibli KI, Donnem T, Al-Saad S, et al. Prognostic Effect of Epithelial and Stromal Lymphocyte Infiltration in Non–Small Cell Lung Cancer. Clinical Cancer Research 2008;14:5220–7.

Allavena P, Sica A, Solinas G, et al. The inflammatory micro-environment in tumor progression: The role of tumor-associated macrophages. Critical Reviews in Oncology/Hematology 2008;66:1–9.

Anastasiou M, Kyriazoglou A, Kotsantis I, et al. Immune checkpoint inhibitors in sarcomas: a systematic review. Immuno-Oncology and Technology 2023;20:100407.

Anderson NM, Simon MC. The tumor microenvironment. Current Biology 2020;30:R921–5.

Ando M, Ito M, Srirat T, et al. Memory T cell, exhaustion, and tumor immunity. Immunological Medicine 2020;43:1–9.

Bae JY, Choi KU, Kim A, et al. Evaluation of immune-biomarker expression in high-grade soft-tissue sarcoma: HLA-DQA1 expression as a prognostic marker. Exp Ther Med 2020;20:1–1.

Bai R-L, Chen N-F, Li L-Y, et al. A brand new era of cancer immunotherapy: breakthroughs and challenges. Chinese Medical Journal 2021;134:1267–75.

Bardales KL, Jiang L, Radaelli E, et al. Intertumoral heterogeneity of the immune microenvironment in high grade canine mast cell tumors. Vet Oncol 2025;2:7.

Becht E, Giraldo NA, Lacroix L, et al. Estimating the population abundance of tissue-infiltrating immune and stromal cell populations using gene expression. Genome Biol 2016;17:218.

Blay J-Y, Penel N, Ray-Coquard IL, et al. High clinical activity of pembrolizumab in chordoma, alveolar soft part sarcoma (ASPS) and other rare sarcoma histotypes: The French AcSé pembrolizumab study from Unicancer. JCO 2021;39:11520–11520.

Borst J, Ahrends T, Bąbała N, et al. CD4+ T cell help in cancer immunology and immunotherapy. Nat Rev Immunol 2018;18:635–47.

Bouhlel MA, Derudas B, Rigamonti E, et al. PPARγ Activation Primes Human Monocytes into Alternative M2 Macrophages with Anti-inflammatory Properties. Cell Metabolism 2007;6:137–43.

Boxberg M, Steiger K, Lenze U, et al. PD-L1 and PD-1 and characterization of tumor-infiltrating lymphocytes in high grade sarcomas of soft tissue – prognostic implications and rationale for immunotherapy. OncoImmunology 2018;7:e1389366.

Brummel K, Eerkens AL, De Bruyn M, et al. Tumour-infiltrating lymphocytes: from prognosis to treatment selection. Br J Cancer 2023;128:451–8.

Bruno TC. New predictors for immunotherapy responses sharpen our view of the tumour microenvironment. Nature 2020;577:474–6.

Cao M, Wang Y, Wang D, et al. Increased High-Risk Human Papillomavirus Viral Load Is Associated With Immunosuppressed Microenvironment and Predicts a Worse Long-Term Survival in Cervical Cancer Patients. American Journal of Clinical Pathology 2020;153:502–12.

Chen C-W, Wang H-C, Tsai I-M, et al. CD204-positive M2-like tumor-associated macrophages increase migration of gastric cancer cells by upregulating miR-210 to reduce NTN4 expression. Cancer Immunol Immunother 2024;73:1.

Chen H, Liu H, Ai J, et al. PD-1/PD-L1 expression is associated with increased TIM3 expression and tumor-infiltrating T lymphocytes in fibroblastic tumors. Clin Transl Oncol 2022;24:586–96.

Cheng S, Li Z, Gao R, et al. A pan-cancer single-cell transcriptional atlas of tumor infiltrating myeloid cells. Cell 2021;184:792-809.e23.

Conley AP, Trinh VA, Zobniw CM, et al. Positive Tumor Response to Combined Checkpoint Inhibitors in a Patient With Refractory Alveolar Soft Part Sarcoma: A Case Report. JGO 2018:1–6.

Cortiana V, Ghazal BSc J, Vallabhaneni Bs H, et al. Immune Modulation in Sarcoma: Targeting the Tumor Microenvironment. Oncology (Williston Park) 2025;null:232–6.

Dancsok AR, Setsu N, Gao D, et al. Expression of lymphocyte immunoregulatory biomarkers in bone and soft-tissue sarcomas. Modern Pathology 2019;32:1772–85.

deLeeuw RJ, Kost SE, Kakal JA, et al. The Prognostic Value of FoxP3+ Tumor-Infiltrating Lymphocytes in Cancer: A Critical Review of the Literature. Clinical Cancer Research 2012;18:3022–9.

Deng J, Zeng W, Kong W, et al. The Study of Sarcoma Microenvironment Heterogeneity Associated With Prognosis Based on an Immunogenomic Landscape Analysis. Front Bioeng Biotechnol 2020;8.

Dieu-Nosjean M-C, Goc J, Giraldo NA, et al. Tertiary lymphoid structures in cancer and beyond. Trends in Immunology 2014;35:571–80.

Downs-Canner SM, Meier J, Vincent BG, et al. B Cell Function in the Tumor Microenvironment. Annu Rev Immunol 2022;40:169–93.

Dufresne A, Lesluyes T, Ménétrier-Caux C, et al. Specific immune landscapes and immune checkpoint expressions in histotypes and molecular subtypes of sarcoma. OncoImmunology 2020;9.

Dunn GP, Old LJ, Schreiber RD. The Immunobiology of Cancer Immunosurveillance and Immunoediting. Immunity 2004;21:137–48.

El-Kenawi A, Dominguez-Viqueira W, Liu M, et al. Macrophage-Derived Cholesterol Contributes to Therapeutic Resistance in Prostate Cancer. Cancer Research 2021;81:5477–90.

Erdag G, Schaefer JT, Smolkin ME, et al. Immunotype and Immunohistologic Characteristics of Tumor-Infiltrating Immune Cells Are Associated with Clinical Outcome in Metastatic Melanoma. Cancer Research 2012;72:1070–80.

Eschweiler S, Clarke J, Ramírez-Suástegui C, et al. Intratumoral follicular regulatory T cells curtail anti-PD-1 treatment efficacy. Nat Immunol 2021;22:1052–63.

Fujii H, Arakawa A, Utsumi D, et al. $CD8^+$tumor-infiltrating lymphocytes at primary sites as a possible prognostic factor of cutaneous angiosarcoma: Angiosarcoma and tumor immunity. Int J Cancer 2014;134:2393–402.

Galon J, Costes A, Sanchez-Cabo F, et al. Type, Density, and Location of Immune Cells Within Human Colorectal Tumors Predict Clinical Outcome. Science 2006;313:1960–4.

Germain C, Gnjatic S, Tamzalit F, et al. Presence of B Cells in Tertiary Lymphoid Structures Is Associated with a Protective Immunity in Patients with Lung Cancer. Am J Respir Crit Care Med 2014;189:832–44.

Gray D, Gray M. What are regulatory B cells? Eur J Immunol 2010;40:2677–9.

Gu H-Y, Lin L-L, Zhang C, et al. The Potential of Five Immune-Related Prognostic Genes to Predict Survival and Response to Immune Checkpoint Inhibitors for Soft Tissue Sarcomas Based on Multi-Omic Study. Front Oncol 2020;10.

Hanahan D, Weinberg RA. Hallmarks of Cancer: The Next Generation. Cell 2011;144:646–74.

Helmink BA, Reddy SM, Gao J, et al. B cells and tertiary lymphoid structures promote immunotherapy response. Nature 2020;577:549–55.

Hemminger JA, Iwenofu OH. NY-ESO-1 is a sensitive and specific immunohistochemical marker for myxoid and round cell liposarcomas among related mesenchymal myxoid neoplasms. Modern Pathology 2013;26:1204–10.

Hernández-Prieto S, Romera A, Ferrer M, et al. A 50-gene signature is a novel scoring system for tumor-infiltrating immune cells with strong correlation with clinical outcome of stage I/II non-small cell lung cancer. Clin Transl Oncol 2015;17:330–8.

Hirayama S, Ishii G, Nagai K, et al. Prognostic Impact of CD204-Positive Macrophages in Lung Squamous Cell Carcinoma: Possible Contribution of Cd204-Positive Macrophages to the Tumor-Promoting Microenvironment. Journal of Thoracic Oncology 2012;7:1790–7.

Hu C, Chen B, Huang Z, et al. Comprehensive profiling of immune-related genes in soft tissue sarcoma patients. J Transl Med 2020;18.

Hwang W-T, Adams SF, Tahirovic E, et al. Prognostic significance of tumor-infiltrating T cells in ovarian cancer: A meta-analysis. Gynecologic Oncology 2012;124:192–8.

Igase M, Inanaga S, Tani K, et al. Long-term survival of dogs with stage 4 oral malignant melanoma treated with anti-canine PD -1 therapeutic antibody: A follow-up case report. Vet Comparative Oncology 2022;20:901–5.

Jiang Y, Li Y, Zhu B. T-cell exhaustion in the tumor microenvironment. Cell Death Dis 2015;6:e1792–e1792.

Judge SJ, Darrow MA, Thorpe SW, et al. Analysis of tumor-infiltrating NK and T cells highlights IL-15 stimulation and TIGIT blockade as a combination immunotherapy strategy for soft tissue sarcomas. J Immunother Cancer 2020;8:e001355.

Jumaniyazova E, Lokhonina A, Dzhalilova D, et al. Immune Cells in the Tumor Microenvironment of Soft Tissue Sarcomas. Cancers 2023;15:5760.

Kasikova L, Rakova J, Hensler M, et al. Tertiary lymphoid structures and B cells determine clinically relevant T cell phenotypes in ovarian cancer. Nat Commun 2024;15.

Kerrison WGJ, Lee ATJ, Thway K, et al. Current Status and Future Directions of Immunotherapies in Soft Tissue Sarcomas. Biomedicines 2022;10:573.

Komohara Y, Ohnishi K, Kuratsu J, et al. Possible involvement of the M2 anti-inflammatory macrophage phenotype in growth of human gliomas. The Journal of Pathology 2008;216:15–24.

Ladányi A, Kiss J, Mohos A, et al. Prognostic impact of B-cell density in cutaneous melanoma. Cancer Immunol Immunother 2011;60:1729–38.

Lawrence MS, Stojanov P, Polak P, et al. Mutational heterogeneity in cancer and the search for new cancer-associated genes. Nature 2013;499:214–8.

Lee C-H, Espinosa I, Vrijaldenhoven S, et al. Prognostic Significance of Macrophage Infiltration in Leiomyosarcomas. Clinical Cancer Research 2008;14:1423–30.

Lee S, Margolin K. Tumor-Infiltrating Lymphocytes in Melanoma. Curr Oncol Rep 2012;14:468–74.

Liu Y, Feng W, Dai Y, et al. Single-Cell Transcriptomics Reveals the Complexity of the Tumor Microenvironment of Treatment-Naive Osteosarcoma. Front Oncol 2021;11.

Lund FE, Randall TD. Effector and regulatory B cells: modulators of CD4+ T cell immunity. Nat Rev Immunol 2010;10:236–47.

Maekawa N, Konnai S, Takagi S, et al. A canine chimeric monoclonal antibody targeting PD-L1 and its clinical efficacy in canine oral malignant melanoma or undifferentiated sarcoma. Sci Rep 2017;7:8951.

Maggi E, Munari E, Landolina N, et al. T cell landscape in the microenvironment of human solid tumors. Immunology Letters 2024;270:106942.

Malfitano AM, Pisanti S, Napolitano F, et al. Tumor-Associated Macrophage Status in Cancer Treatment. Cancers 2020;12:1987.

Mantovani A, Marchesi F, Malesci A, et al. Tumour-associated macrophages as treatment targets in oncology. Nat Rev Clin Oncol 2017;14:399–416.

Mei Z, Liu Y, Liu C, et al. Tumour-infiltrating inflammation and prognosis in colorectal cancer: systematic review and meta-analysis. Br J Cancer 2014;110:1595–605.

Muscatello LV, Avallone G, Brunetti B, et al. Standardized approach for evaluating tumor infiltrating lymphocytes in canine mammary carcinoma: Spatial distribution and score as relevant features of tumor malignancy. The Veterinary Journal 2022;283–284:105833.

Muscatello LV, Gobbo F, Avallone G, et al. PD-L1 immunohistochemistry in canine neoplasms: Validation of commercial antibodies, standardization of evaluation, and scoring systems. Vet Pathol 2024;61:393–401.

Nabeshima A, Matsumoto Y, Fukushi J, et al. Tumour-associated macrophages correlate with poor prognosis in myxoid liposarcoma and promote cell motility and invasion via the HB-EGF-EGFR-PI3K/Akt pathways. Br J Cancer 2015;112:547–55.

Nakajima K, Raz A. T-cell infiltration profile in musculoskeletal tumors. Journal Orthopaedic Research 2021;39:536–42.

Noy R, Pollard JW. Tumor-Associated Macrophages: From Mechanisms to Therapy. Immunity 2014;41:49–61.

Nyström H, Jönsson M, Nilbert M, et al. Immune-cell infiltration in high-grade soft tissue sarcomas; prognostic implications of tumor-associated macrophages and B-cells. Acta Oncologica 2023;62:33–9.

Ohtaki Y, Ishii G, Nagai K, et al. Stromal Macrophage Expressing CD204 is Associated with Tumor Aggressiveness in Lung Adenocarcinoma. Journal of Thoracic Oncology 2010;5:1507–15.

Pardoll DM. The blockade of immune checkpoints in cancer immunotherapy. Nat Rev Cancer 2012;12:252–64.

Petitprez F, De Reyniès A, Keung EZ, et al. B cells are associated with survival and immunotherapy response in sarcoma. Nature 2020;577:556–60.

Pollack SM, He Q, Yearley JH, et al. T-cell infiltration and clonality correlate with programmed cell death protein 1 and programmed death-ligand 1 expression in patients with soft tissue sarcomas. Cancer 2017;123:3291–304.

Razmara AM, Judge SJ, Gingrich AA, et al. Natural Killer and T Cell Infiltration in Canine Osteosarcoma: Clinical Implications and Translational Relevance. Front Vet Sci 2021;8:771737.

Salah S, Lewin JH, Davidson S, et al. Immunoprofiling in alveolar soft part sarcoma. JCO 2017;35:11059–11059.

Salgado R, Denkert C, Demaria S, et al. The evaluation of tumor-infiltrating lymphocytes (TILs) in breast cancer: recommendations by an International TILs Working Group 2014. Annals of Oncology 2015;26:259–71.

Sautès-Fridman C, Petitprez F, Calderaro J, et al. Tertiary lymphoid structures in the era of cancer immunotherapy. Nat Rev Cancer 2019;19:307–25.

Sharma P, Hu-Lieskovan S, Wargo JA, et al. Primary, Adaptive, and Acquired Resistance to Cancer Immunotherapy. Cell 2017;168:707–23.

Sharonov GV, Serebrovskaya EO, Yuzhakova DV, et al. B cells, plasma cells and antibody repertoires in the tumour microenvironment. Nat Rev Immunol 2020;20:294–307.

Smolle MA, Herbsthofer L, Granegger B, et al. T-regulatory cells predict clinical outcome in soft tissue sarcoma patients: a clinico-pathological study. Br J Cancer 2021;125:717–24.

Sorbye SW, Kilvaer T, Valkov A, et al. Prognostic Impact of Lymphocytes in Soft Tissue Sarcomas. PLoS ONE 2011;6:e14611.

Sousa LM, Almeida JS, Fortes-Andrade T, et al. Tumor and Peripheral Immune Status in Soft Tissue Sarcoma: Implications for Immunotherapy. Cancers 2021;13:3885.

Stevenson VB, Klahn S, LeRoith T, et al. Canine melanoma: A review of diagnostics and comparative mechanisms of disease and immunotolerance in the era of the immunotherapies. Front Vet Sci 2023;9:1046636.

Stevenson VB, Gudenschwager-Basso EK, Klahn S, et al. Inhibitory checkpoint molecule mRNA expression in canine soft tissue sarcoma. Vet Comparative Oncology 2023;21:709–16.

Sun G, Liu Y. Tertiary lymphoid structures in ovarian cancer. Front Immunol 2024;15.

Tang T, Huang X, Zhang G, et al. Advantages of targeting the tumor immune microenvironment over blocking immune checkpoint in cancer immunotherapy. Sig Transduct Target Ther 2021;6.

Tazzari M, Bergamaschi L, De Vita A, et al. Molecular Determinants of Soft Tissue Sarcoma Immunity: Targets for Immune Intervention. IJMS 2021;22:7518.

Thorsson V, Gibbs DL, Brown SD, et al. The Immune Landscape of Cancer. Immunity 2018;48:812-830.e14.

Tsagozis P, Augsten M, Zhang Y, et al. An immunosuppressive macrophage profile attenuates the prognostic impact of CD20-positive B cells in human soft tissue sarcoma. Cancer Immunol Immunother 2019;68:927–36.

Tseng WW, Malu S, Zhang M, et al. Analysis of the Intratumoral Adaptive Immune Response in Well Differentiated and Dedifferentiated Retroperitoneal Liposarcoma. Sarcoma 2015;2015:1–9.

Verreck FAW, De Boer T, Langenberg DML, et al. Human IL-23-producing type 1 macrophages promote but IL-10-producing type 2 macrophages subvert immunity to (myco)bacteria. Proc Natl Acad Sci USA 2004;101:4560–5.

Von Rueden SK, Fan TM. Cancer-Immunity Cycle and Therapeutic Interventions-Opportunities for Including Pet Dogs With Cancer. Front Oncol 2021;11:773420.

Yuen GJ, Demissie E, Pillai S. B Lymphocytes and Cancer: A Love–Hate Relationship. Trends in Cancer 2016;2:747–57.

Zhang J, Yan Y, Yang Y, et al. High Infiltration of Tumor-Associated Macrophages Influences Poor Prognosis in Human Gastric Cancer Patients, Associates With the Phenomenon of EMT. Medicine 2016;95:e2636.

Zhu N, Hou J. Assessing immune infiltration and the tumor microenvironment for the diagnosis and prognosis of sarcoma. Cancer Cell Int 2020;20.

## *Experimental Part*

In recent years, increasing attention has been dedicated to the tumor immune microenvironment (TIME), recognized as a key factor in tumor progression and response to immunotherapy. Soft tissue sarcomas (STSs) have traditionally been regarded as poorly immunogenic tumors; however, emerging evidence suggests that certain histological subtypes may produce a more prominent immune response, making them potential candidates for immune-based therapeutic approaches.

In dogs, data on the immune composition of the TIME in different STS histotypes are still limited and often not stratified by tumor type. In this context, the present experimental work aimed to gain deeper insight into the immune landscape of five canine STS subtypes: perivascular wall tumors (PWTs), myxosarcomas, liposarcomas, fibrosarcomas, and leiomyosarcomas.

The first study focused on the immunohistochemical analysis of lymphocyte infiltration, quantifying T-cells (CD3+), B-cells (CD20+), and regulatory T-cells (FoxP3+). This allowed for the assessment of total tumor-infiltrating lymphocyte (TIL) density, the B/T-cell ratio, and the proportion of Tregs within the T-cell population.

The second study concentrated on the macrophage component of the TIME, particularly the infiltration of CD204+ macrophages, a marker associated with alternatively activated (M2-like) macrophages, which are known to exert immunosuppressive and tumor-promoting functions in various neoplastic contexts.

Taken together, the studies aimed to provide a more comprehensive and comparative view of the immune responses characterizing different canine STS histotypes, with the goal of identifying potential associations between immune cell infiltration and tumor behavior.

**Tumor-infiltrating lymphocytes vary in different canine soft tissue sarcoma histological types**

Avallone G, Brigandì E, Tugnoli C, Rigillo A, Bacci B, and Roccabianca P

Vet Pathol. 2025 May;62(3):276-283. doi: 10.1177/03009858241300556.

Epub 2024 Dec 9. PMID: 39651618.

**Abstract**

Soft tissue sarcomas (STSs) are conventionally viewed as poorly immunogenic tumors; however, some human STSs have recently been reported to elicit an immune response, thus representing potential candidates for immunotherapy. Data regarding immune cell infiltrates in canine STSs are limited and reported without tumor-type stratification. The aim of this study was to retrospectively assess tumor-infiltrating lymphocytes (TILs) in canine STSs of 5 different histotypes. Eighty-seven canine STSs were collected: 22 perivascular wall tumors (PWTs), 19 liposarcomas, 17 fibrosarcomas, 16 myxosarcomas, and 13 leiomyosarcomas. The tumors were graded and immunolabeled for CD3, CD20, and FoxP3, and slides were scanned. T-cell, B-cell, Treg, and total TIL densities were quantified with QuPath software and expressed as cells/mm$^2$. The B/T-cells ratio and Treg/T-cell proportions were calculated. Total TIL densities were higher in PWTs and myxosarcomas (median = 225 and 303, respectively). PWTs had higher T-cell density but lower Treg proportion (median = 152 and 7.6% respectively). Myxosarcomas had higher Treg densities and B/T-cell ratios (median = 24.4 and 1.57, respectively). No association with grade was found among STSs as a group. In myxosarcomas, higher grade was significantly associated with higher total TILs, and CD20+ and FoxP3+ cell densities ($p < .05$). The results suggest that PWTs and myxosarcomas may represent the most immunogenic STS types. Myxosarcomas elicit a B-cell and Treg-rich immune response; PWTs stimulate a T-cell-rich

and Treg-poor reaction. The immune system response may contribute to the more aggressive behavior of myxosarcomas and the more indolent course of PWTs.

## Introduction

Soft tissue sarcomas (STSs) comprise a diverse group of neoplasms traditionally regarded as poorly immunogenic (“immunogenically cold”) (Kerrison et al., 2022a).

However, in recent years, there has been a surge of interest in immune therapies, with numerous studies in human medicine suggesting that STSs can indeed incite an immune response (H. Chen et al., 2022; Chen et al., 2020; Dancsok et al., 2019; Jumaniyazova et al., 2023; Nyström et al., 2023). This discovery carries significant implications, particularly as STSs often exhibit resistance to chemotherapy, and treatment options are scarce. Central to these investigations is the study of the tumor immune microenvironment (TIME), focusing on tumor-infiltrating lymphocytes (TILs), tumor-associated macrophages (TAMs), and the expression of immune checkpoints, including the PD-1/PD-L1 (programmed cell death protein 1/ programmed death-ligand 1) axis (H. Chen et al., 2022; Chen et al., 2020; Dancsok et al., 2019; Jumaniyazova et al., 2023; Nyström et al., 2023).

In veterinary medicine, canine melanoma stands out as one of the most extensively studied malignancies regarding the immune TIME, owing to its well-established immunogenicity and allowing for the development of effective immune therapies (Stevenson et al., 2023). While TILs, TAMs, and PD-1/PD-L1 axis expression have been explored in various canine tumors (Muscatello et al., 2022), information specific to canine STSs remains limited. Some studies have reported on TILs and TAMs in canine STSs, correlating their presence with PD-1/PD-L1 axis expression and histologic grade, respectively (Finotello et al., 2021; Stevenson et al., 2023). However, comprehensive data on TIME differences among different canine STS histotypes are lacking. In contrast, in humans, complex karyotype STSs tend to provoke a

stronger immune response compared with translocational STSs, likely due to their higher mutational burden (Dancsok et al., 2019).

While standardized guidelines exist for assessing TILs in other tumor types (e.g. mammary carcinomas) and can be applied to epithelial tumors (Muscatello et al., 2022; Salgado et al., 2015), evaluating TILs in STSs is more complex and thus less standardized. This complexity stems from the relatively low number of TILs in STSs and the absence of clearly delineated supporting stroma in these tumors. Consequently, TIL assessment in STSs typically relies on immunolabeled sections rather than conventional hematoxylin and eosin staining (H. Chen et al., 2022; Dancsok et al., 2019; Stevenson et al., 2023).

The **aim** of this study was to characterize the lymphocytic immune response in canine STSs by evaluating TILs in immunohistochemically labeled sections using image analysis.

Additionally, the study aimed to evaluate the comparison of the immune response in relation to different STS histotypes, grades, and additional histologic parameters.

## Materials and Methods

*Cases Selection*

Formalin-fixed, paraffin-embedded samples of canine STSs with defined histotypes were retrospectively selected from the histologic archive of three institutions according to the following inclusion criteria: STS tumor types included perivascular wall tumor (PWT), fibrosarcoma, liposarcoma, myxosarcoma, and leiomyosarcoma and excluded visceral (e.g., splenic and intestinal) sarcomas; hematoxylin and eosin-stained slides were reviewed by two pathologists to confirm the diagnosis; and the paraffin blocks checked for availability of tissue. The histotype of the tumors was confirmed based on the following criteria:

- PWTs: the presence of at least 1 of the 4 classical perivascular patterns as previously described (Roccabianca et al., 2020), and absence of patterns suggestive of nerve sheath tumors, such as nuclear palisading, Verocay bodies, and tactile like structure.
- Myxosarcoma: spindle to stellate neoplastic cells embedded in various amounts of mucinous matrix, which nevertheless represents the majority of the extracellular matrix of the tumor. Histologic patterns indicative of PWTs and patterns indicative of nerve sheath tumors are absent.
- Liposarcoma: polygonal to spindle cells containing optically empty vacuole(s) with sharp margins, displacing and indenting the nucleus.
- Leiomyosarcoma: intersecting bundles of spindle cells with abundant eosinophilic cytoplasm, scant to absent extracellular matrix, and immunohistochemical (IHC) expression of smooth muscle actin and/or desmin. Some of the leiomyosarcomas were included in a previously published study (Avallone et al., 2022).
- Fibrosarcoma: bundles and streams of spindle cells, perpendicularly arranged or forming herringbone pattern, with moderate amounts of cytoplasm, elongated nuclei, and embedded in various amounts of collagen, which represented the majority of the extracellular matrix of the tumor. These cases were differentiated from leiomyosarcomas by lack of smooth muscle actin expression and a vimentin-only phenotype.

The histologic grade was assigned according to the literature (Avallone et al., 2021; Roccabianca et al., 2020). The amount of necrosis was assessed at the microscope and classified as absent, ≤ 50% of the sarcoma, and > 50% of the sarcoma (Avallone et al., 2021; Roccabianca et al., 2020). Mitotic count (MC) was assessed in 2.37 $mm^2$ in the most cellular and proliferative areas of the tumor (Avallone et al., 2021).

*Immunohistochemistry*

All cases underwent IHC assessment for CD3, CD20, and FoxP3. Three-micrometer-thick sections were dewaxed and rehydrated. Endogenous peroxidase was blocked by immersion in 3% $H_2O_2$ in methanol for 30 minutes. Source, dilution, and retrieval protocols for each antibody are reported in Table 3.1. Each slide was incubated with the primary antibody overnight at 4°C. The reaction was amplified by the avidin-biotin method (Vectastain® Elite ABC-HRP kit, Vector, Burlingame, CA, USA) and visualized with 0.04% 3,3' diaminobenzidine (Code: 10-0048, Histoline Milano, IT) for 4 minutes. Sections were counterstained with hematoxylin, rinsed in tap water, and dehydrated before a coverslip was added. Sections of canine hyperplastic lymph nodes were used as positive controls. Negative controls comprised slides incubated with the omission of the primary antibody, and internal negative controls were constituted by the neoplastic cells of the same samples known to be nonreactive for the specific antibody.

**Table 3.1:** Antibody source and protocols.

| **Antibody** | **Source** | **Retrieval** | **Dilution** |
|---|---|---|---|
| **CD20 (rabbit polyclonal)** | Invitrogen, Rockford, Illinois (USA) | Citrate buffer pH 6, pressure cooker (110°C), 10 min | 1:1000 |
| **CD3 (mouse monoclonal, clone F7.2.38)** | Dako, Glostrup (Denmark) | EDTA buffer pH 8, pressure cooker (110°C), 10 min | 1:1000 |
| **FoxP3 (rat monoclonal, clone FJK-16s)** | eBioscience, Invitrogen, Carlsbad, CA (USA) | Citrate buffer pH 6, pressure cooker (110°C), 20 min | 1:400 |

*IHC Evaluation and Image Analysis*

The IHC slides were scanned with Grundium Ocus 20 (Tampere, Finland) at 20X magnification (0.25 µm/pixel) to obtain a whole-slide image (WSI). The digital images were analyzed with the open-source DIA software QuPath v0.5.0.3. For each marker, positive cells were counted in WSIs. Automatic cell counting was performed using the Positive cell detection tool. As the intensity of labeling varied within the cohort, the IHC and hematoxylin stain estimates for each digitized slide were adjusted (estimate stain vectors tool in QuPath). Analysis was performed starting with manual selection of all the neoplastic tissue in each section and Positive cell detection tool (Analyze → Cell analysis → Positive cell detection → adjust parameters based on Optical Density Sum, Score compartment: Nucleus DAB OD Mean). Default parameters for cell detection were adjusted to best match the outline of lymphocytes, and the results for each case were visually checked by the operator for satisfactory quality of the analysis results (Figure 3.2). CD3+, CD20+, and FoxP3+ cell densities were calculated as number of cells/$mm^2$, as previously reported (H. Chen et al., 2022; Dancsok et al., 2019). The total TIL density was calculated as the total of CD3+ and CD20+ cells. The B-cell/T-cell ratio and the percentage of FoxP3+ T-cells were also calculated. WSIs were searched for the presence of tertiary lymphoid structures (TLSs) that were manually counted if present.

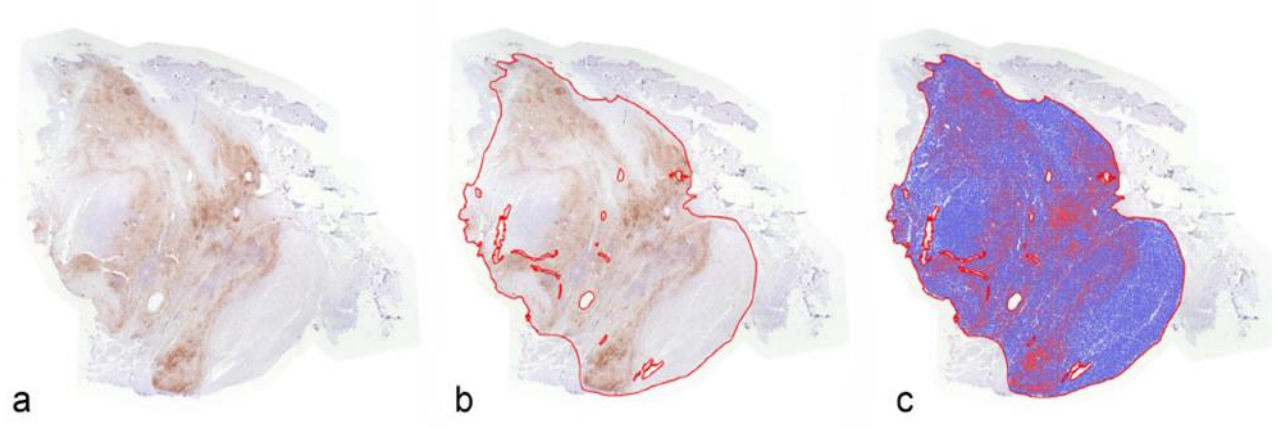


**Figure 3.2:** Image analysis for the quantification of CD3+ cells in a canine perivascular wall tumor. (a) Whole-slide image (WSI), CD3 immunohistochemistry. (b) Selection of the region of interest on the WSI, excluding non-neoplastic tissues, holes, cracks, and folds of the section. (c) Cell detection of CD3+ cells (red) and CD3-negative cells (blue).

*Statistical Analysis*

A Kruskal-Wallis 1-way analysis of variance was used to assess the association of TIL variables with histotype, grade, MC, and amount of necrosis. MC and amount of necrosis were classified according to the STS grading scheme (Avallone et al., 2021). Post-hoc pairwise analysis was performed with the Dwass-Steel-Critchlow-Fligner test. MC was further analyzed as a continuous variable by calculating Spearman's correlation coefficient with the TIL variables. Furthermore, for statistical purposes, grade 2 and grade 3 cases were grouped together, and necrosis was also categorized as present or absent. The Mann-Whitney U test was then used to assess the difference in TIL variables between these groups. Results were considered significant at a threshold of $p \leq .05$. Statistical analyses were conducted using Jamovi (version 2.4.12.0).

## Results

A total of 87 canine STSs were included: 22 PWTs, 19 liposarcomas, 17 fibrosarcomas, 16 myxosarcomas, and 13 leiomyosarcomas. Fifty-six cases were grade 1, 25 were grade 2, and 6 were grade 3. Necrosis was absent in 57 cases, scored ≤ 50% of the tumor in 29 cases, and > 50% of the tumor in 1 case. The median MC was 4 (range 0–63). TLSs were present in 4 cases, ranging from 1 to 3 per section. The median total TIL density was 139 cells/mm$^2$ (range 0–3538). TILs were not detected in 4 cases: 2 liposarcomas and 2 fibrosarcomas. The median density of CD3+ cells was 59.2 cells/mm$^2$ (range 0–3025), and CD3+ cells were absent in 2 fibrosarcomas that were infiltrated by CD20+ cells. The median density of FoxP3+ cells was 9.06 cells/mm$^2$ (range 0–617); FoxP3+ cells were absent in 3 fibrosarcomas and 1 PWT that nevertheless contained CD3+ cells. The median percentage of T-cells that were FoxP3+ was 12.2% (range 0–91.8%). The median density of CD20+ cells was 34.4 cells/mm$^2$ (range 0–686), and CD20+ cells were absent in 2 additional fibrosarcomas that were infiltrated by CD3+ cells. The median B-cell/T-cell ratio was 0.484 (range 0 to 114). TLSs were identified in 2 myxosarcomas and 2 PWTs. Results of the immunohistochemistry are depicted in Figure 3.3 and summarized in Figure 3.4.

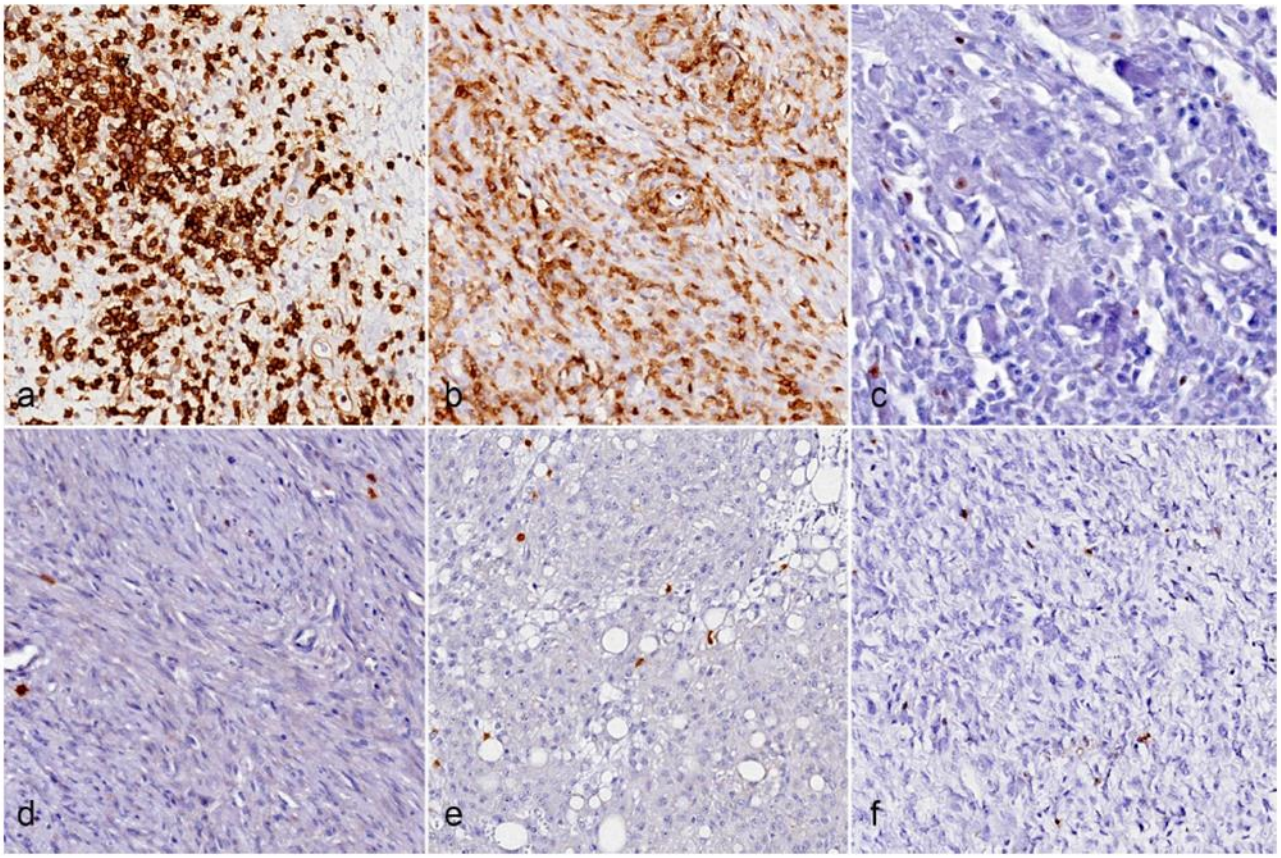


**Figure 3.3:** Tumor-infiltrating lymphocyte immunohistochemistry in canine soft tissue sarcomas. (**a**) Canine myxosarcoma characterized by numerous intratumoral CD20+ cells. CD20 immunohistochemistry (IHC). (**b**) Canine perivascular wall tumor (PWT) infiltrated by numerous CD3+ cells. CD3 IHC. (**c**) Canine PWT, same case as in (b). Numerous lymphocytes infiltrate the tumor and a small proportion express FoxP3. FoxP3 IHC. (**d**) Canine fibrosarcoma infiltrated by rare CD20+ cells. CD20 IHC. (**e**) Canine liposarcoma infiltrated by rare CD3+ cells. CD3 IHC. (**f**) Canine fibrosarcoma infiltrated by rare CD3+ cells. CD3 IHC.

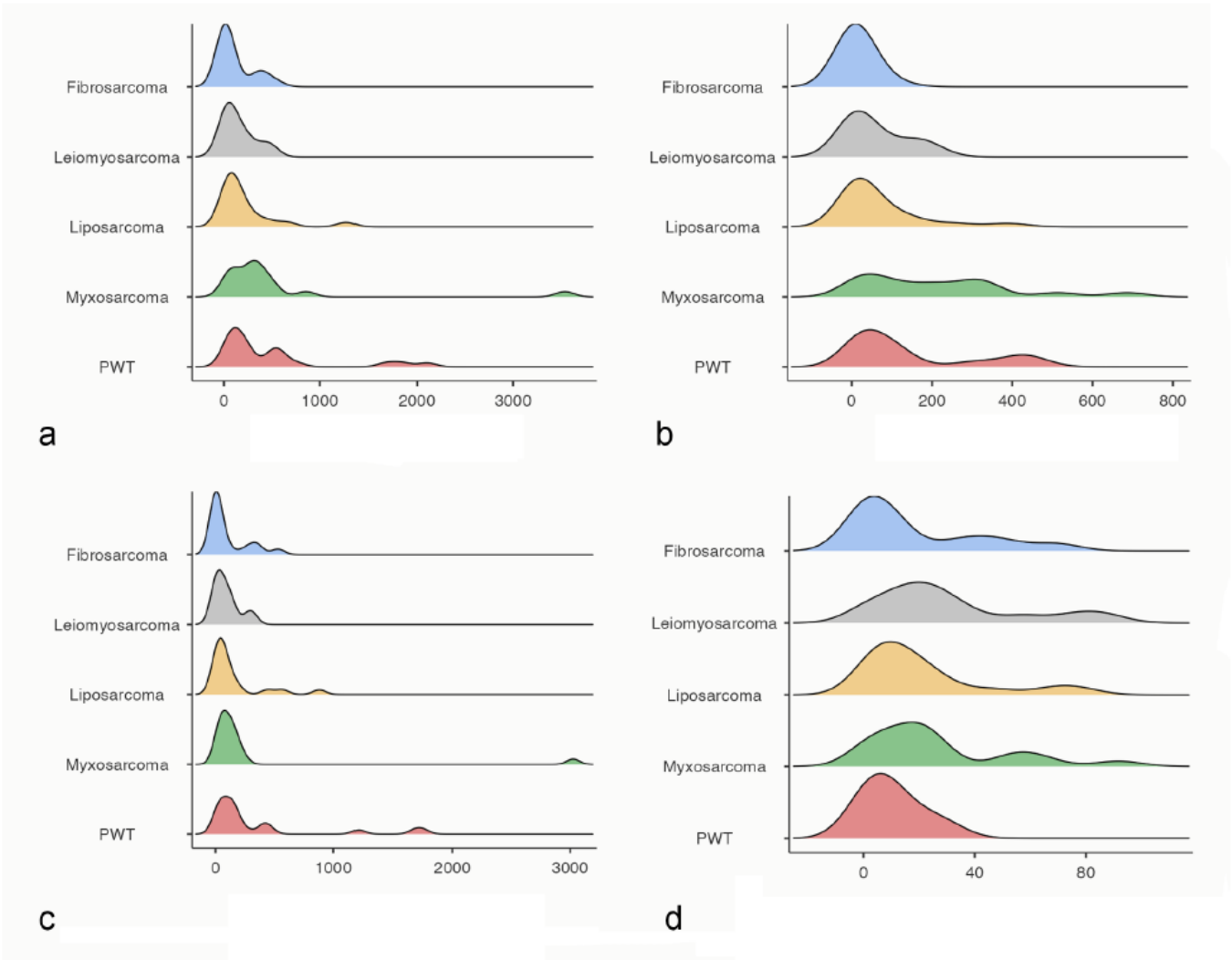


**Figure 3.4:** Total tumor-infiltrating lymphocytes (TILs) and their subpopulations in canine soft tissue sarcomas separated by diagnosis. (a) Total TIL density, (b) CD20+ cell density, (c) CD3+ cell density, and (d) Treg proportion. The densities of total TILs, CD20+, and CD3+ cells are expressed as the number of lymphocytes/mm2, while Treg proportion is expressed as percentage of FoxP3+ cells/ CD3+ cells.

A statistically significant association was found between the diagnosis and the total TIL density; CD20+, CD3+, and FoxP3+ cell density; percentage FoxP3+ T-cells; and the B-cell/T-cell ratio (Table 3.2).

**Table 3.2:** Kruskall-Wallis analysis assessing the difference of tumor infiltrating lymphocyte (TIL) variables in canine soft tissue sarcoma histotypes.

| | **Chi square** | **p** |
|---|---|---|
| **Total TIL density** | 19.52 | <.001 |
| **CD20+ cell density** | 27.51 | <.001 |
| **CD3+ cell density** | 13.80 | .008 |
| **FoxP3+ cell density** | 9.74 | .045 |
| **Treg proportion (% of T-cells)** | 10.43 | .034 |
| **B/T-cell ratio** | 10.65 | .031 |

Based on the Dwass-Steel-Critchlow-Fligner test, the total density of TILs was significantly higher in myxosarcomas and PWTs compared with fibrosarcomas; the CD20+ cell density was significantly higher in myxosarcomas compared with fibrosarcomas and liposarcomas, and in PWTs compared with fibrosarcomas; the CD3+ cell density was significantly higher in PWTs compared with fibrosarcomas; and the B-cell/T-cell ratio was higher in myxosarcomas compared with fibrosarcomas (Table 3.3).

**Table 3.3:** Dwass-Steel-Critchlow-Fligner pairwise comparison of tumor-infiltrating lymphocyte (TIL) variables among soft tissue sarcoma histotypes. Only statistically significant differences are reported.

| | | | W | p |
|---|---|---|---|---|
| **Total TIL density** | Fibrosarcoma | Myxosarcoma | 4.178 | .026 |
| **Total TIL density** | Fibrosarcoma | PWT | 5.047 | .003 |
| **CD20+ cell density** | Fibrosarcoma | Myxosarcoma | 5.8633 | <.001 |
| **CD20+ cell density** | Fibrosarcoma | PWT | 5.7706 | <.001 |
| **CD20+ cell density** | Liposarcoma | Myxosarcoma | 3.9339 | .043 |
| **CD3+ cell density** | Fibrosarcoma | PWT | 4.368 | .017 |
| **B/T-cell ratio** | Fibrosarcoma | Myxosarcoma | 3.970 | .040 |

Considering all histotypes together, no statistically significant associations between grade, MC, amount of necrosis, and TIL variables were observed. Considering each single histotype separately (Figure 3.5), a higher grade of myxosarcomas was significantly associated with higher total TILs (Chi square = 5.309, $p$ = .021) and CD20+ (Chi square = 4.765, $p$ = .029) and FoxP3+ (Chi square = 4.765, $p$ = .029) cell densities; the amount of necrosis was significantly higher in cases with higher CD3+ cell densities (Chi square = 4.25, $p$ = .039). No other statistically significant association was found. Analysis of the association of TIL variables with MC as a continuous variable, amount of necrosis (present vs absent), and grade (I vs II+III) did not find any associations.

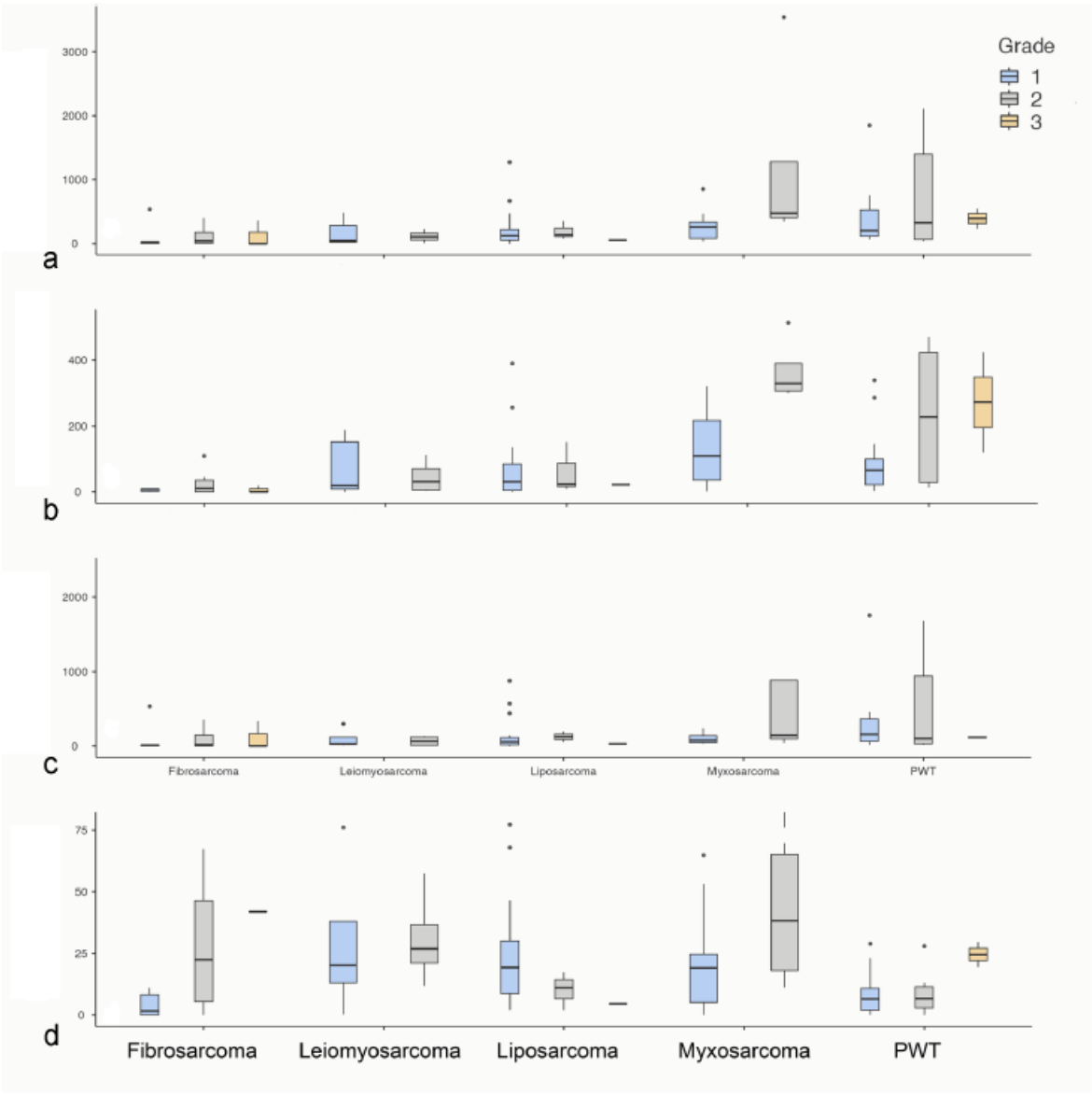


**Figure 3.5:** Total tumor-infiltrating lymphocytes (TILs) and their subpopulations in canine soft tissue sarcomas separated by diagnosis and histological grade. (a) Total TIL density, (b) CD20+ cell density, (c) CD3+ cell density, and (d) Treg proportion. The densities of total TILs, CD20+, and CD3+ cells are expressed as the number of lymphocytes/mm2, while Treg proportion is expressed as percentage of FoxP3+ cells/ CD3+ cells. PWT, perivascular wall tumor.

## Discussion

Interest in TIME and TILs in canine cancers has increased in recent years, mainly because of their therapeutic implications. Among canine neoplasms, the immunogenicity of STSs has not been extensively studied because STSs are traditionally considered poorly immunogenic (H. Chen et al., 2022; Chen et al., 2020; Dancsok et al., 2019; Petitprez et al., 2020). Recently, in human medicine, the paradigm of “immune-cold” STS has been revised and several studies have reported that TIL infiltration can be significant, varies according to sarcoma type, and can be correlated with prognosis and/or response to therapies (H. Chen et al., 2022; Chen et al., 2020; Dancsok et al., 2019; Petitprez et al., 2020).

Defined guidelines are available for breast cancer (Salgado et al., 2015) and have recently been applied also to canine mammary tumors (Muscatello et al., 2022). This protocol relies on a semiquantitative assessment of TILs in the stromal compartment of the tumor on hematoxylin and eosin-stained slides (Salgado et al., 2015) and can be easily translated to other epithelial tumors; however, guidelines for the assessment of TILs in STSs are lacking. Furthermore, the lack of a clearly discernible supporting stroma in STSs and the smaller number of TILs does not allow the application of this approach; thus, some of the studies have assessed TILs by manual count on immunohistochemically labeled slides (Judge et al., 2020; Stevenson et al., 2023). The majority of studies report the amount of TILs as cell numbers in 1 $mm^2$, but the criteria for the choice of the area in which to perform the count and its size vary among studies (Dancsok et al., 2019; Petitprez et al., 2020). In veterinary medicine, the few studies investigating TIME in canine STSs have not specified tumor types and have not provided specific criteria for the quantification of intraneoplastic immune cells (Finotello et al., 2021; Stevenson et al., 2023). Therefore, in order to provide the most reliable data, we quantified TILs with the aid of image analysis on WSIs, to express the density of TILs and TIL subpopulations as the number of cells/$mm^2$ and to characterize TILs

in 5 specific STS histotypes, allowing for a comparison among different tumor types. Overall, TILs were frequently observed in our caseload, with only a few cases being devoid of TILs, the so-called “immune-desert cases”. Nevertheless, high variability in total TIL density and type of lymphocytes were evident. This variability may be partially attributed to the striking differences in the immune response depending on the histotype, but not on the histologic grade, identified in this study. This finding is similar to what has been described in a large study of human STSs, where the grade did not correlate with TIL density and their subpopulation, with the exception of the number of regulatory T-cells (Tregs), which was positively associated with tumor grade (Dancsok et al., 2019). The same study revealed that non-translocation-associated sarcomas had a higher TIL density compared with translocation-associated sarcomas, likely because of their higher tumor mutational burden and probability of producing neo-antigens (Dancsok et al., 2019). Canine myxosarcomas and PWTs had the highest total TIL densities, while fibrosarcomas had the lowest. Leiomyosarcomas and liposarcomas were generally TIL poor, even if the difference with the other tumor types was not statistically significant. Interestingly, in human medicine, myxosarcoma is also the tumor type with the highest TIL density (Smolle et al., 2021). In canine myxosarcomas, TILs were characterized by a relatively high number of B-cells, with a B-cell/T-cell ratio of almost 1.6, and a median proportion of Tregs of 20% of T-cells. Increased B-cell infiltration has been found to be associated with prolonged survival and better prognosis in some human STSs (Petitprez et al., 2020). Their role has not been fully elucidated, but it seems to be related to the presence of TLSs and their role in neo-antigen presentation, stimulating a cytotoxic T-cell response (Nyström et al., 2023). Hence, the finding of tertiary lymphoid structures is considered prognostically favorable (Petitprez et al., 2020). On the contrary, other studies report that intratumoral TLSs and TAMs may sustain the immunosuppressive niche of STSs in tumor types where B-cells are concentrated in TLSs (Chen et al., 2020). In our caseload, TLSs were present in only 2 myxosarcomas out

of 16, and therefore, no conclusion can be drawn on the role of TLSs. Nevertheless, the overall TIL profile suggests the prevalence of a humoral immune response associated with an immune-suppressive Treg-rich TIME. Further characterization of the myxosarcoma TIME should be performed to better elucidate the role of B-cell infiltration. Notably, considering only the myxosarcoma group, a higher histologic grade was associated with higher TIL, B-cell, and Treg densities. This may suggest that the presence of B-cells and Tregs is associated with a poorer prognosis. Furthermore, it is interesting that myxosarcoma is the tumor type with the highest B-cell density, considering that it has been recently suggested to bear a more aggressive behavior and metastatic potential compared with the other canine STSs (Iwaki et al., 2019). Unfortunately, no grade 3 myxosarcomas were present in our study population, and studies on a larger case series are needed to confirm this result. In PWTs, TILs were characterized by a higher density of B- and T-cells and a lower Treg density compared with other STSs. Furthermore, the B-cell/T-cell ratio was significantly lower in PWTs compared with myxosarcomas, because of a higher proportion of T-cells. Thus, it seems that PWTs elicit a T-cell-rich/Treg-poor immune response that is likely to be cell mediated. Unfortunately, the lack of an anti-CD8 antibody working on formalin-fixed, paraffin-embedded canine tissues prevented further characterization of the T-cell component and did not allow confirmation of this hypothesis. PWTs are the most common STS in the dog and are considered neoplasms with intermediate biological behavior, characterized by low metastatic and variable recurrence rates (Roccabianca et al., 2020). Recurrence of PWTs usually occurs in cases with tumor extension to the histologic tissue margins or histologic tumor-free margins smaller than 3 mm, but a variable proportion of tumors that extend to the tissue margins does not recur (Avallone et al., 2014; LE. Chiti et al., 2021; Roccabianca et al., 2020). While the recurrence of cases with clean margins has been explained with a false negative margin evaluation, that may be linked to the trimming protocol, the nonrecurrence of cases with infiltrated margins has been more difficult to

explain. Based on our results, we hypothesize that the T-cell-rich/Treg-poor immune response may contribute to the control of the residual disease for these cases. This hypothesis is consistent with the finding, in human medicine, of an increased risk of local recurrence in STSs with high Treg density (Smolle et al., 2021). Furthermore, despite the lack of statistical significance, the Treg density and Treg proportion of T-cells were higher in grade 3 PWTs, similar to what has been described in human STSs (Dancsok et al., 2019). Nevertheless, this finding needs further support considering the small number of grade 3 PWTs in this study. Fibrosarcomas were the group of canine STSs with the lowest TIL density and were devoid of significant differences in TIL variables among the different grades. This is similar to what has been reported in a study of fibroblastic sarcoma in humans, where adult-type fibrosarcomas were the STS with the lowest CD4 and CD8-cell density, and myxosarcomas were the ones with the highest density (H. Chen et al., 2022). The same study reported no differences in TIL density among different histologic grades, as occurred in our caseload (H. Chen et al., 2022).

Leiomyosarcomas had a similar TIL density to fibrosarcomas. This agrees with what has been described in human medicine since most soft tissue leiomyosarcomas are immune-low sarcomas (Petitprez et al., 2020). In leiomyosarcomas, as in other human STSs, the presence of TLSs is a favorable prognostic feature (Petitprez et al., 2020). Nevertheless, we did not find TLSs in our canine leiomyosarcoma series. Despite a low TIL density, the Treg proportion of T-cells in fibrosarcomas and leiomyosarcomas increased with the increase of histologic grade, as reported for human STSs (Dancsok et al., 2019). On the contrary, liposarcomas showed a decreased Treg proportion of T-cells in cases with higher grades. This finding may deserve further investigation since liposarcoma is the only sarcoma type in our study with this trend. A possible reason for this discrepancy may be the peculiarity in the architecture of liposarcomas, which can be organized in lobules with supporting stroma as

occurs in epithelial tumors. For this reason, the TIL evaluation protocol used for breast cancer (Amgad et al., 2020; Muscatello et al., 2022), which assesses TIL density only in the supporting stroma, has also been successfully applied to human liposarcomas (Snow et al., 2021). The specific role of stromal TILs should therefore be investigated to better elucidate liposarcoma TIME. Limits of the study include its retrospective nature, which does not allow for knowledge of possible presurgical treatments that could have affected the lymphocytic infiltrate in the tumors. Furthermore, the selection of cases diagnosed mainly based on histologic evaluation led to the exclusion of undifferentiated sarcomas, which could be an interesting topic for further investigations. Summarizing, we characterized the TIL subpopulation density in canine STSs, finding differences among STS histotypes. Myxosarcomas and PWTs seem to be the most immunogenic canine STS types, which elicit very different immune responses: a B-cell/Treg-rich response in myxosarcomas and a T-cell-rich/Treg-poor response in PWTs. These two types of response may contribute to the higher propensity of myxosarcomas to metastasize (Iwaki et al., 2019) and the lack of recurrence in some PWTs with infiltrated margins (Avallone et al., 2014; LE. Chiti et al., 2021a; LE Chiti et al., 2021b). Further studies evaluating TAM density and the expression of the PD-1/PD-L1 axis may add useful information regarding the TIME of canine STSs.

## References


Amgad M, Stovgaard ES, Balslev E, et al. Report on computational assessment of Tumor Infiltrating Lymphocytes from the International Immuno-Oncology Biomarker Working Group. Npj Breast Cancer 2020;6.

Avallone G, Boracchi P, Stefanello D, et al. Canine Perivascular Wall Tumors: High Prognostic Impact of Site, Depth, and Completeness of Margins. Vet Pathol 2014;51:713–21.

Avallone G, Pellegrino V, Muscatello LV, et al. Canine smooth muscle tumors: A clinicopathological study. Vet Pathol 2022;59:244–55.

Avallone G, Rasotto R, Chambers JK, et al. Review of Histological Grading Systems in Veterinary Medicine. Vet Pathol 2021;58:809–28.

Chen H, Liu H, Ai J, et al. PD-1/PD-L1 expression is associated with increased TIM3 expression and tumor-infiltrating T lymphocytes in fibroblastic tumors. Clin Transl Oncol 2022;24:586–96.

Chen L, Oke T, Siegel N, et al. The Immunosuppressive Niche of Soft-Tissue Sarcomas is Sustained by Tumor-Associated Macrophages and Characterized by Intratumoral Tertiary Lymphoid Structures. Clinical Cancer Research 2020;26:4018–30.

Chiti LE, Ferrari R, Boracchi P, et al. Prognostic impact of clinical, haematological, and histopathological variables in 102 canine cutaneous perivascular wall tumours. Vet Comparative Oncology 2021;19:275–83.

Chiti LE, Ferrari R, Roccabianca P, et al. Surgical Margins in Canine Cutaneous Soft-Tissue Sarcomas: A Dichotomous Classification System Does Not Accurately Predict the Risk of Local Recurrence. Animals 2021;11:2367.

Dancsok AR, Setsu N, Gao D, et al. Expression of lymphocyte immunoregulatory biomarkers in bone and soft-tissue sarcomas. Modern Pathology 2019;32:1772–85.

Finotello R, Whybrow K, Scarin G, et al. Correlation between Tumour Associated Macrophage (TAM) Infiltration and Mitotic Activity in Canine Soft Tissue Sarcomas. Animals 2021;11:684.

Iwaki Y, Lindley S, Smith A, et al. Canine myxosarcomas, a retrospective analysis of 32 dogs (2003–2018). BMC Vet Res 2019;15.

Judge SJ, Darrow MA, Thorpe SW, et al. Analysis of tumor-infiltrating NK and T cells highlights IL-15 stimulation and TIGIT blockade as a combination immunotherapy strategy for soft tissue sarcomas. J Immunother Cancer 2020;8:e001355.

Jumaniyazova E, Lokhonina A, Dzhalilova D, et al. Immune Cells in the Tumor Microenvironment of Soft Tissue Sarcomas. Cancers 2023;15:5760.

Kerrison WGJ, Lee ATJ, Thway K, et al. Current Status and Future Directions of Immunotherapies in Soft Tissue Sarcomas. Biomedicines 2022;10:573.

Muscatello LV, Avallone G, Brunetti B, et al. Standardized approach for evaluating tumor infiltrating lymphocytes in canine mammary carcinoma: Spatial distribution and score as relevant features of tumor malignancy. The Veterinary Journal 2022;283–284:105833.

Nyström H, Jönsson M, Nilbert M, et al. Immune-cell infiltration in high-grade soft tissue sarcomas; prognostic implications of tumor-associated macrophages and B-cells. Acta Oncologica 2023;62:33–9.

Petitprez F, De Reyniès A, Keung EZ, et al. B cells are associated with survival and immunotherapy response in sarcoma. Nature 2020;577:556–60.

Roccabianca P, Schulman FY, Avallone G, et al. Surgical Pathology of Tumors of Domestic Animals. vol. 3. 3rd ed. Kiupel M.; 2020.

Salgado R, Denkert C, Demaria S, et al. The evaluation of tumor-infiltrating lymphocytes (TILs) in breast cancer: recommendations by an International TILs Working Group 2014. Annals of Oncology 2015;26:259–71.

Smolle MA, Herbsthofer L, Granegger B, et al. T-regulatory cells predict clinical outcome in soft tissue sarcoma patients: a clinico-pathological study. Br J Cancer 2021;125:717–24.

Snow H, Mitchell C, Hendry S, et al. Characterising the immune microenvironment in liposarcoma, its impact on prognosis and the impact of radiotherapy. Journal of Surgical Oncology 2021;123:117–26.

Stevenson VB, Klahn S, LeRoith T, et al. Canine melanoma: A review of diagnostics and comparative mechanisms of disease and immunotolerance in the era of the immunotherapies. Front Vet Sci 2023;9.

Stevenson VB, Gudenschwager-Basso EK, Klahn S, et al. Inhibitory checkpoint molecule mRNA expression in canine soft tissue sarcoma. Vet Comparative Oncology 2023;21:709–16.

**Characterization of tumor-associated macrophages in canine soft tissue sarcomas reveals histotype-dependent immune microenvironments and correlations with mitotic count and histological grade**

Avallone G., Brigandì E., Rigillo A., Bacci B., Tugnoli C., Roccabianca P.

Vet Pathol. 2026 Jan 11:3009858251409221. doi: 10.1177/03009858251409221.

Epub ahead of print. PMID: 41520222.

## Abstract

The tumor immune microenvironment (TIME) plays a pivotal role in cancer progression, yet its characterization in veterinary oncology remains limited. Eighty-five STS cases, comprising fibrosarcomas, leiomyosarcomas, liposarcomas, myxosarcomas, and perivascular wall tumors (PWTs), were immunohistochemically assessed for Iba-1 (total TAMs) and CD204 (M2-like macrophages) expression, scored by image analysis, and correlated with histological parameters. Iba-1 score was higher in grade 3 STSs compared with grade 1 STSs (W=3.40, *p*=0.043) and in PWTs compared with myxosarcomas (W=6.037, *p*<0.001). CD204 score was lower in PWTs compared with fibrosarcomas (W=5.152, p=0.003), leiomyosarcomas (W=4.394, *p*=0.016), and myxosarcomas (W=4.812, *p*=0.006). Stratifying by STS type, Iba-1 was higher in grade 2 myxosarcomas compared with grade 1 (Mann U=4, *p*=0.018). Iba-1 and CD204 were higher in myxosarcomas with necrosis compared with those without (Mann U=5, *p*=0.026, and Mann U=0, p=0.001, respectively). In PWTs, MC was higher in cases with higher Iba-1 (Spearman's rho=0.438, *p*=0.041) and in cases with lower CD204 (Spearman's rho=-0.459, *p*=0.035). Considering the entire group of STSs, Iba-1 directly correlated with total TILs, T cells, and Tregs. In fibrosarcomas, Iba-1 and CD204 directly correlated with total TILs, T cells, and Tregs. In myxosarcomas, CD204 directly correlated with Tregs. In leiomyosarcomas, Iba-1 score

directly correlated with Tregs and CD204 with T cells and Tregs. In PWTs, B cells directly correlated with Iba-1 and inversely with CD204. These findings suggest the presence of a TIME favoring anti-tumor immunity in PWTs and a pro-tumoral TIME in myxosarcomas, reinforcing the concept that canine STS histotypes elicit distinct immune responses.

**Introduction**

The study of the tumor immune microenvironment (TIME) in veterinary medicine has expanded in the last few years, increasing knowledge of the complex interactions between neoplastic cells and the immune system in domestic animal tumors.

The most studied immune cell types of the TIME are tumor-infiltrating lymphocytes (TILs) and tumor-associated macrophages (TAMs) (Avallone et al., 2025; Dancsok et al., 2020; Finotello et al., 2021; Jumaniyazova et al., 2023; Nyström et al., 2023).

Different types of TILs and TAMs populations may produce a microenvironment that can either favor or inhibit tumor progression, depending on their phenotype and function (Boutilier and Elsawa, 2021; Nyström et al., 2023; Smolle et al., 2021).

The role of TAMs is linked to their activation: classically activated (Type 1) TAMs inhibit tumor progression by inhibition of cell proliferation and causing tissue damage through the secretion of pro-inflammatory cytokines and nitric oxide; alternatively activated (Type 2) TAMs may support neoplastic cell immune evasion as they exhibit typical anti-inflammatory and immunosuppressive functions with poor antigen-presenting capabilities (Boutilier and Elsawa, 2021; Pan et al., 2020).

Recently, the role of TIME in canine soft tissue sarcomas (STSs) has been explored (Avallone et al., 2025; Finotello et al., 2021; VB. Stevenson et al., 2023), suggesting that TIL density and cell type are linked to STS histotype and histological grade (Avallone et al., 2025). Myxosarcomas and perivascular wall tumors (PWTs) are more immunogenic than

other STSs (such as fibrosarcoma, leiomyosarcoma, and liposarcoma) (Avallone et al., 2025). Furthermore, while myxosarcomas seem to have a pro-tumoral TIL infiltrate, PWTs have anti-tumoral TILs (Avallone et al., 2025). Regarding the role of TAMs in canine STSs, information is scarce, with one study reporting an association between total TAM density and mitotic count (MC) (Finotello et al., 2021). Nevertheless, the specific role of Type1 and Type 2 macrophages has not been investigated for canine STSs, and different STS types have not been compared in this regard.

The **aim** of this study was to quantify and characterize TAMs in a case series of canine STSs on immunohistochemically labeled sections using image analysis, and to assess possible associations with STS histotype, histological grade, necrosis, and mitotic count. Results regarding TAMs were also compared with already published data regarding TILs population densities (Avallone et al., 2025).

## Materials & Methods

*Case selection*

Eighty-five cases of canine STSs from the caseload of a previous study on TILs in canine STSs were included based on the availability of sufficient tumor tissue in paraffin blocks. Cases were selected according to the following inclusion criteria: STS tumor types included PWT, fibrosarcoma, liposarcoma, myxosarcoma, and leiomyosarcoma, and excluded visceral (e.g., splenic and intestinal) sarcomas; hematoxylin and eosin-stained slides were reviewed by two pathologists (GA and PR), and appropriate immunohistochemistry was performed when necessary to confirm the diagnosis based on the most recent classification system (Roccabianca et al., 2020).

The histologic grade was assigned according to the literature: the amount of necrosis was assessed microscopically and classified as absent, $\leq$ 50% of the sarcoma, or > 50% of the

sarcoma; MC was assessed in 2.37 $mm^2$ in the most cellular and proliferative areas of the tumor (Roccabianca et al., 2020).

*Immunohistochemistry*

All cases underwent immunohistochemical (IHC) assessment for Iba-1 (pan-histiocytic marker) and CD204 (M2-like macrophages). The source, dilution, and retrieval protocols for each antibody are reported in Table 3.4.

**Table 3.4:** Antibodies and corresponding immunohistochemical protocols used.

| | **Species** | **Clone** | **Dilution** | **Antigen retrieval** |
|---|---|---|---|---|
| **Iba-1** | Goat | Polyclonal (code NB100-1028) | 1:2000 | pH6 citrate; 2 microwave cycles, 5 minutes each at 750 W |
| **CD204** | Mouse | SRA-E5P6 | 1:800 | pH9 EDTA; 3 microwave cycles, 5 minutes each at 750 W |

Three-micrometer-thick sections (one section per case) were dewaxed and rehydrated. Endogenous peroxidase was blocked by immersion in 3% $H_2O_2$ in methanol for 30 minutes. Each slide was incubated with the primary antibody overnight at 4°C.

The reaction was amplified by the avidin-biotin method (Vectastain® Elite ABC-HRP kit, Vector, Burlingame, CA, USA) and visualized with 0.04% 3,3′-diaminobenzidine (Code: 10-0048, Histoline, Milano, IT) for 4 minutes. Sections were counterstained with hematoxylin, rinsed in tap water, dehydrated, and coverslipped. Sections of a canine hyperplastic lymph node were used as positive controls. Negative controls comprised slides incubated with omission of the primary antibody, and internal negative controls were constituted by the neoplastic cells of the same samples, known to be non-reactive for the specific antibody.

*Image analysis*

The immunohistochemically stained slides were scanned with Grundium Ocus 20 (Tampere, Finland) at 20x magnification (0.25 µm/pixel) to obtain a whole-slide image (WSI). Digital slides (.svs files) were analyzed using the open-source digital image analysis (DIA) software QuPath v0.5.0.1.2 Expression of Iba-1 and CD204 was quantified by calculating the positively stained area as a percentage of the total tumor area. The tumor region of interest (ROI) was manually selected and included all the neoplastic tissue present in the section. Areas of necrosis, hemorrhage, and non-involved vessels were excluded. Pixel classification was performed on the ROI to detect the positively stained area by following the workflow: Classify → Pixel Classification → Train Pixel Classification on the highly representative image of the project. The resulting classifier was then applied to the entire dataset, and the outcomes for each case were visually reviewed by the operator to ensure adequate quality of the analysis.

The percentage of tumor area labeled for Iba-1 (Iba-1 score) was used to quantify total TAMs, and the percentage of tumor area labeled for CD204 (CD204 score) was used to quantify M2-like TAMs. The log10-transformed ratio between Iba-1 score and CD204 score (log10 Iba-1/CD204 score) was also calculated to assess the proportion of M2-like macrophages in the total TAMs.

*Statistical analysis*

Descriptive analysis was performed by calculating the mean, standard deviation, median, minimum, and maximum values. The Kruskal-Wallis test was used to assess differences in TAM scores across histotype, grade, MC, and amount of necrosis. MC and amount of necrosis were classified according to the STS grading scheme. Post-hoc pairwise analysis was performed with Dwass-Steel-Critchlow-Fligner test. MC was also analyzed as a

continuous variable by calculating Spearman's correlation coefficient with TAMs scores. Furthermore, for statistical purposes, grade 2 and grade 3 cases were also grouped together, necrosis was also categorized as present or absent, and the Mann-Whitney U test was used to assess the differences of TAM scores between these groups. Spearman's correlation coefficient was used to quantify the association between TAM scores and the previously published TIL scores (Avallone et al., 2025). All the analyses were performed for the entire case series and for each STS histotype separately. Results were considered statistically significant at a threshold of $p \leq 0.05$. Statistical analyses were conducted using Jamovi (version 2.4.12.0).

**Results**

Eighty-five STSs were included based on selection criteria: 56 were grade 1, 23 grade 2, and 6 grade 3. There were 18 fibrosarcomas (8 grade 1, 7 grade 2, and 3 grade 3), 13 leiomyosarcomas (9 grade 1, 3 grade 2, and 1 grade 3), 17 liposarcomas (14 grade 1 and, 3 grade 2), 15 myxosarcomas (11 grade 1, and 4 grade 2), and 22 perivascular wall tumors (PWTs) (14 grade 1, 6 grade 2, and 2 grade 3). Necrosis was absent in 56 cases, present in less than 50% of the tumor in 28 and present in more than 50% of the tumor in 1. Median MC was 4 (range, 0-63). Cells expressing Iba-1 and cells expressing CD204 were evidenced in all cases (Figures 3.6 (1-10)). Median Iba-1 score was 4.58% (range, 0.31%-71.3%), median CD204 score was 0.886% (range, 0.001%-23%), median log10 Iba-1/CD204 score was 0.59 (range, -1.83 to -9.73). Descriptive statistics of continuous variables stratified by histotype are reported in Table 3.5.

**Table 3.5:** Statistically significant correlations of Tumor Associated Macrophages (TAMs) scores with tumor infiltrating lymphocytes (TILs) densities in canine soft tissue sarcoma (STS).

| | | | **Total TILS density** | **CD20+ cell density** | **CD3+ cell density** | **FoxP3+ cell density** |
|---|---|---|---|---|---|---|
| **STS** | Iba-1 score | Spearman's rho | 0.292 | | 0.309 | 0.332 |
| | | p-value | 0.007 | | 0.004 | 0.002 |
| **Fibrosarcomas** | Iba-1 score | Spearman's rho | 0.573 | | 0.705 | 0.602 |
| | | p-value | 0.016 | | 0.002 | 0.011 |
| | CD204 score | Spearman's rho | 0.542 | | 0.612 | 0.589 |
| | | p-value | 0.025 | | 0.009 | 0.013 |
| **Leiomyosarcoma** | Iba-1 score | Spearman's rho | | | | 0.753 |
| | | p-value | | | | 0.004 |
| | CD204 score | Spearman's rho | | | 0.687 | 0.566 |
| | | p-value | | | 0.012 | 0.047 |
| **Perivascular wall tumors** | Iba-1 score | Spearman's rho | | 0.525 | | |
| | | p-value | | 0.013 | | |
| | CD204 score | Spearman's rho | | -0.446 | | |
| | | p-value | | 0.039 | | |

* p < .05, ** p < .01, *** p < .001

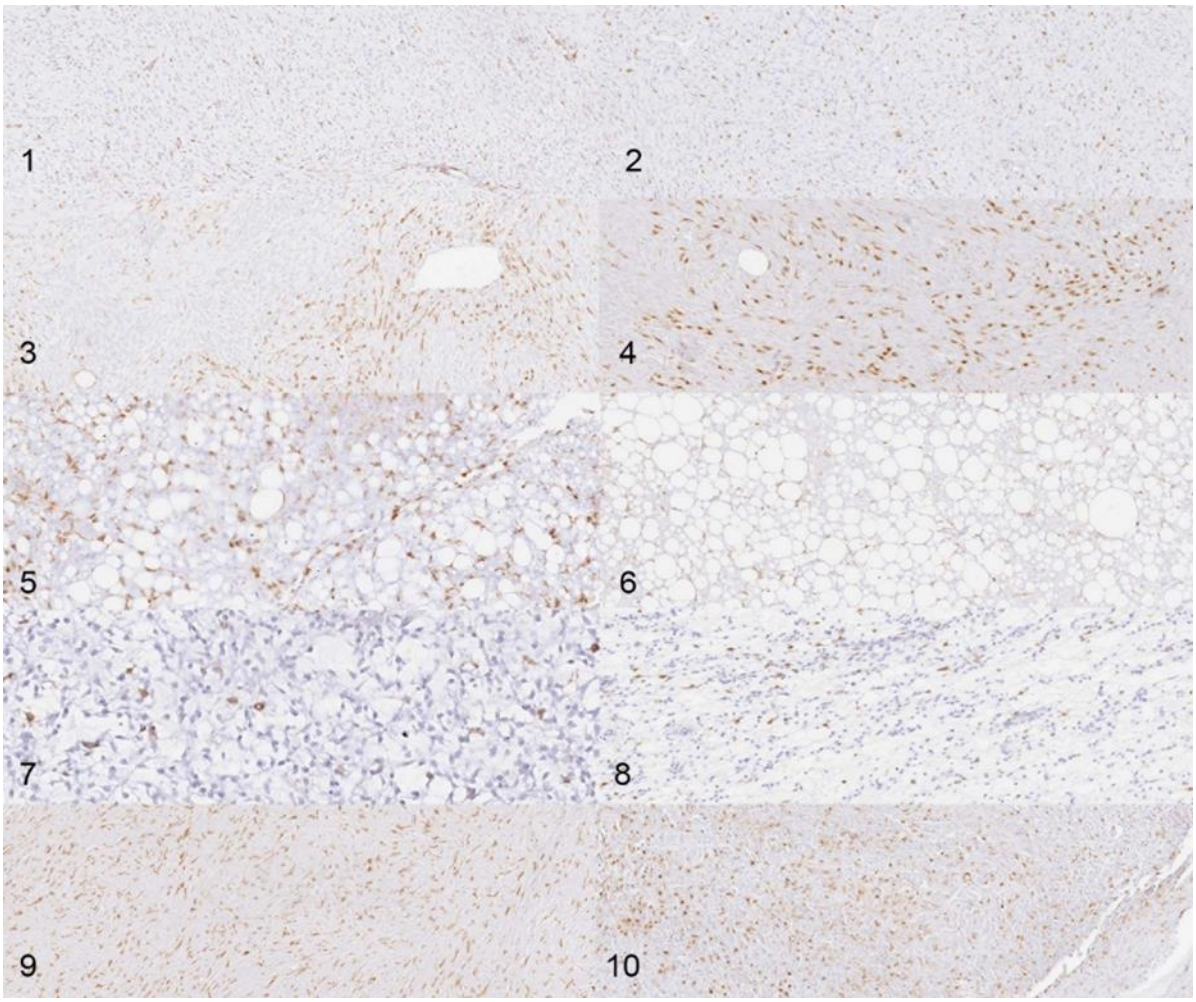


**Figure 3.6 (1-10):** Immunohistochemistry for tumor associated macrophages (TAMs) in canine soft tissue sarcomas. 1) Canine fibrosarcoma characterized by a moderate to high number of Iba-1 and 2) CD204 positive macrophages. 3) Canine leiomyosarcoma containing numerous Iba-1 and 4) CD204 positive macrophages. 5) Canine liposarcoma characterized by a moderate number of Iba-1 positive and 6) CD204 positive macrophages. 7) Canine myxosarcoma containing scant Iba-1 and 8) CD204 positive macrophages. 9) Canine perivascular wall tumor containing numerous Iba-1 and 10) CD204 positive macrophages.

Considering all the STS types together, all three TAMs scores were significantly associated with diagnosis (Figure 3.7): total Iba-1 score was higher in PWTs compared with myxosarcomas (W = 6.037, $p < 0.001$); CD204 score was lower in PWTs compared with fibrosarcomas (W = 5.152, $p = 0.003$), with leiomyosarcomas (W = 4.394, $p = 0.016$), and with myxosarcomas (W = 4.812, $p = 0.006$); log10 Iba1/CD204 score was higher in PWTs compared with fibrosarcomas (W = 5.113, $p = 0.003$), with leiomyosarcomas (W = 4.876, p = 0.005), with liposarcomas (W = 4.206, $p = 0.025$), myxosarcomas (W = 6.168, $p < 0.001$). Iba-1 score was significantly associated with grade, being higher in grade 3 STSs (median = 8.91%) compared with grade 1 STSs (median = 2.97%) (W = 3.40, $p = 0.043$) (Figure 3.7).

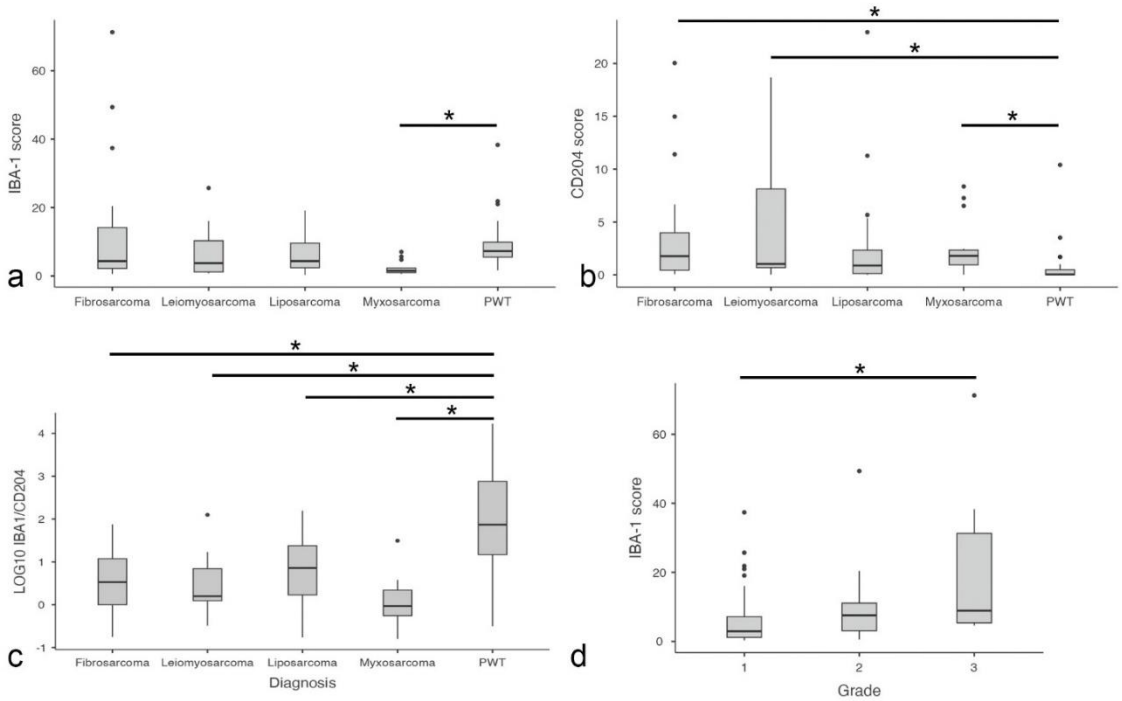


**Figure 3.7:** Boxplots depicting the associations of TAMs scores with histotype and histological grade in canine STSs. a) Iba-1 score is significantly higher in PWTs compared with myxosarcoma; b) CD204 score is significantly lower in PWTs compared with fibrosarcomas, leiomyosarcomas and myxosarcomas; c) Log10 Iba-1/CD204 score is significantly higher in PWTs compared with all the other histotypes; d) Iba-1 score is significantly higher in grade 3 STSs compared with grade one.

This significant association was confirmed merging grade 2 and 3 cases being higher (median = 7.58%) than in grade 1 cases (Mann U = 511, $p$ = 0.005).

Analyses were repeated stratifying by STS type, revealing a significant association of Iba-1 score with grade in myxosarcomas, being higher in grade 2 (median = 5.21%) compared with grade 1 cases (median = 1.16%) (Mann U = 4, $p$ = 0.018). A similar trend, although not statistically significant, was found for CD204 score (grade 1 median = 1.18%; grade 2 median = 4.51%) (Mann U = 7, $p$ = 0.056). In myxosarcomas, cases with necrosis had a significantly higher Iba-1 (median = 5.21%) and CD204 score (median = 6.90%) compared with cases without necrosis (iba-1 median score = 1.16%; CD204 median score = 1.18%) (Mann U = 5, $p$=0.026, and Mann U = 0, $p$ = 0.001 respectively) (Figure 3.8).

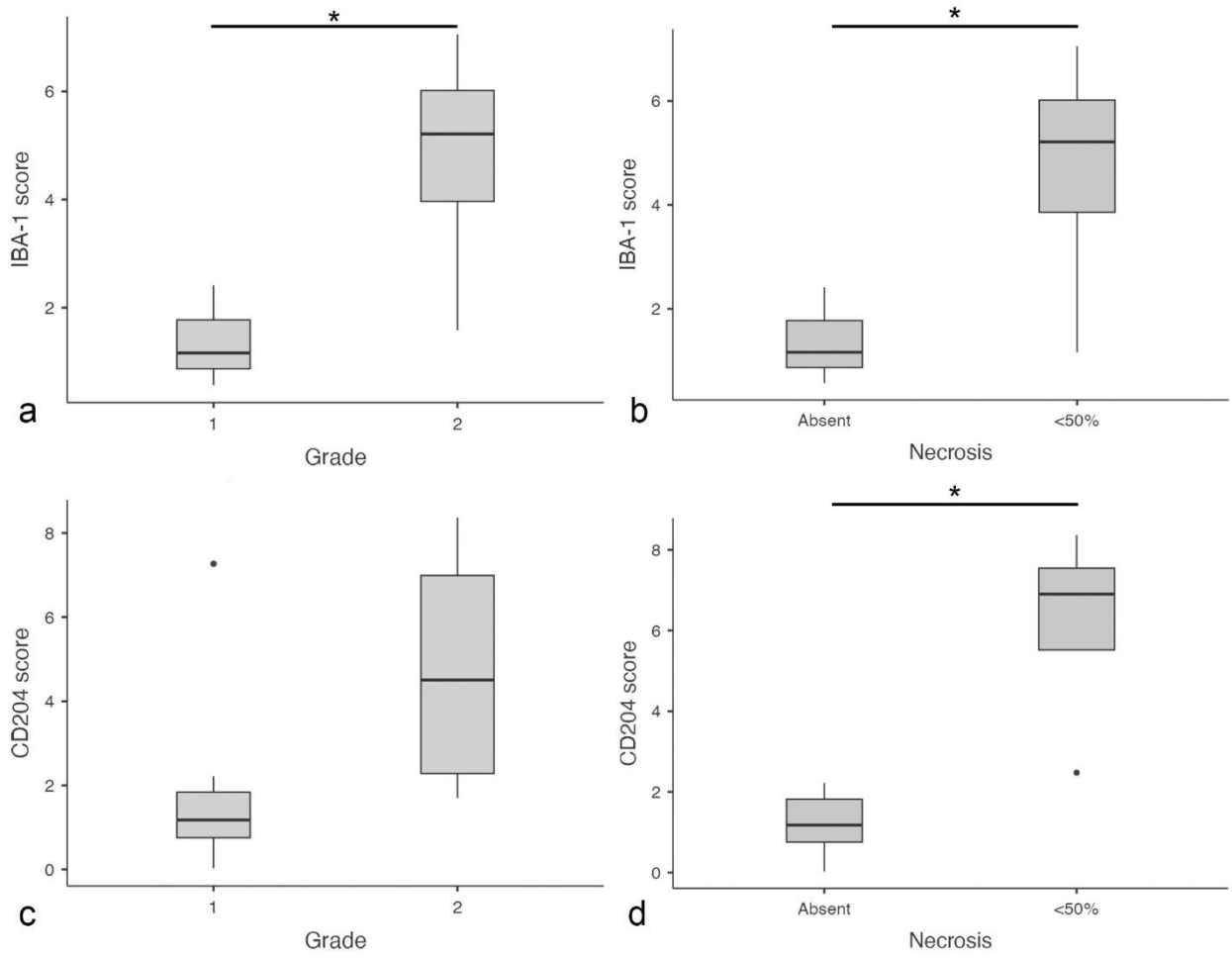


**Figure 3.8:** Boxplots depicting the associations of Tumor Associated Macrophages (TAMs) scores with histological grade and necrosis in canine myxosarcomas. a) and b) Iba-1 score is significantly higher in grade 2 myxosarcomas compared with grade 1 and in cases with necrosis compared with cases without; c) and d) CD204 score is significantly higher in grade 2 myxosarcomas compared with grade 1 and in cases with necrosis compared with cases without. Grade 3 myxosarcomas were not present in this case series.

In PWTs, MC was significantly correlated with TAM scores (Figure 3.9), being higher in cases with higher Iba-1 score (Spearman's rho = 0.438, $p$ = 0.041) and in cases with lower CD204 score (Spearman's rho = -0.459, $p$ = 0.035).

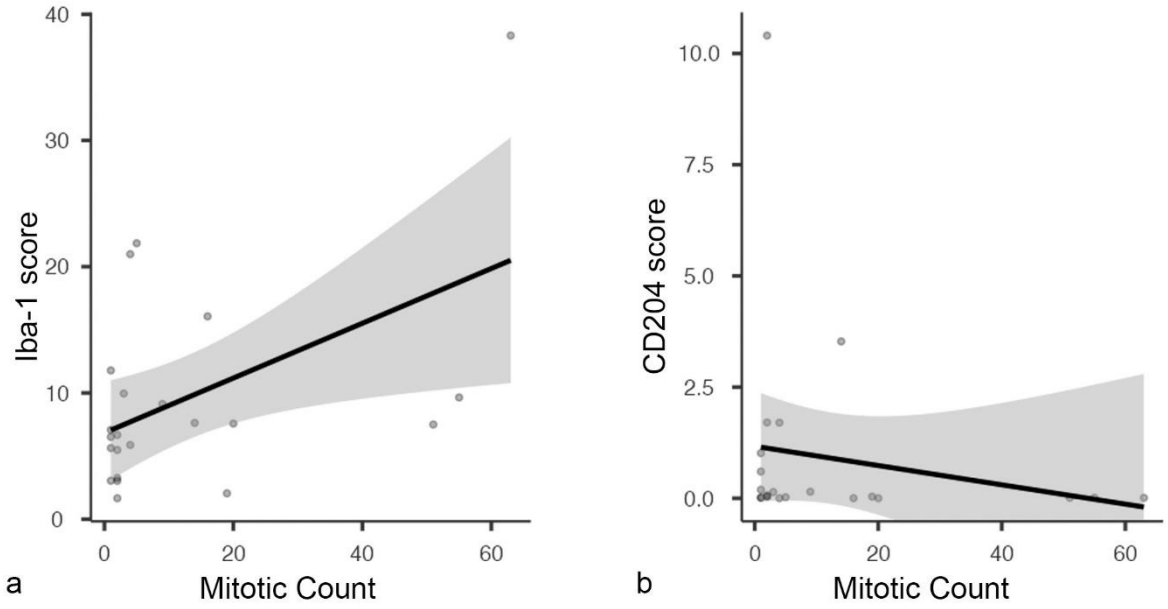


**Figure 3.9:** Scatterplots depicting the direct correlation of mitotic count with Iba-1 score (a) and the inverse correlation with CD204 score (b), in canine perivascular wall tumors.

Considering the entire group of STSs, Iba-1 score was directly correlated with total TILs, T-cell and Treg density (Figure 3.10). In fibrosarcomas, Iba-1 and CD204 scores were directly correlated with total TILs, T-cell and Treg densities (Figure 3.10). In myxosarcomas, CD204 score was directly correlated with Treg density. In leiomyosarcomas, Iba-1 score was directly correlated with Treg density and CD204 score with T-cell and Treg densities. In PWTs, B-cell density was directly correlated with Iba-1 score and inversely correlated with CD204 score (Figure 3.11).

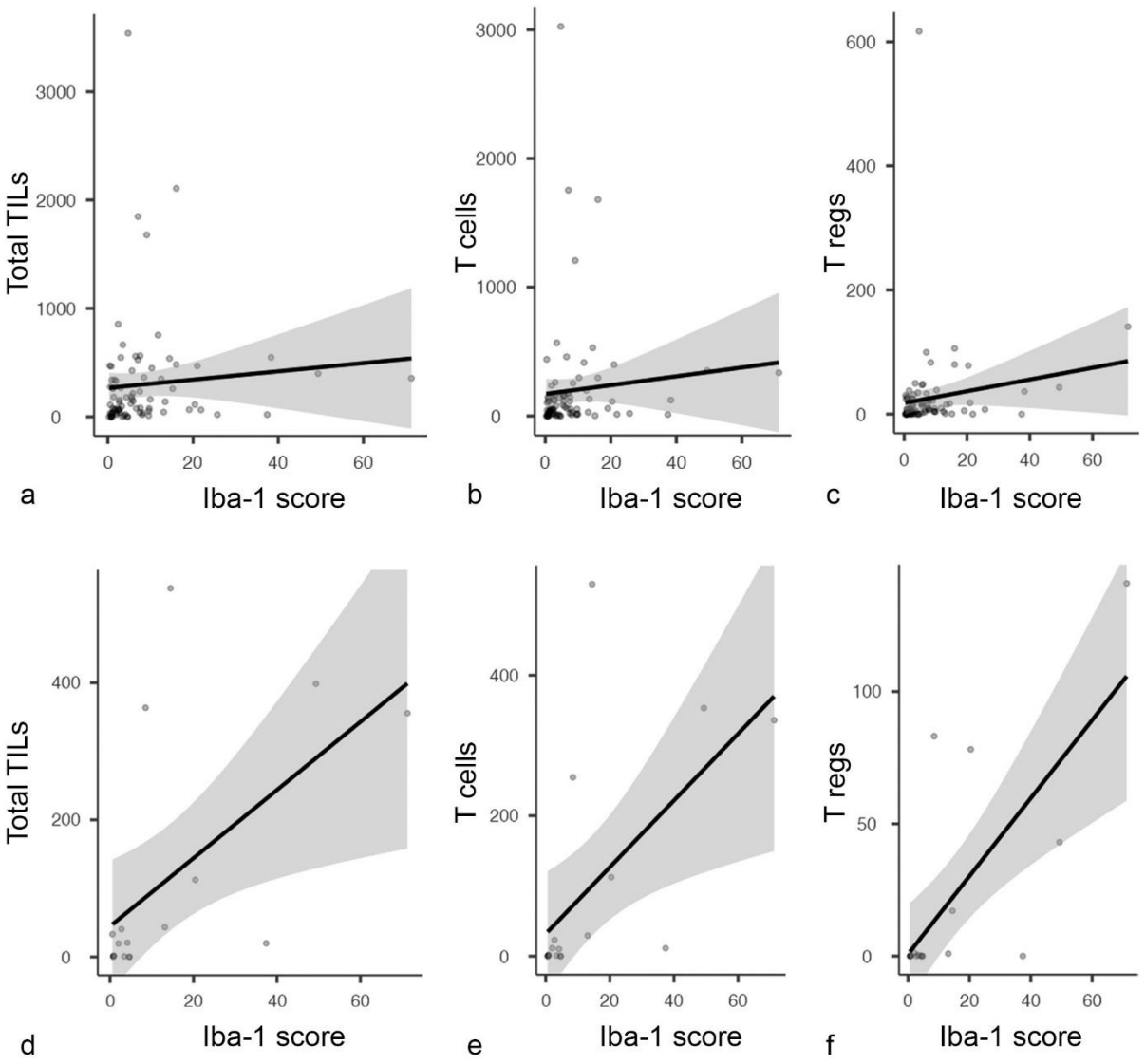


**Figure 3.10:** Scatterplots depicting the correlation of Iba-1 score with tumor infiltrating lymphocytes (TILs) densities in canine soft tissue sarcomas (STSs) and in fibrosarcomas. a, b and c) In canine STSs Iba-1 score is directly correlated with total TILs, T cell and T reg densities. Similar but stronger correlation is found in fibrosarcomas (d, e and f).

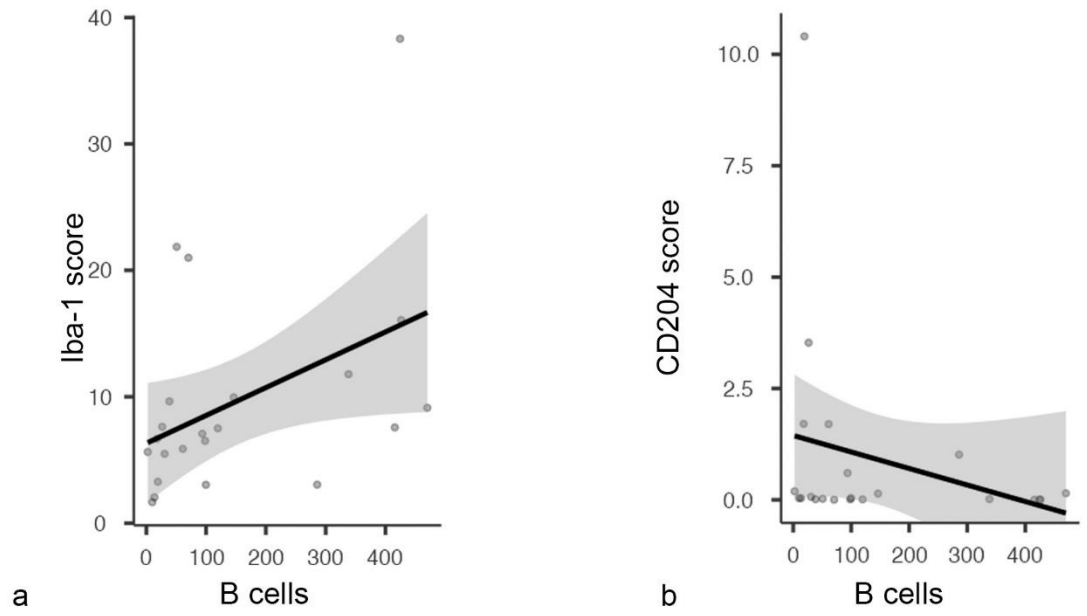


**Figure 3.11:** Scatterplots depicting the correlation of Iba-1 score with CD20 positive cell density in canine perivascular wall tumors. a) Iba-1 score is directly correlated with CD20 positive cell density; b) CD204 score is inversely correlated with CD20 positive cell density.

**Discussion**

In this study, we were able to quantify Iba-1 (total TAMs) and CD204 (M2-like macrophages) positive TAMs in canine STSs, revealing a variation of TAM type and quantity according to STS type.

Specifically, PWTs exhibited lower CD204 scores compared to myxosarcomas, leiomyosarcomas, and fibrosarcomas, as well as a lower proportion of CD204-positive cells relative to the Iba-1 score when compared with all other STS types. Additionally, total TAM density was higher in PWTs than in myxosarcomas. These findings align with previous observations suggesting that PWTs possess a TIME more effective at restraining tumor growth, whereas myxosarcomas - despite their immunogenicity - tend to develop a pro-tumoral TIME. These results seem to support the hypothesis that different types of canine

soft tissue sarcomas elicit a different type of immune response, as suggested in a previous study on TILs (Avallone et al., 2025).

A direct association of total TAMs with histological grade was also found, but it was not paralleled by a similar association of M2-like macrophages. This discrepancy is interesting, since M2 macrophages have been associated with poor prognosis in other canine tumor types, such as oral melanoma (Porcellato et al., 2022) and mammary tumors (Seung et al., 2018).

One possible explanation could be that STSs with higher grade may bear a greater tumor mutational burden, thus stimulating a more intense immune response, but that TAMs do not shift to a M2-like phenotype. This hypothesis is also based on a study in human medicine (Dancsok et al., 2020), which described a higher macrophage infiltration in sarcomas with complex karyotype compared with translocation sarcomas (Seung et al., 2018).

When considering the entire case series, no association was found between MC and infiltration of Iba-1-positive macrophages. This result contrasts with a previous study that reported an increase in Iba-1 positive macrophages in STSs with higher MC (Finotello et al., 2021).

However, when stratifying the analysis by tumor type, a significant association between MC and Iba-1 score emerged in perivascular wall tumors (PWTs), but not in other STS subtypes. The discrepancy between our findings and those of Finotello and colleagues (Finotello et al., 2021) may be attributed to differences in case composition. In our study, a balanced number of cases was included for each STS subtype, whereas in Finotello's study, the specific tumor types were not specified (Finotello et al., 2021).

Given that PWTs represent the most common canine STSs (Roccabianca et al., 2020), it is likely that this subtype was overrepresented in their cohort, potentially influencing the overall results.

When comparing the TAM scores with the previously published data on TIL densities in the same cases (Avallone et al., 2025), a statistically significant correlation of Iba-1 score was found with total TIL density, T-cell density, and Treg density. This may suggest that the lymphocytic immune response to cancer cells is sustained by TAMs.

When stratifying the cohort of cases by diagnosis, the association of total Iba-1 score and histological grade was evident only in myxosarcomas, in which CD204 score showed a similar trend even if not significant. Furthermore, in this tumor type, both TAM scores are associated with presence of necrosis and CD204 score with Treg density. Taken together, these results suggest that TAMs infiltrating myxosarcomas bear a putative prognostic significance and may support the pro-tumoral lymphocytic infiltrate previously described (Avallone et al., 2025). On the other hand, grade and necrosis were not associated with TAMs scores in other STS types, suggesting that the prognostic significance of TAMs is less relevant in these tumors than in myxosarcomas.

Nevertheless, in fibrosarcomas and leiomyosarcomas, which are characterized by a low TIL density (Avallone et al., 2025), CD204 score (indicative of M2-like macrophages) was directly correlated with T-cell and Tregs density. This correlation may be additional evidence of a pro-tumoral TIME in these poorly immunogenic tumor types.

In PWTs, grade and necrosis were not associated with TAMs, but Iba-1 score was directly correlated with MC. As previously discussed, this is consistent with a previous study on TAMs infiltration in canine STSs, which likely included a high number of PWTs (Finotello et al., 2021). Additionally, an inverse correlation of MC with CD204 score was found. These

results seem to suggest that in PWTs with higher MC there is an increase in non-M2 TAMs, putatively M1 TAMs with anti-tumor functions, which may be related to an increased mutational burden in highly proliferative PWTs.

Furthermore, in PWTs, B-cell density directly correlated with Iba-1 scores and inversely correlated with CD204 scores. This finding suggests that, in this context, B cells play an anti-tumor role together with T-cells and non-M2 TAMs. As a matter of fact, B cells can have a dual role within the tumor microenvironment: on one hand, they may contribute to the establishment of an immunosuppressive milieu, impairing the immune system's capacity to recognize and eliminate tumor cells; on the other hand, they can enhance anti-tumor immunity by providing co-stimulatory signals, promoting T cell activation and clonal expansion, and activating other immune cells, thereby supporting tumor suppression (Milardi and Lleo, 2023; Yang et al., 2024). This appears to be the case for B cells in PWTs, which exist within a microenvironment enriched in T cells but poor in Tregs and M2-like macrophages, potentially contributing to a more effective anti-tumor response.

In conclusion, this study confirms that the composition of TAMs in canine STSs is highly dependent on tumor histotype. PWTs exhibited a distinctive immune microenvironment characterized by a high total TAM density, a lower proportion of M2-like (CD204-positive) macrophages, higher mitotic counts, and an immune infiltrate enriched in T-cells but poor in Tregs - features suggestive of a more effective anti-tumor immune response. In this context, B cells also appear to play an anti-tumoral role alongside other immune cells. Conversely, myxosarcomas demonstrated a pro-tumoral TIME, with TAM infiltration correlating with tumor grade, necrosis, and Treg density. In fibrosarcomas and leiomyosarcomas, the association of M2-like macrophages with lymphocytic infiltrates in otherwise poorly immunogenic tumors suggests a role for TAMs in sustaining an immunosuppressive milieu. Collectively, these findings reinforce the concept that different STS histotypes elicit distinct

immune responses, with TAMs assuming context-specific functions. Additionally, the study highlights the utility and efficiency of image analysis on whole-slide images for accurately quantifying immune cell infiltrates, offering an objective tool for assessing the tumor microenvironment that would be challenging to evaluate through conventional methods alone.

**References**

Avallone G, Brigandì E, Tugnoli C, et al. Tumor-infiltrating lymphocytes vary in different canine soft tissue sarcoma histological types. Vet Pathol 2025;62:276–83.

Boutilier AJ, Elsawa SF. Macrophage Polarization States in the Tumor Microenvironment. IJMS 2021;22:6995.

Dancsok AR, Gao D, Lee AF, et al. Tumor-associated macrophages and macrophage-related immune checkpoint expression in sarcomas. OncoImmunology 2020;9:1747340.

Finotello R, Whybrow K, Scarin G, et al. Correlation between Tumour Associated Macrophage (TAM) Infiltration and Mitotic Activity in Canine Soft Tissue Sarcomas. Animals 2021;11:684.

Jumaniyazova E, Lokhonina A, Dzhalilova D, et al. Immune Cells in the Tumor Microenvironment of Soft Tissue Sarcomas. Cancers 2023;15:5760.

Milardi G, Lleo A. Tumor-Infiltrating B Lymphocytes: Promising Immunotherapeutic Targets for Primary Liver Cancer Treatment. Cancers 2023;15:2182.

Nyström H, Jönsson M, Nilbert M, et al. Immune-cell infiltration in high-grade soft tissue sarcomas; prognostic implications of tumor-associated macrophages and B-cells. Acta Oncologica 2023;62:33–9.

Pan Y, Yu Y, Wang X, et al. Tumor-Associated Macrophages in Tumor Immunity. Front Immunol 2020;11:583084.

Porcellato I, Sforna M, Lo Giudice A, et al. Tumor-Associated Macrophages in Canine Oral and Cutaneous Melanomas and Melanocytomas: Phenotypic and Prognostic Assessment. Front Vet Sci 2022;9:878949.

Roccabianca P, Schulman FY, Avallone G, et al. Surgical Pathology of Tumors of Domestic Animals. vol. 3. 3rd ed. Kiupel M.; 2020.

Seung B-J, Lim H-Y, Shin J-I, et al. CD204-Expressing Tumor-Associated Macrophages Are Associated With Malignant, High-Grade, and Hormone Receptor–Negative Canine Mammary Gland Tumors. Vet Pathol 2018;55:417–24.

Smolle MA, Herbsthofer L, Granegger B, et al. T-regulatory cells predict clinical outcome in soft tissue sarcoma patients: a clinico-pathological study. Br J Cancer 2021;125:717–24.

Stevenson VB, Gudenschwager-Basso EK, Klahn S, et al. Inhibitory checkpoint molecule mRNA expression in canine soft tissue sarcoma. Vet Comparative Oncology 2023;21:709–16.

Yang H, Zhang Z, Li J, et al. The Dual Role of B Cells in the Tumor Microenvironment: Implications for Cancer Immunology and Therapy. IJMS 2024;25:11825.

## Chapter 4: Proteomic Profiling

### *Chapter Overview*

Soft tissue sarcomas (STSs) represent a complex and heterogeneous group of neoplasms, for which the diagnosis and the prognosis are often challenging due to the overlap of histological features. At the same time, classification is crucial as different histotypes show distinct behaviors (Bode-Lesniewska et al., 2025; Dell'Anno et al., 2024; Husain and Verma, 2011; Patrichi and Gurzu, 2024; Yamaguchi and Hasegawa, 2004). This biological heterogeneity is reflected in differences on local recurrence, metastasis and response to therapy (Burns et al., 2020).

Consequently, the exploration of molecular markers – encompassing genomic alterations, proteomic profiles, and immunohistochemical signatures – offers valuable insights into tumor classification, aggressiveness, metastatic potential and clinical outcome.

At the genomic level, STSs fall into two main categories: those with complex karyotypes or those with simple karyotypes and specific genetic alterations such as translocations and point mutations (Burns et al., 2023).

In Ewing sarcoma, synovial sarcoma, and myxoid liposarcoma, up to 90-95% of tumors harbor a translocation specific to the tumor type (Mitelman et al., 2007). In contrast, in sarcomas such as fibrosarcoma, leiomyosarcoma, or high-grade pleomorphic sarcoma, specific genetic alterations are not found, exhibiting a more complex karyotype (Bovée and Hogendoorn, 2010; De Álava, 2007).

As regards translocations in sarcomas, the *EWSR1* or the *FUS* gene are involved in many tumor types (Bovée and Hogendoorn, 2010), acting as aberrant transcription factors dysregulating gene expression patterns initiating tumor formation (Janknecht, 2005).

Some STSs can also carry specific somatic mutations, such as KIT mutations in gastrointestinal stromal tumors (GISTs) (Bovée and Hogendoorn, 2010).

Or else, some sarcomas are characterized by a highly reproducible amplification such as the amplification of *CDK4* and *MDM2* in well-differentiated and dedifferentiated liposarcoma (Dei Tos et al., 2000; Sandberg, 2004).

Interestingly, the STS genotype influences the composition of the TIME (Jumaniyazova et al., 2023) as totality of somatic mutations, accounting for the tumor mutational burden (TMB), correlates with both the tumor's ability to induce anticancer immunity and its response to immunotherapy (Tazzari et al., 2021; Tuccitto et al., 2019). From the other side, TMB can allow tumor cells to escape immune surveillance, which is considered a key hallmark of cancer (Hanahan and Weinberg, 2011). Thus, in contexts favorable to an immune response, such as tumors with high TMB, cancer genotypes may sometimes evolve to acquire genetic alterations that promote immunosuppression (Tazzari et al., 2021).

In general, it can be stated that sarcomas with complex karyotypes are characterized by highly immune-infiltrated tumor microenvironments (so-called 'immune hot'), which may serve as a predictor of a favorable response to immunotherapy (Keenan et al., 2019; Tazzari et al., 2021).

For this reason, genetic STSs profiling and characterization of the specific mutations that play a key role in their tumorigenesis, can be a driving force for understanding tumor pathogenesis and identifying accurate diagnostic markers (Tazzari et al., 2021).

Despite the insights gained from large-scale genomic and epigenomic profiling of STSs, these data provide only a partial view of tumor biology (Chibon et al., 2010; Koelsche et al., 2021; Nacev et al., 2022; Thorsson et al., 2018), as they do not directly reflect protein

function or dynamic cellular processes and entirely explain the phenotypic diversity observed across different subtypes (Burns et al., 2023).

In this context, proteomic approaches have become increasingly important, offering complementary and sometimes contrasting perspectives that refine the molecular understanding of sarcomas biology (Burns et al., 2020) (Figure 4.1).

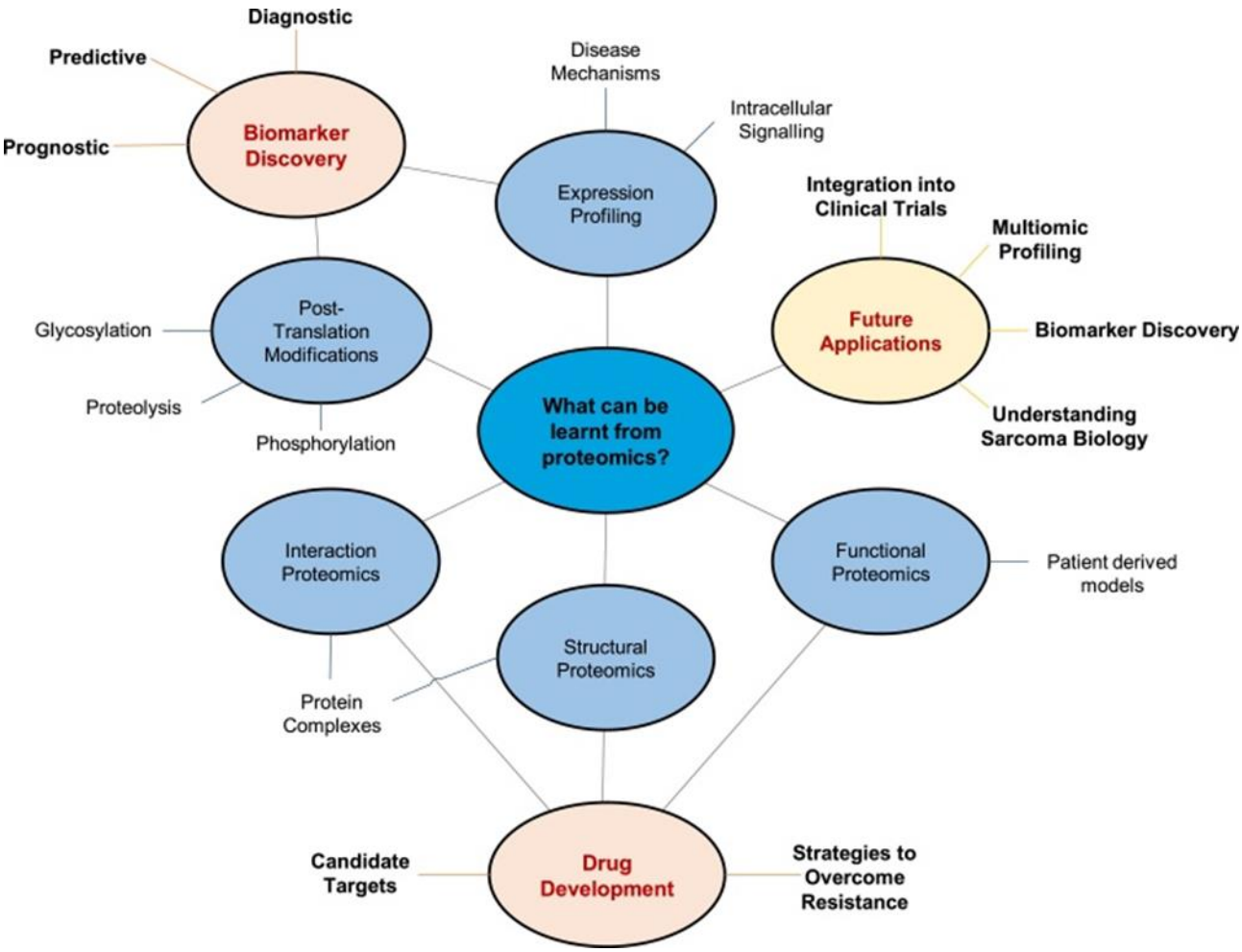


**Figure 4.1**: The potential benefit of using proteomic approaches in sarcoma research (Burns et al., 2020).

## References


Bode-Lesniewska B, Dürr HR, Wang D, et al. Rethinking the Prognostic Role of Necrosis in Soft-Tissue Sarcoma: Multidisciplinary Insights from the Sarcoma Academy. Cancers 2025;17:1779.

Bovée JVMG, Hogendoorn PCW. Molecular pathology of sarcomas: concepts and clinical implications. Virchows Arch 2010;456:193–9.

Burns J, Wilding CP, Krasny L, et al. The proteomic landscape of soft tissue sarcomas. Nat Commun 2023;14.

Burns J, Wilding CP, L Jones R, et al. Proteomic research in sarcomas - current status and future opportunities. Semin Cancer Biol 2020;61:56–70.

Chibon F, Lagarde P, Salas S, et al. Validated prediction of clinical outcome in sarcomas and multiple types of cancer on the basis of a gene expression signature related to genome complexity. Nat Med 2010;16:781–7.

De Álava E. Molecular pathology in sarcomas. Clin Transl Oncol 2007;9:130–44.

Dei Tos AP, Doglioni C, Piccinin S, et al. Coordinated expression and amplification of theMDM2,CDK4, andHMGI-C genes in atypical lipomatous tumours. J Pathol 2000;190:531–6.

Dell'Anno F, Giugliano R, Listorti V, et al. A Review on Canine and Human Soft Tissue Sarcomas: New Insights on Prognosis Factors and Treatment Measures. Vet Sci 2024;11:362.

Hanahan D, Weinberg RA. Hallmarks of Cancer: The Next Generation. Cell 2011;144:646–74.

Husain N, Verma N. Curent concepts in pathology of soft tissue sarcoma. Indian J Surg Oncol 2011;2:302–8.

Janknecht R. EWS–ETS oncoproteins: The linchpins of Ewing tumors. Gene 2005;363:1–14.

Jumaniyazova E, Lokhonina A, Dzhalilova D, et al. Immune Cells in the Tumor Microenvironment of Soft Tissue Sarcomas. Cancers 2023;15:5760.

Keenan TE, Burke KP, Van Allen EM. Genomic correlates of response to immune checkpoint blockade. Nat Med 2019;25:389–402.

Koelsche C, Schrimpf D, Stichel D, et al. Sarcoma classification by DNA methylation profiling. Nat Commun 2021;12:498.

Mitelman F, Johansson B, Mertens F. The impact of translocations and gene fusions on cancer causation. Nat Rev Cancer 2007;7:233–45.

Nacev BA, Sanchez-Vega F, Smith SA, et al. Clinical sequencing of soft tissue and bone sarcomas delineates diverse genomic landscapes and potential therapeutic targets. Nat Commun 2022;13:3405.

Patrichi AI, Gurzu S. Pathogenetic and molecular classifications of soft tissue and bone tumors: A 2024 update. Pathology - Research and Practice 2024;260:155406.

Sandberg AA. Updates on the cytogenetics and molecular genetics of bone and soft tissue tumors: liposarcoma. Cancer Genetics and Cytogenetics 2004;155:1–24.

Tazzari M, Bergamaschi L, De Vita A, et al. Molecular Determinants of Soft Tissue Sarcoma Immunity: Targets for Immune Intervention. IJMS 2021;22:7518.

Thorsson V, Gibbs DL, Brown SD, et al. The Immune Landscape of Cancer. Immunity 2018;48:812-830.e14.

Tuccitto A, Shahaj E, Vergani E, et al. Immunosuppressive circuits in tumor microenvironment and their influence on cancer treatment efficacy. Virchows Arch 2019;474:407–20.

Yamaguchi U, Hasegawa T. [Pathological evaluation of soft tissue sarcoma for diagnosis, prognosis and treatment]. Gan To Kagaku Ryoho 2004;31:1340–5.

## *Experimental Part*

### Proteomic profiling of canine STSs

#### Introduction

Proteomic analysis has emerged as a powerful tool to distinguish histotypes, identify diagnostic and prognostic biomarkers, and highlight biological pathways involved in tumor pathogenesis (Burns et al., 2023).

Recent large-scale proteomic profiling studies from The Clinical Proteomic Tumor Analysis Consortium (CPTAC) have highlighted the importance of protein-level analysis, empowering advanced molecular classification and the identification of clinically relevant cancer drivers and biomarkers (Huang et al., 2021; Mertins et al., 2016; Petralia et al., 2020; Satpathy et al., 2021; Zhang et al., 2014)

Proteomic studies aimed at first at distinguishing histotypes but also at identifying candidate biomarkers which could improve diagnosis, patient stratification, prognosis and prediction of clinical course (Burns et al., 2020). Moreover, proteins represent the targets of many therapies; therefore, the identification of key proteins or protein modifications driving sarcoma progression, metastasis, and resistance to current treatments may reveal new paths for therapy (Burns et al., 2020).

Proteomics describes the study of entire protein complement in a system of interest, which is not limited to the study of protein abundance, but also involves analysis of protein regulation and activity, including the detection of protein isoforms, post-translational modifications, and protein-protein interactions (Burns et al., 2020).

The primary objective of this project was to characterize the proteomic profile of canine STSs, in order to achieve a deeper understanding of their pathogenesis, identifying potential

biomarkers and assessing the biological pathways involved through comparative analysis of different histological subtypes.

To this end, a collaboration has been established with **The Institute of Cancer Research** (London, UK) and the Molecular and Systems Oncology Group, coordinated by Professor Paul Huang. The group specialized in the study of human STSs, with a particular focus on explaining how signaling proteins regulate tumor progression and drug resistance in cancer, employing a wide range of molecular techniques (Burns et al., 2023, 2020). Specifically, the laboratory is engaged in the following research areas:

- Proteomic profiling in large retrospective cohorts (Burns et al., 2023).
- Investigation of mechanisms underlying therapeutic resistance (Elms et al., 2025; Jenks et al., 2018; Vyse et al., 2018; Wilding et al., 2019).
- Development of patient-derived models for drug screening (Kerrison et al., 2022b; Pasquali et al., 2025).
- Identification of prognostic and predictive biomarkers for patient stratification and early diagnosis (Merry et al., 2021).

An advantage of the protocol adopted by the group is the ability to perform the methodology on FFPE samples. This capability, which remains relatively uncommon, is crucial for rare tumors such as STSs, where the availability of fresh tissue samples is limited, and access to FFPE archived material represents a valuable opportunity for large-scale studies. Furthermore, the technique allows for the extraction of the majority of proteins from the samples without the necessity to preselect a specific target, thereby enabling broad-spectrum analysis.

## Materials & Methods

A cohort of 80 STSs was selected from the archives of the Department of Veterinary Medical Sciences (DIMEVET), University of Bologna, Department of Veterinary Medicine and Animal Sciences, University of Milan and i-VET Veterinary Diagnostic Laboratory, comprising 16 samples for each histotype: perivascular wall tumors (PWTs), myxosarcomas, fibrosarcomas, leiomyosarcomas, and liposarcomas. FFPE samples required a specific protein extraction procedure capable of reversing the formalin-induced protein cross-links induced by formalin fixation (Burns et al., 2023).

The protocol could be summarized as follows and a schematic representation of the workflow is presented in Figure 4.2.

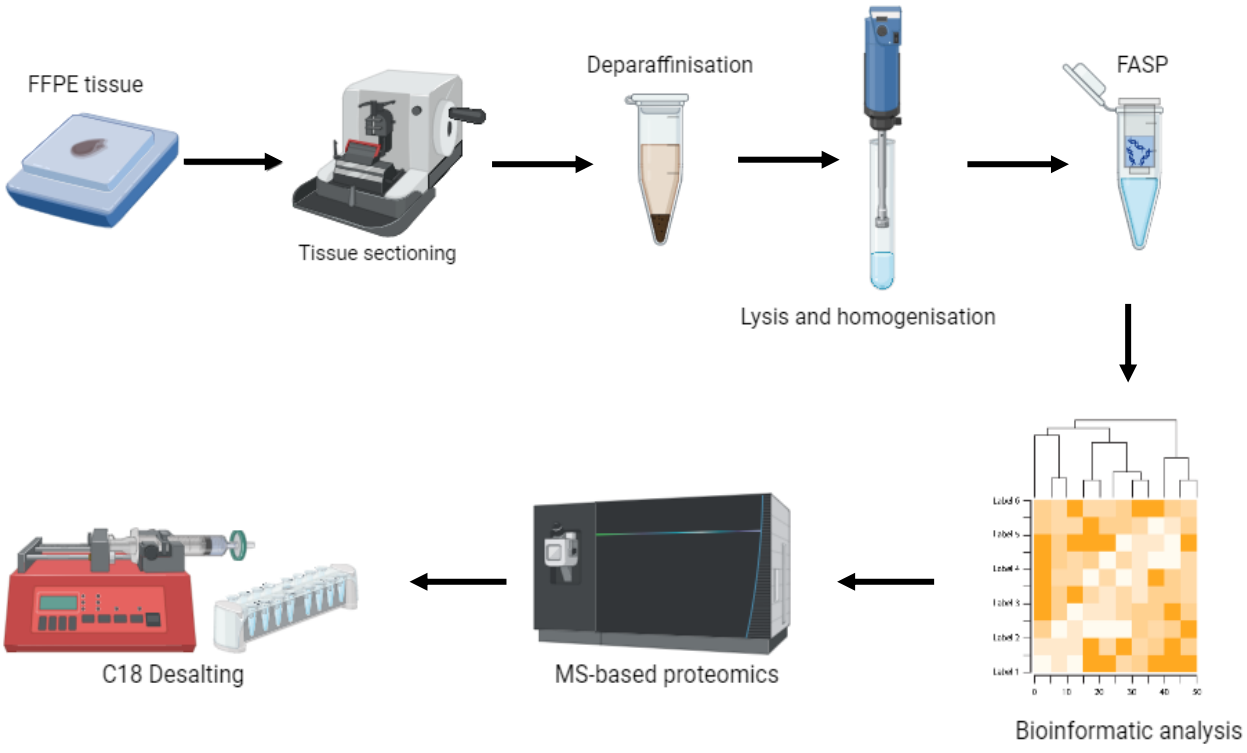


**Figure 4.2:** Schematic representation of protein extraction and quantification workflow from FFPE tissue.

*Sectioning of FFPE tissue*

Each FFPE sample was sectioned with a section depth of 300µm. Tissue sections were placed in an Eppendorf tube of known weight in order to determine the exact weight of the samples.

*Deparaffination*

Deparaffination includes xylene passages, which dissolves the paraffin, followed by decreasing concentrations of ethanol (100%, 96% and 70%) to gradually rehydrate the tissue.

In each passage 1 ml of solvent (xylene or ethanol) was added, vortexed, shaken for 10 minutes, centrifuged for 5 minutes at 14000g and the supernatant was removed. For xylene, same passages were repeated 3 times, and for ethanol two times each.

Following these steps, all samples were completely dried in the SpeedVac for 30 minutes and subsequently weighed.

*Homogenization*

Based on the final weight of each sample, an appropriate volume of PTS buffer was added (200 µl/mg) to ensure effective protein solubilization and stabilization. Homogenization was performed with a homogenizer, to mechanically disrupt the tissue. The homogenization procedure consisted of three rounds of 30 seconds each, alternated with 30-second pauses. Between samples, the homogenizer probe was cleaned by sequential washes with methanol and distilled water. All homogenized samples underwent sonication by adding ice for 10 minutes to further lyse cells and shear gDNA. The lysate was transferred into a single Eppendorf to mix up all the proteins and, to reverse formalin cross-links, incubated at 95°C for 1 hour and on a Thermomixer at 80°C for 2 hours at 750 rpm.

Following incubation, samples were allowed to return to room temperature and centrifugated at 14000g for 15 minutes at 4°C. Finally, supernatant was collected and protein concentration measured, as required by following step.

*Protein quantification*

This step is necessary to define the amount of lysate to be collected and processed in the subsequent steps.

Protein quantification was performed using the Pierce BCA Protein Assay Microplate Procedure, following the manufacturer's instructions. Samples were mixed with the reagent at a 10:200 µl ratio in a 96-well plate, each measured in triplicate, using BSA to generate the standard curve. Once quantified, lysate was stocked at -80°C.

*FASP (Filter-Aided Sample Preparation)*

The lysate is loaded into a device containing a membrane that retains molecules larger than 10 kDa, allowing smaller contaminants to pass through. The urea buffer employed at this stage assists in removing residual contaminants. The procedure was performed as follow:

- PTS buffer was added to the lysate to reach an amount divisible by 750 µl (the volume of lysate required for each round).
- Urea buffer (3 ml for each round) and 750 µl of lysate for each round were added in an Amicon 4 filter column and centrifuged at 14000g for 15 minutes (as many times as required to achieve purification of the entire lysate volume).
- The volume retained in the filter was transferred in a smaller Amicon 0.5 by adding 200 µl of Urea buffer and centrifuged at 14000g for 15 minutes.

*Reduction and Alkylation*

The filtered lysate was incubated with a reducing agent (Dithiothreitol (DTT)) and an alkylating agent (Iodoacetamide (IAA)), both required to prepare proteins for enzymatic digestion.

Samples were incubated at 56 °C for 1 hour with a concentration of 10 mM DTT, breaks disulfide bonds between cysteines, converting them into free thiol groups (-SH). After that, samples were incubated at room temperature for 45 minutes in the dark with a concentration

of 55 mM of IAA, that reacts with the free thiol groups generated by DTT, forming alkylated cysteines.

*Enzymatic digestion*

Preparation for enzymatic digestion consisted of adding 100 µl of trypsin-ABC solution (Ammonium Bicarbonate) to each sample, followed by passage through the filter over 5 rounds of centrifugation.

Trypsin-ABC solution provides a slightly basic environment, optimal for proteolytic enzymes.

Enzymatic digestion was performed by adding 2 µg of trypsin incubated at 37°C overnight in heatblock. This digestion produces peptides of optimal length for mass spectrometry (8-20 amino acids).

Following the overnight incubation, the lysate was transferred to a new collection tube by passing it through the filter by centrifugation (14000 g for 10 minutes) three times with the addition of 200 µl ABC. The enzymatic digestion was stopped by adding 60 µl of 10% TFA (trifluoroacetic acid, a strong organic acid commonly used to inactivate proteolytic enzymes). To the resulting lysate, 340 µl of 0,1% TFA were added to reach a final volume of 1 ml. The solution was adjusted to have a pH around 4.

*Desalting*

This step involves loading digested peptides in a C18 column (hydrophobic stationary phase) using an infusion pump. The procedure was carried out as follows:

- 5 ml of 60% acetonitrile (ACN) + 0.1% TFA were passed through the column to activate and equilibrate the C18 resin, ensuring efficient binding of peptides.
- 10 ml of 0.1% TFA were used to wash the column and remove residual organic solvent, preparing it for sample loading.

- 1 ml of the peptide sample was loaded on the column for binding.
- 10 ml of 0.1% TFA were used to wash away salts and other impurities, while the peptides remained bound to the C18 resin.
- 3 ml of 60% ACN + 0.1% TFA were used to elute the purified peptides, which were collected and then dried completely using the SpeedVac (approximately 3 hours).

*Peptide Quantification*

This step is required to establish the concentration of peptides to be subjected to mass spectrometry. The procedure was identical to that used for protein quantification.

Based on the peptide concentration, a specific volume of the lysate (corresponding to 10 µg of peptides) was transferred to a new tube to perform Liquid Chromatography and Tandem Mass Spectrometry (LC-MS/MS). This analytical technique enables the accurate identification and quantification of peptides through measurement of the mass-to-charge ratio of generated ions. Tandem mass spectrometry allows selective fragmentation of peptides, providing structural information for reconstructing their amino acid sequence and detecting post-translational modifications.

Raw data obtained from LC-MS/MS are processed using a quantitative proteomics software (MaxQuant), in combination with protein search engines, such as UniProt, for protein identification and quantification.

Following data normalization, appropriate biostatistical tests are applied to determine whether samples cluster according to histotype or other clinicopathological parameters.

**Results from the Pilot Study**

Preliminary results from a pilot study conducted prior to the establishment of the collaboration have provided a promising basis for the success of the project. Specifically, 8 samples from four different histotypes of canine STSs were analyzed. The analysis revealed

a distinct clustering pattern for perivascular wall tumors and liposarcomas, whereas myxosarcomas and leiomyosarcomas displayed a more heterogeneous clustering, suggesting greater variability in their proteomic profiles (Figure 4.3).

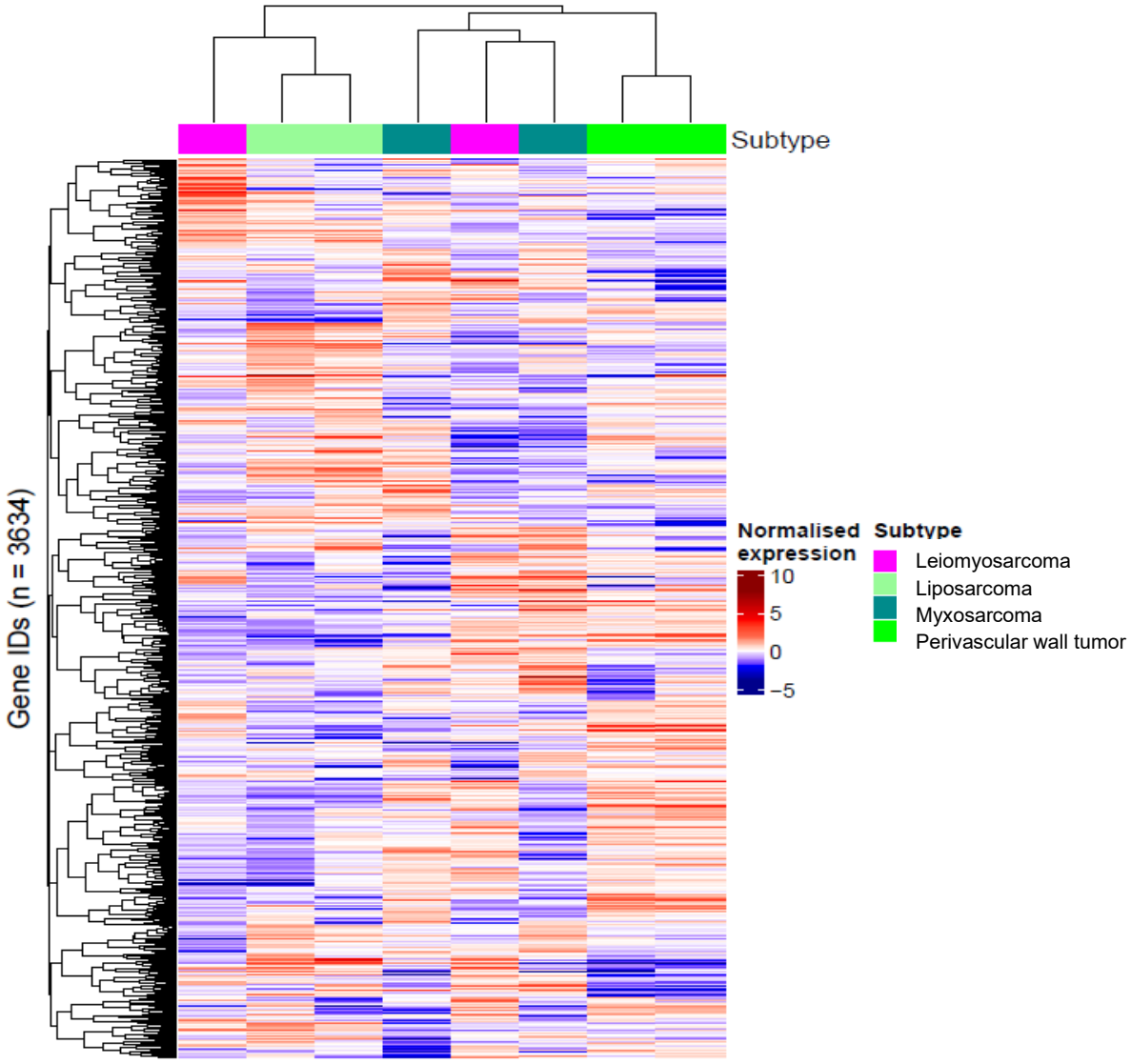


**Figure 4.3:** Annotated heatmap of eight STSs represented by four distinct histotypes (2 leiomyosarcomas, 2 liposarcomas, 2 myxosarcomas, and 2 perivascular wall tumors). The analysis shows that liposarcomas and perivascular wall tumors are grouped into distinct clusters, whereas myxosarcomas and leiomyosarcomas appears to be more heterogeneous.

**Expected results**

Consistently with our previous findings on the tumor microenvironment and with evidence from the human literature, proteomic profiling of the different histological subtypes of canine STSs is expected to yield distinctive proteomic signatures. These signatures will contribute to a deeper understanding of the underlying molecular mechanisms and enhance biological and histopathological characterization. Furthermore, the identification of potential biomarkers associated with specific histotypes may provide valuable information for diagnosis, prognosis, and the development of more targeted therapeutic strategies. Finally, comparative analysis of canine data with existing human datasets may uncover molecular similarities that reinforce the role of the dog as a spontaneous model in translational research, particularly in light of the higher incidence of STSs in dogs compared to humans.

**Proteomic limitations in biomarkers identification and future integrative strategies**

Biomarker identification represents a central objective of proteomics, as it seeks to uncover molecules that reflect normal biological processes, disease-associated alterations, or responses to therapeutic strategies (Gianazza et al., 2020). However, the results must be interpreted with caution when used for the definition of histotype-specific biomarkers.

Proteomics provides a relative measurement of protein abundance, which is often influenced by technical variables, such as sample preparation, ionization efficiency, instrument dynamics, as well as biological factors, including tumor heterogeneity, stromal or inflammatory contamination. An additional limitation is the complexity and intratumoral heterogeneity of STSs. Samples from the same histotype can exhibit marked proteomic variability, which reduces the specificity of certain candidate proteins as discriminative biomarkers (Proietto et al., 2023).

Considering all of the above, although preliminary proteomic analysis has revealed significant differences in protein expression profiles among the different histotypes of canine STSs, future results should be interpreted as exploratory.

From a future perspective, the identified candidate biomarkers will need to be deepen investigated and confirmed using more specific and quantitative techniques, such as immunohistochemistry, Western blot, and ELISA.

**References**

Burns, J. et al. The proteomic landscape of soft tissue sarcomas. Nat Commun 14, (2023).

Burns, J., Wilding, C. P., L Jones, R. & H Huang, P. Proteomic research in sarcomas - current status and future opportunities. Semin Cancer Biol 61, 56–70 (2020).

Elms, M. L. et al. Exploiting collateral sensitivity in the evolution of resistance to tyrosine kinase inhibitors in soft tissue sarcomas. Commun Biol 8, 1185 (2025).

Gianazza, E. et al. Platelets in Healthy and Disease States: From Biomarkers Discovery to Drug Targets Identification by Proteomics. IJMS 21, 4541 (2020).

Huang, C. et al. Proteogenomic insights into the biology and treatment of HPV-negative head and neck squamous cell carcinoma. Cancer Cell 39, 361-379.e16 (2021).

Jenks, A. D. et al. Primary Cilia Mediate Diverse Kinase Inhibitor Resistance Mechanisms in Cancer. Cell Reports 23, 3042–3055 (2018).

Kerrison, W. G. J. et al. Characterisation of a Novel Cell Line (ICR-SS-1) Established from a Patient-Derived Xenograft of Synovial Sarcoma. Cells 11, 2418 (2022).

Merry, E., Thway, K., Jones, R. L. & Huang, P. H. Predictive and prognostic transcriptomic biomarkers in soft tissue sarcomas. NPJ Precis Oncol 5, 17 (2021).

Mertins, P. et al. Proteogenomics connects somatic mutations to signalling in breast cancer. Nature 534, 55–62 (2016).

Pasquali, S. et al. Preclinical models of soft tissue sarcomas – generation and applications to enhance translational research. Critical Reviews in Oncology/Hematology 207, 104621 (2025).

Petralia, F. et al. Integrated Proteogenomic Characterization across Major Histological Types of Pediatric Brain Cancer. Cell 183, 1962-1985.e31 (2020).

Proietto, M. et al. Tumor heterogeneity: preclinical models, emerging technologies, and future applications. Front. Oncol. 13, 1164535 (2023).

Satpathy, S. et al. A proteogenomic portrait of lung squamous cell carcinoma. Cell 184, 4348-4371.e40 (2021).

Vyse, S. et al. Quantitative phosphoproteomic analysis of acquired cancer drug resistance to pazopanib and dasatinib. Journal of Proteomics 170, 130–140 (2018).

Wilding, C. P. et al. The landscape of tyrosine kinase inhibitors in sarcomas: looking beyond pazopanib. Expert Review of Anticancer Therapy 19, 971–991 (2019).

Zhang, B. et al. Proteogenomic characterization of human colon and rectal cancer. Nature 513, 382–387 (2014).

## Chapter 5: Other Studies

### The immunohistochemical expression of EMA is not informative in the differential diagnosis of Perivascular Wall Tumors and Nerve Sheath Tumors

#### Introduction

The differential diagnosis between Nerve Sheath Tumors (NSTs) and Perivascular Wall Tumors (PWTs) in dogs represents a significant challenge in veterinary oncology, as there are many overlaps in both clinical presentation and histology (Roccabianca et al., 2020).

PWTs are a class of soft tissue neoplasms that originate from the cells constituting the walls of blood vessels. They include hemangiopericytoma, myopericytoma, angioleiomyoma, and its malignant counterpart angioleiomyosarcoma, angiofibroma, angiomyofibroblastoma (Avallone et al., 2007).

The histological appearance of PWTs is characterized by a proliferation of spindle-shaped cells organized around capillaries or larger vascular structures, forming a distinctive whirling pattern. The stroma of these neoplasms is highly variable, ranging from dense collagen to a myxoid matrix (Avallone et al., 2007).

In contrast, NSTs originate from the cells of the peripheral nervous system that surround nerve fibers, specifically Schwann cells, perineurial cells, and perineurial and endoneurial fibroblasts (Morabito et al., 2023). They have generally been classified as NSTs and subdivided based on malignancy into benign nerve sheath tumors (BNSTs), which include neurofibromas, schwannomas, and perineuriomas, and malignant nerve sheath tumors (MNSTs) (Roccabianca et al., 2020).

NSTs are histologically composed of pleomorphic spindle-shaped or polygonal neoplastic cells, which are derived from Schwann cells, perineurial cells, or both and are arranged in irregularly interwoven bundles, nuclear palisades, whorls, storiform patterns, or sheets. In

addition, NSTs contain various amounts of collagenous stroma (Goldschmidt and Hendrick, 2002; Koestner and Higgins, 2002).

NSTs and PWTs both can manifest in the skin, subcutaneous tissue, or as intramuscular masses, forming nodules or lumps (Avallone et al., 2007; Suzuki et al., 2014).

These two lesions also share similarities in terms of invasiveness, as both exhibit a tendency for invasive growth with infiltration of surrounding tissues (Suzuki et al., 2014).

Histologically, the presence of whorls is a common feature in both tumors. In NSTs, particularly in perineuriomas, neoplastic cells are organized in a whirling pattern around nerve fibers and blood vessels. Similarly, in canine PWTs, whorls are observed, but with the distinction that the vessels at the center of these structures may collapse, mimicking nerve fibers (Goldblum et al., 2020).

Another common characteristic is the presence of Antoni A and Antoni B areas, which are typical of NSTs (such as in schwannomas). Antoni A areas are characterized by the presence of compact spindle-shaped cells arranged in bundles, with a palisading pattern. Antoni B areas, on the other hand, consist of spindle-shaped cells arranged in a myxoid background. In PWTs, the myxoid pattern is one of the most common among non-perivascular types, showing a similarity to Antoni B areas (Avallone et al., 2007).

The most important diagnostic criterion for NSTs is proving that the neoplastic cells originate from nerve sheath components (Weiss and Goldblum, 2008).

In veterinary medicine, there are several studies on the immunohistochemical or ultrastructural subclassification of PWTs (Avallone et al., 2007; Jakab et al., 2012; Palmieri et al., 2013), but very few studies on the comparison of immunohistochemical features for the differential diagnosis between canine NSTs and PWTs (Chijiwa et al., 2004; Jakab et al., 2012).

In PWTs, various markers are used, including CD34, vimentin, alpha-smooth muscle actin, and calponin (Avallone et al., 2007).

In contrast, NSTs are identified using markers such as SOX10 and S100. S100 has been historically considered the most specific marker for identifying schwannomas and neurofibromas in dogs (Karamchandani et al., 2012). Additionally, nerve growth factor receptor (NGFR), allows for a proper distinction between MPNSTs and PWTs (Suzuki et al., 2014).

In human medicine, the epithelial membrane antigen (EMA) and the S100 protein are among the most commonly used markers in the differential diagnosis of these neoplasms (Friedrich et al., 2022; Johnson et al., 2022).

EMA is a transmembrane glycoprotein with a highly glycosylated extracellular portion, found at a basal level in almost all epithelial tissues and perineurial fibroblasts, and a mucin encoded by the *MUC1* gene in humans (Chen et al., 2021).

*MUC1* encodes a glycosylated membrane phosphoprotein, with a protein mass ranging from 250 to 500 kDa. It is anchored to the apical surface of many tissues, including the perineurium (Singh and Hollingsworth, 2006). It is often found to be overexpressed or over-glycosylated, leading to cellular alterations (Qing et al., 2022). In fact, this protein can be involved in the development and progression of neoplasms by altering various cellular activities, thereby promoting tumor growth and hindering the efficacy of therapies (Hollingsworth and Swanson, 2004; Qing et al., 2022).

In particular, *MUC1* is involved in several processes that promote tumor progression:

- Tumor cell proliferation: its glycosylated domains can bind and concentrate growth factors near their receptors, leading to stronger and prolonged receptor activation (Hollingsworth and Swanson, 2004).

- Immune evasion: *MUC1* prevents immune cells from interacting with receptors on the tumor cell surface through steric hindrance, thereby inhibiting an antitumor immune response (Hollingsworth and Swanson, 2004).
- Cell cycle deregulation: it alters the balance of p53 responses, favoring cell cycle arrest (via increased p21 expression) over apoptosis (through Bax suppression) (Wei et al., 2005).
- Inhibition of apoptosis via AKT signaling: *MUC1* overexpression increases AKT phosphorylation, which phosphorylates BAD, causing its dissociation from BCL-2 and BCL-XL. This leaves BCL-2 and BCL-XL free to prevent cytochrome c release from mitochondria, thereby blocking apoptosis (Raina et al., 2004).
- Promote tumor invasion: the cytoplasmic tail of *MUC1* can interact with β-catenin, stabilizing it in the cytoplasm and promoting the expression of vimentin and *CDH2*. These proteins drive epithelial-mesenchymal transition, increasing motility, invasiveness, and metastatic potential (Koelsche et al., 2021; Schroeder et al., 2003).

However, the use of EMA as a marker for perineurial cells has some limitations. First, the cytoplasmic processes of perineurial cells are extremely thin and widely spaced, making EMA expression difficult to detect. Second, EMA expression can sometimes be focal and weak (Macarenco et al., 2007).

The **aims** of this study are to validate the cross reactivity with canine tissues of a commercial antibody for EMA, and to evaluate its effectiveness in differentiating PWTs from NSTs, thereby making the diagnosis more definitive and accurate.

## Materials & Methods

### Western Blot

*Sample collection*

Samples were collected from dogs undergoing autopsy at the Department of Veterinary Medical Sciences (DIMEVET), University of Bologna, including the positive control (mucosa of the small intestine obtained by scraping, known to express the EMA antigen) and the negative control (inguinal and femoral lymph nodes, known not to express the EMA antigen). The sampled tissues showed no significant pathological alterations, and no extraneous diseases affecting other organs were observed. Each sample was divided into 100 ± 0.5 mg aliquots to facilitate homogenization and stored at -80°C to prevent the activation of proteolytic processes.

*Samples preparation*

Two for negative controls and two for positive controls aliquots were prepared and homogenized using an automated mechanical homogenizer, starting with the negative samples to avoid cross-contamination. Then, two aliquots were treated with 1 ml of SDS Lysis Buffer (62.5 mM Tris-HCl, pH 6.8; 2% SDS; 20% glycerol) at a final volume-to-weight ratio of 1 ml buffer per 100 mg of tissue, while the remaining two aliquots were treated with 1 ml of RIPA buffer (Radioimmunoprecipitation Assay Buffer) at the same final volume-to-weight ratio.

Afterwards, samples were centrifuged at 12,000 x g for 5 minutes, yielding a supernatant containing the protein phase, which was subsequently separated from the pellet into a new microcentrifuge tube and appropriately labeled as RIPA buffer and SDS buffer.

The selection of these two buffers was driven by their capacity to promote protein denaturation through disruption of covalent interactions. The key distinction between them

consists in the extent of their denaturing effects: RIPA buffer, which combines neutral and anionic detergents (including SDS), induces a more pronounced and comprehensive protein denaturation than SDS alone.

*Protein quantification*

To quantify the total protein concentration, a colorimetric assay kit was used, specifically the Total Protein Kit, Micro Lowry, Peterson's modification (SIGMA®). The Lowry method is based on two successive steps: the biuret reaction, where a copper solution is added to the protein solution in a basic environment, resulting in a purple coloration with a maximum absorbance at 540 nm. The second reaction occurs when the Folin reagent (phosphomolybdic-phosphotungstic reagent) is added, which reacts with the tyrosine and tryptophan residues in the proteins, producing a blue color with a maximum absorbance at 750 nm. The Peterson method employed in this study includes an additional modification, as it uses sodium dodecyl sulfate (SDS), included in the Lowry reagent, to facilitate the solubilization of relatively insoluble lipoproteins. Aliquots of 10 and 30 µL from each sample prepared in both SDS Buffer and RIPA Buffer were used for protein quantification following the procedure outlined in the data sheet provided by the kit manufacturer.

The development of the colorimetric reaction was achieved, and it was subsequently analyzed using spectrophotometric reading. For each sample, the absorbance value was measured at 750 nm and then interpolated on the standard curve to determine the actual concentration of total proteins present in each sample. This allowed for the calculation of the required sample volume to achieve the desired protein concentrations, specifically 10 µg of protein. Following the quantification, samples were subjected to separation using SDS-PAGE technique, followed by Coomassie blue staining to verify the quality of the extracted proteins.

*SDS-PAGE electrophoresis*

The samples were subsequently subjected to SDS-PAGE electrophoresis to separate the proteins based on their molecular weight. For the analysis, four aliquots derived from four distinct samples were prepared, including two negative and two positive controls. The samples were divided into two groups: one pair of controls (one negative and one positive) derived from resuspension in SDS buffer, while the other pair was prepared in RIPA buffer. In both cases, the samples were prepared with a final volume of 10 µL, consisting of 2.5 µL of LDS (Lithium Dodecyl Sulfate), 1 µL of reducing agent, variable amounts of sample, and variable amounts of distilled water for each sample, as the aliquots were prepared to achieve 10 µg of protein in each sample. The same procedure was repeated to obtain a final quantity of 30 µg of protein.

This procedure was also applied to the standard molecular weight marker (Spectra™ Multicolor High Range Protein Ladder), with the difference that no dilution was performed; thus, a solution was prepared consisting of 2.5 µL of LDS (Lithium Dodecyl Sulfate), 1 µL of reducing agent, and 6.5 µL of ladder. Once the samples were prepared, they were incubated in a heating block at 95°C for 10 minutes to ensure complete denaturation of the proteins, facilitating the electrophoretic run.

During the incubation period, the electrophoresis chamber was prepared, consisting of two compartments to which two different buffers were added: an external chamber containing 800 mL of 1X Tris acetate SDS buffer (tris(hydroxymethyl)aminomethane Sodium Dodecyl Sulfate Buffer), prepared from a 20X concentrated stock solution, and an internal chamber containing 200 mL of 1X Tris acetate SDS buffer plus 500 µL of reducing agent, allowing the electrophoretic run to be performed in a reducing environment.

After the incubation period, the samples were loaded onto the gel (NuPAGE™ 3-8% Tris-Acetate Gel, Thermo Fisher Scientific©), with 10 µg and 30 µg of protein loaded into each well. Alongside the samples, 7 µL of ladder were loaded, which would be used for the semi-qualitative determination of the proteins. Finally, the electrophoresis was initiated, maintaining a constant voltage of 200 V, with an initial current of approximately 65 A and a final current of 45 A.

At the end of the electrophoretic run, the gel was stained for a few minutes with Coomassie Blue (EZBlue™ Gel Staining Reagent, SIGMA©) to evaluate the quality of the extracted proteins. This procedure was repeated, using only 10 µg of protein for samples.

*Gel transfer to membrane*

Subsequently, the gel was transferred to a container with milliQ water under agitation, where it was kept for 10 minutes. After the first wash, the gel was transferred to a second container containing Tris-glycine (tris(hydroxymethyl)aminomethane) and maintained under agitation for 30-60 minutes. Meanwhile, a solution of 100 mL of PBS-Tween with 5% powdered milk was prepared and left to stir with a magnetic stirrer for 60 minutes to completely mix the solution, which would then be used in the blocking phase.

After equilibrating the gel in Tris-Glycine, the transfer of proteins to a PVDF membrane (Trans-Blot Turbo, 0.2 µm PVDF, Biorad ©) was performed using the Trans-Blot Turbo™ apparatus (BIO-RAD©). The transfer program utilized was specific for high molecular weight (HIGH MW) proteins, set with the following parameters: 1.3 A, 24 V for 10 minutes.

*Western Blot*

Upon completion of the transfer, the membrane was carefully removed to preserve its integrity and was washed under agitation in milliQ water for 10 minutes. Subsequently, the

membrane was transferred to a second container containing a blocking solution with 5% powdered milk, incubating it at room temperature with agitation for at least 1 hour.

At the same time, a solution containing the primary antibody against EMA was prepared, diluted 1:200 in a final volume of 5 mL of PBS-Tween 20. Finally, the membrane was placed inside a 50 mL conical tube containing the antibody solution, ensuring that the side with the proteins faced in direct contact with the antibody solution. The membrane was then incubated under agitation at 4°C overnight.

At the end of the incubation period, three washes were performed for 5, 15, and 5 minutes, respectively, using a PBS-Tween 20 solution to remove excess unbound antibodies. Meanwhile, a solution of secondary antibody (Goat anti-Mouse IgG (H+L) Cross-Adsorbed Secondary Antibody HRP; Invitrogen™, Thermo Fisher Scientific©) was prepared, diluted 1:10,000 in a total volume of 10 mL of PBS-Tween 20. The membrane was then placed in a 50 mL falcon with the antibody solution and agitated at room temperature for one hour.

After the incubation time, the three washes of 5, 15, and 5 minutes were repeated to prepare the membrane for the development and amplification of the chemiluminescent signal, using a 1:1 solution of enhancer/luminol and substrate with a final volume of 6 mL. This step facilitated the development of the chemiluminescent signal, which was analyzed using the ChemiDoc instrument (BioRad©). The results obtained allowed for the qualitative determination of the presence of the target protein in the samples analyzed indicated by the appearance of bands at specific molecular weights.

**Immunohistochemistry**

*Sample collection*

Cases of canine PWTs and NSTs were selected from the archives of the DIMEVET, University of Bologna.

*Immunohistochemistry*

From each tissue block, four sections of 3 μm thickness underwent immunohistochemistry for EMA, NGFR, Calponin, and α-SMA, following standardized protocols.

Positive control sections were included in each test according to standardized methods. The tissues used as positive controls were mammary gland for calponin, small intestine for α-SMA and NGFR and sciatic nerve for EMA.

The sections were maintained at 37°C the day before the assay and then incubated at 60°C for 1 hour. The sections were then subjected to:

- Deparaffinization: The sections were subjected to two passes of X-free solvent, each lasting 15 minutes.
- Inhibition of Endogenous Peroxidases: The sections were treated with a 3% hydrogen peroxide solution in methanol for 30 minutes to inhibit any endogenous peroxidase activity.
- Rehydration: The sections underwent rehydration in decreasing concentrations of ethanol for 2 minutes each, using 100%, 90%, and 70% ethanol, followed by a final wash in distilled water for 5 minutes.

The procedures for antigen retrieval, incubation with primary and secondary antibodies are outlined in Table 5.1.

**Table 5.1:** Immunohistochemistry procedures for EMA, Calponin, NGFR, and α-SMA

| | Antigen retrieval | Primary Ab | Secondary Ab |
|---|---|---|---|
| **EMA** | Citrate buffer pH 6, pressure cooker, Low pressure mode, 110 °C, 10 minutes | Mouse monoclonal antibody clone E29, cod. MO613, Agilient DAKO, Santa Clara, CA 95051, USA. Dilution: 1:200 | Goat Anti-mouse cod. BA9200, Vector Laboratories, Newark, CA 94560, USA. 1:200 in blocking solution, room temperature, 30 minutes |
| **Calponin** | Enzymatic pre-digestion in 0.01% Proteinase K for 10 minutes, followed by heating using citrate buffer at pH 6, microwave for two cycles of 5 minutes at 750 W | Mouse monoclonal antibody clone CALP cod. M3556, Agilient DAKO, Santa Clara, CA 95051, USA. Dilution: 1:2000 | |
| **NGFR** | Heating using EDTA buffer at pH 8, microwave for two cycles of 5 minutes at 750 W | Mouse monoclonal antibody clone ME20Y, cod. H-9400-82, Invitrogen, Rockford, Illinois, USA. Dilution: 1:500 | |
| **α-SMA** | Heating using Citrate bufffer at pH 6, microwave for 2 cycles of 5 minutes at 750 W | Mouse monoclonal antibody clone 1A4, cod. MO851, Agilient DAKO, Santa Clara, CA 95051, USA. Dilution: 1:450 | |

The reaction was amplified by the avidin-biotin method (Vectastain® Elite ABC-HRP kit, Vector, Burlingame, CA, USA) and visualized with 0.04% 3,3-diaminobenzidine (Code: 10-0048, Histoline Milano, IT) for 7, 3, 1.5 and 3 minutes respectively.

After three rinses of 3 minutes in distilled water to remove excess DAB, Harris Hematoxylin staining was applied for 60 seconds for NGFR, Calponin, and α-SMA, while EMA was stained for 40 seconds to contrast the cells in the section.

The sections then underwent a dehydration process, which included 2 minutes immersions in distilled water followed by increasing concentrations of ethanol (70%, 90%, 100%) for 2 minutes each, concluding with two immersions in X-Free solvent for clarification.

All sections were then mounted using DPX (Distyrene Plasticizer Xylene) and left to dry.

**Results**

*Case collection*

For this study, 16 cases of canine STSs were collected (11 PWTs, 3 NSTs, 2 STS). Data related to breed, age, gender location and diagnosis are reported in Table 5.2.

**Table 5.2:** Cases collection

| Case | Breed | Age | Sex | Location | Diagnosis |
|---|---|---|---|---|---|
| 1 | Mixed-breed | 16 years | F | Right knee | PWT |
| 2 | Boxer | 10 years | M | Left elbow | PWT |
| 3 | Boxer | 9 years | M | Right forearm | PWT |
| 4 | Mixed-breed | 11 years | M | Right elbow | PWT |
| 5 | German Shepherd | 10 years | M | Sternum | PWT |
| 6 | Bolognese | 11 years | M | Toe | PWT |
| 7 | Pomeranian Spitz | ND | F | ND | PWT |
| 8 | Boxer | 8 years | F | Left hind limb | PWT |
| 9 | Mixed-breed | 7 years | M | Right elbow | PWT |
| 10 | Mixed-breed | 14 years | F | Left metatarsus | PWT |
| 11 | Mixed-breed | 7 years | F | Right thigh | PWT |
| 12 | German Shepherd | ND | M | Nasopharynx | MNST |
| 13 | Jack Russell Terrier | ND | M | Flank | NST |
| 14 | Mixed-breed | 14 years | M | Right flank | NST |
| 15 | Mixed-breed | 6 years | F | Left medial tibia | STS |
| 16 | French Bulldog | 12 years | F | Neck | STS |

*Protein quantification*

Regarding protein quantification, the calibration curve obtained from the analysis of samples containing BSA allowed for the calculation of the total protein content in each sample (Figure 5.1, Table 5.3, Table 5.4).

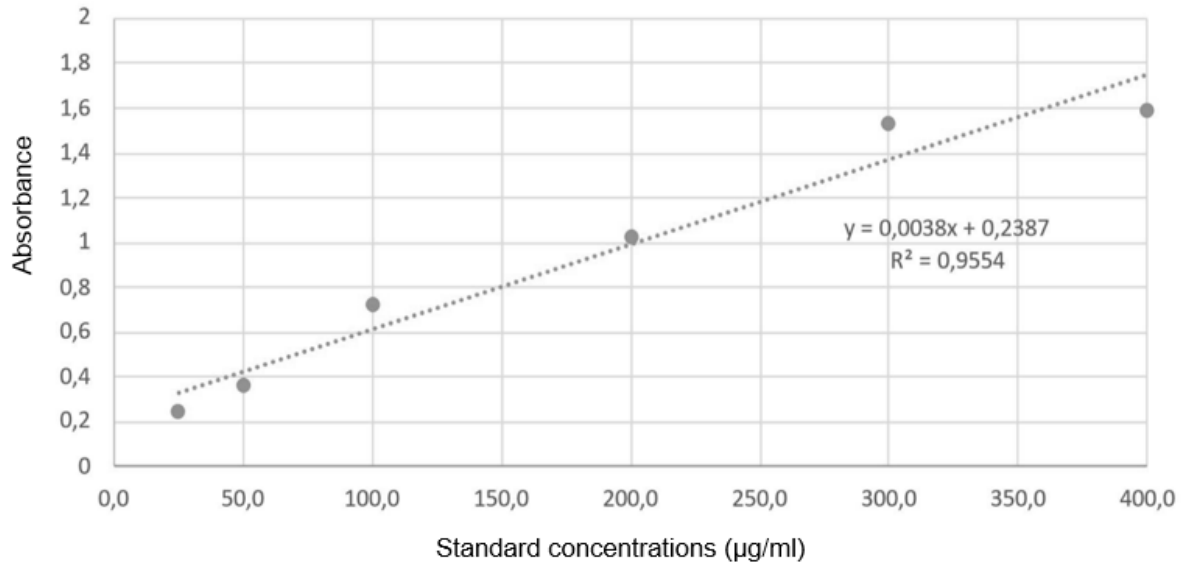


**Figure 5.1:** Calibration curve for protein quantification. The equation of the linear regression is y = 0.0038x + 0.2387 with an $R^2$ value of 0.9554.

**Table 5.3:** Standard concentrations (25.0–400.0 µg/ml) with absorbance values measured at 750 nm.

| Concentration (µg/ml) | Absorbance (750 nm) |
|---|---|
| 25.0 | 0.244 |
| 50.0 | 0.367 |
| 100.0 | 0.72 |
| 200.0 | 1.028 |
| 300.0 | 1.533 |
| 400.0 | 1.595 |

**Table 5.4:** Quantitative analysis with the evaluation of µg of protein contained in 1 µL of solution and the total µg present in the samples.

| Sample | Concentration (mg/mL) | Absorbance (750 nm) |
|---|---|---|
| 1 | 5,44 | 0,813 |
| 2 | 5,58 | 0,559 |
| 3 | 8,07 | 0,471 |
| 4 | 12,45 | 0,486 |

The analyses performed using Coomassie Blue staining (EZBlue™ Gel Staining Reagent, SIGMA©) revealed that the proteins were intact and properly separated, confirming the successful outcome of the electrophoretic separation (Figure 5.2, Table 5.5).

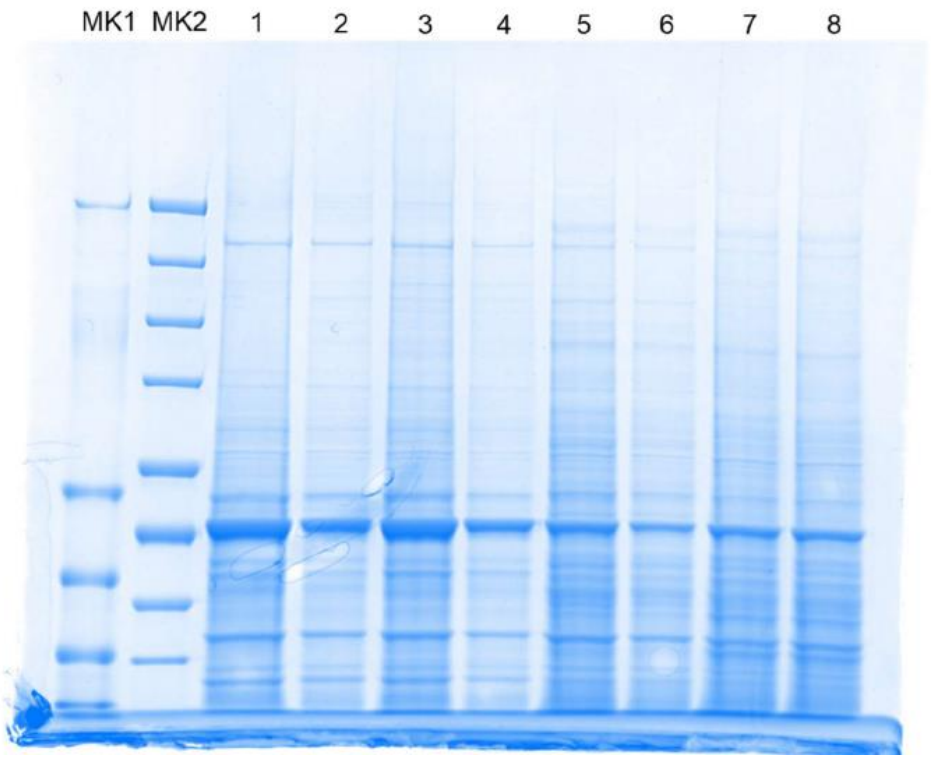


**Figure 5.2:** Gel stained with Coomassie Blue (EZBlue™ Gel Staining Reagent, SIGMA©).

**Table 5.5:** Arrangement of the ladders and samples on the gel.

| **Lane** | **MK1** | **MK2** | **1** | **2** | **3** | **4** | **5** | **6** | **7** | **8** |
|---|---|---|---|---|---|---|---|---|---|---|
| **Buffer** | Marker 1 (See Blue 2) | Marker 2 (high molecular weight) | RIPA | RIPA | SDS | SDS | RIPA | RIPA | SDS | SDS |
| **µg prot** | | | 30 | 10 | 30 | 10 | 30 | 10 | 30 | 10 |
| **Tissue** | | | Lymph nodes (-) | | | | Intestinal mucosa (+) | | | |

In the intestinal mucosa samples used as positive controls a band with a molecular weight of 135 kDa was highlighted, which was absent in the lymph node samples used as negative controls, where an aspecific band with a molecular weight of 109 kDa was present (Figure 5.3).

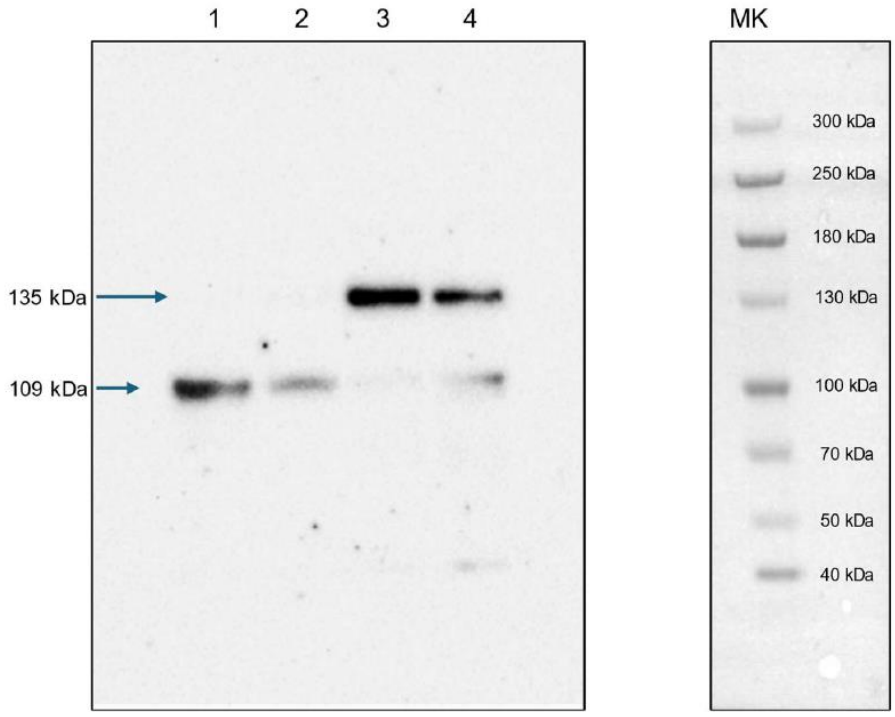


**Figure 5.3:** On the left are the results of the Western blot for EMA: 1) Lymph node (-) SDS; 2) Lymph node (-) RIPA; 3) Intestinal mucosa (+) SDS; 4) Intestinal mucosa (+) RIPA. On the right is the Spectra™ Multicolor High Range Protein Ladder, to which molecular weights have been assigned for each band according to the specifications of the data sheet.

*Immunohistochemistry*

For the analyzed samples, four immunohistochemical analyses were performed to identify the presence of cells positive for the markers EMA, NGFR, α-SMA, and Calponin (Table 5.6).

**Table 5.6:** Immunohistochemistry results.

| Case | EMA | NGFR | α-SMA | Calponin | Diagnosis |
|---|---|---|---|---|---|
| 1 | + | - | - | - | PWT |
| 2 | + | + | - | + | PWT |
| 3 | + | - | - | - | PWT |
| 4 | + | - | - | - | PWT |
| 5 | + | - | + | - | PWT |
| 6 | + | - | - | - | PWT |
| 7 | - | - | - | - | PWT |
| 8 | - | - | - | - | PWT |
| 9 | + | - | + | - | PWT |
| 10 | + | - | + | + | PWT |
| 11 | + | - | + | - | PWT |
| 12 | + | + | - | - | MNST |
| 13 | + | + | - | - | NST |
| 14 | + | + | - | - | NST |
| 15 | + | + | - | - | STS |
| 16 | + | - | + | + | STS |

The immunohistochemical analysis of the 16 cases examined revealed the expression of the EMA antigen in 14 samples (87.5%). Among the positive cases, 9 were initially classified as PWTs, accounting for approximately 82% of all PWTs, 3 as NSTs, and 2 as STSs, which together constitute 100% of the samples belonging to these histotypes. The remaining two cases, which were negative for EMA, belonged to the group of PWTs. Regarding the NGFR

antigen, 5 samples (31.3%) tested positive. Of these, 3 were NSTs (100%), 1 was a PWT (9.1%), and 1 was classified as STS (50%). The 11 negative samples predominantly included PWTs (90.9%), and only one case was diagnosed as an undifferentiated STS (50%). The α-SMA antigen was detected in 5 cases (31.3%), of which 4 were PWTs (36.4%) and 1 was a STS (50%). Among the 11 negative samples (68.8%), 7 belonged to the group of PWTs (63.6%), 3 NSTs (100%), and one case was diagnosed as an undifferentiated STS (50%). Calponin expression was observed in 3 samples (18.8%). Of these, 2 were PWTs (18.2%) and 1 was classified as an STS (50%). The remaining 13 cases (81.3%) were negative, divided into 9 PWTs (81.8%), 3 NSTs (100%), and 1 undifferentiated STS (50%).

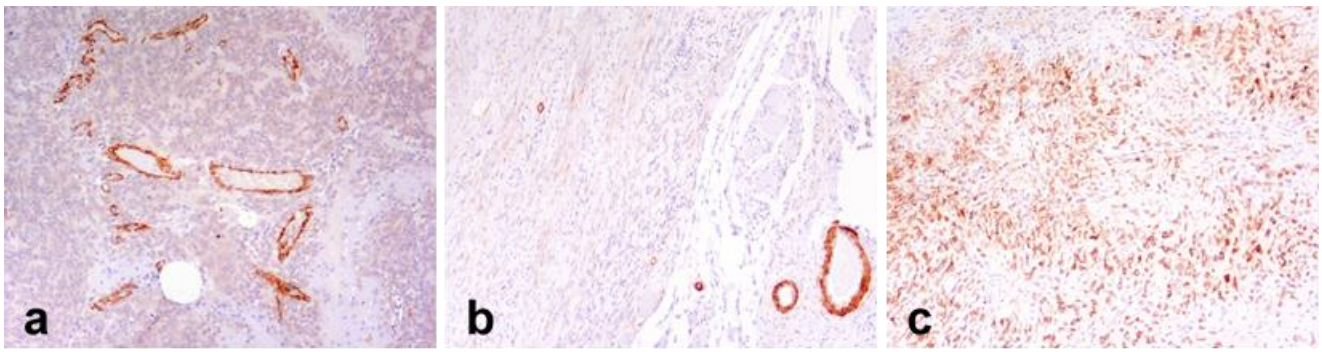


**Figure 5.4:** Immunohistochemical reactivity for α-SMA in a PWT (a), Calponin (b), in a PWT and NGFR (c), in a NST.

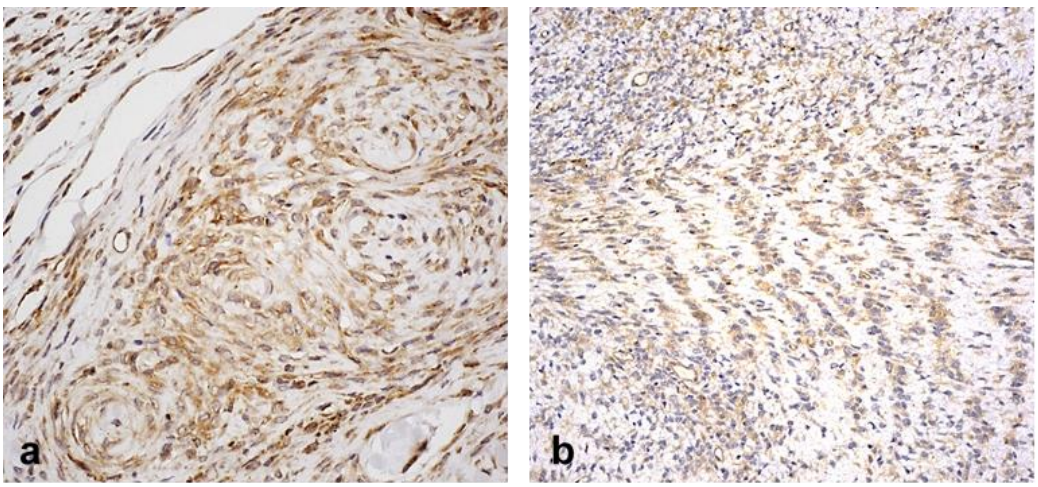


**Figure 5.5:** Immunohistochemical reactivity for EMA in PWT (a) and NST (b).

## Discussion

The aim of this study was to assess EMA expression in two histotypes of canine NST and PWT, with the objective of facilitating differential diagnosis between these variants, since they may exhibit overlapping morphological features at the histological level. In particular, both can exhibit spindle-shaped neoplastic cells (Avallone et al., 2007; Roccabianca et al., 2020), presence of whorls and alternating hypercellular and hypocellular areas, characteristics that can complicate their distinction (Avallone et al., 2007; Roccabianca et al., 2020). EMA expression could represent a useful tool for more accurately distinguishing, as this marker has been proven to be highly effective in recognizing perineural cells and distinguishing between the two neoplasms in human medicine (Hirose et al., 2003).

However, since there is no validation of the cross reactivity of this antibody in the literature, and therefore its specificity for canine EMA was not guaranteed, the validation was initially carried out using Western blot, confirmed the expression of the EMA antigen in the intestinal tissue samples used as positive controls. In particular, the analysis via Western blot highlighted the presence of a band at approximately 135 kDa, consistent with the expected molecular weight of EMA in dogs. This finding, along with the immunohistochemical reactivity of canine meningiomas already described (Mandara et al., 2021), allowed for the validation of the anti-EMA antibody (C29) used in this study.

Regarding immunohistochemical analyses, particularly related to the expression of the EMA antigen, it was found that out of the 16 samples analyzed, 14 were positive, specifically 9 out of 11 PWTs, 3 out of 3 NSTs, and 1 out of 2 STS. These data indicate that while the EMA antigen appears to be consistently expressed in NST, its expression in PWT limits its use for diagnostic purposes. However, the expression of EMA in PWT remains of uncertain nature, as this antigen is absent in normal perivascular cells. This raises questions about

the mechanism underlying its appearance in such neoplasms, suggesting the need for further studies.

This study represents a preliminary analysis, and as such, specific markers for neural cells were not used, unlike the studies by Suzuki et al. (2014) and Sisó et al. (2022), which utilized markers such as S-100 (Sisó et al., 2022; Suzuki et al., 2014), Periaxin-1 (Sisó et al., 2022) and SOX-10 (Sisó et al., 2022; Suzuki et al., 2014). The absence of these markers in the present study represents a limitation, as these antigens have proven to be highly specific, facilitating the distinction between NST and PWT (Suzuki et al., 2014).

**References**

Avallone G, Helmbold P, Caniatti M, et al. The Spectrum of Canine Cutaneous Perivascular Wall Tumors: Morphologic, Phenotypic and Clinical Characterization. Vet Pathol 2007;44:607–20.

Chen W, Zhang Z, Zhang S, et al. MUC1: Structure, Function, and Clinic Application in Epithelial Cancers. Int J Mol Sci 2021;22:6567.

Chijiwa K, Uchida K, Tateyama S. Immunohistochemical Evaluation of Canine Peripheral Nerve Sheath Tumors and Other Soft Tissue Sarcomas. Vet Pathol 2004;41:307–18.

Friedrich RE, Nörnberg LKN, Hagel C. Peripheral Nerve Sheath Tumors in Patients With Neurofibromatosis Type 1: Morphological and Immunohistochemical Study. Anticancer Res 2022;42:1247–61.

Goldblum JR, Folpe AL, Weiss SW. Enzinger & Weiss's soft tissue tumors. Seventh edition. Philadelphia, PA: Elsevier; 2020.

Goldschmidt MH, Hendrick MJ. Tumors of the Skin and Soft Tissues. Tumors in Domestic Animals. 1st ed., Wiley; 2002, p. 45–117.

Hirose T, Tani T, Shimada T, et al. Immunohistochemical Demonstration of EMA/Glut1-Positive Perineurial Cells and CD34-Positive Fibroblastic Cells in Peripheral Nerve Sheath Tumors. Modern Pathology 2003;16:293–8.

Hollingsworth MA, Swanson BJ. Mucins in cancer: protection and control of the cell surface. Nat Rev Cancer 2004;4:45–60.

Jakab C, Gálfi P, Jerzsele Á, et al. Expression of claudin-1 in canine peripheral nerve sheath tumours and perivascular wall tumours. Immunohistochemical study. Histol Histopathol 2012;27:905–17.

Johnson C, Brazen B, Ross R, et al. Sclerosing perineurioma: a rare benign tumor in a pediatric patient. DOJ 2022;27.

Karamchandani JR, Nielsen TO, Van De Rijn M, et al. Sox10 and S100 in the Diagnosis of Soft-tissue Neoplasms. Applied Immunohistochemistry & Molecular Morphology 2012;20:445–50.

Koelsche C, Schrimpf D, Stichel D, et al. Sarcoma classification by DNA methylation profiling. Nat Commun 2021;12:498.

Koestner A, Higgins RJ. Tumors of the Nervous System. Tumors in Domestic Animals. 1st ed., Wiley; 2002, p. 697–738.

Macarenco RS, Ellinger F, Oliveira AM. Perineurioma: A Distinctive and Underrecognized Peripheral Nerve Sheath Neoplasm. Archives of Pathology & Laboratory Medicine 2007;131:625–36.

Mandara MT, Foiani G, Silvestri S, et al. Immunoexpression of epithelial membrane antigen in canine meningioma: Novel results for perspective considerations. Vet Comparative Oncology 2021;19:115–22. https://doi.org/10.1111/vco.12648.

Morabito S, Specchi S, Di Donato P, et al. Relationship between magnetic resonance imaging findings and histological grade in spinal peripheral nerve sheath tumors in dogs. Veterinary Internal Medicine 2023;37:2278–90.

Palmieri C, Avallone G, Cimini M, et al. Use of Electron Microscopy to Classify Canine Perivascular Wall Tumors. Vet Pathol 2013;50:226–33.

Qing L, Li Q, Dong Z. MUC1: An emerging target in cancer treatment and diagnosis. Bulletin Du Cancer 2022;109:1202–16.

Raina D, Kharbanda S, Kufe D. The MUC1 Oncoprotein Activates the Anti-apoptotic Phosphoinositide 3-Kinase/Akt and Bcl-xL Pathways in Rat 3Y1 Fibroblasts. Journal of Biological Chemistry 2004;279:20607–12.

Roccabianca P, Schulman FY, Avallone G, et al. Surgical Pathology of Tumors of Domestic Animals. vol. 3. 3rd ed. Kiupel M.; 2020.

Schroeder JA, Adriance MC, Thompson MC, et al. MUC1 alters β-catenin-dependent tumor formation and promotes cellular invasion. Oncogene 2003;22:1324–32.

Singh PK, Hollingsworth MA. Cell surface-associated mucins in signal transduction. Trends in Cell Biology 2006;16:467–76.

Sisó S, Marco-Salazar P, Roccabianca P, et al. Nerve Fiber Immunohistochemical Panel Discriminates between Nerve Sheath and Perivascular Wall Tumors. Veterinary Sciences 2022;10:1.

Suzuki S, Uchida K, Nakayama H. The Effects of Tumor Location on Diagnostic Criteria for Canine Malignant Peripheral Nerve Sheath Tumors (MPNSTs) and the Markers for Distinction Between Canine MPNSTs and Canine Perivascular Wall Tumors. Vet Pathol 2014;51:722–36.

Wei X, Xu H, Kufe D. Human MUC1 oncoprotein regulates p53-responsive gene transcription in the genotoxic stress response. Cancer Cell 2005;7:167–78.

Weiss, Goldblum. Malignant tumors of the peripheral nerves, 2008, p. 903–44.

## Immunohistochemical Expression of PDGFRβ in Canine Intestinal Leiomyosarcomas

### Introduction

Canine gastrointestinal mesenchymal neoplasms are rare, accounting for 2% of all tumors and for approximately 10-30% of all intestinal neoplasms, including three different entities: gastrointestinal stromal tumors (GISTs), smooth muscle tumors (SMTs) (leiomyomas and leiomyosarcomas), and non-GIST/non-smooth muscle tumors (Avallone et al., 2022; Hayes et al., 2013; Pellegrino et al., 2018).

Leiomyosarcomas (malignant SMTs) and GISTs share similar biological behavior and histological appearance, usually characterized by interlacing bundles of spindle-shaped cells and collagen fibers. Immunohistochemical (IHC) analysis is essential for their distinction and diagnosis (Del Alcazar et al., 2021; Pellegrino et al., 2018). IHC analysis is based on the expression of c-Kit, desmin and smooth muscle actin (α-SMA):

- GISTs express c-Kit, are negative for desmin, and occasionally express α-SMA;
- SMTs are positive for α-SMA and/or desmin and negative for c-Kit;
- non-GIST/non-SMT tumors are negative for α-SMA, c-Kit, and desmin (Pellegrino et al., 2018).

Smooth muscle tumors are classified as leiomyomas or leiomyosarcomas according to mitotic activity, cytologic atypia, and additional morphological parameters, where leiomyomas are benign smooth muscle tumors, commonly found in the gastrointestinal tract, with no tendency for malignant transformation, whereas leiomyosarcomas are their malignant counterparts (Miettinen and Fetsch, 2006).

The histopathological features of leiomyosarcomas may resemble those of other mesenchymal neoplasms, such as fibrosarcoma, myofibroblastic sarcomas, and GISTs, making differential diagnostic challenging (Brady et al., 2022).

Establishing the diagnosis may have implications both for therapeutic decision and prognosis of affected patients (Brady et al., 2022; Hayes et al., 2013).

Leiomyosarcomas are rare, slow-growing tumors that originate from the smooth muscle of the gastrointestinal tract, locally invasive and generally slow to metastasize (Hayes et al., 2013). They are composed of uniform spindle cells, resembling normal smooth muscle cells and pleomorphic spindle cell sarcomas (Hayes et al., 2013).

Unlike GISTs, leiomyomas and leiomyosarcomas are negative for c-Kit and CD34 (Gillespie et al., 2011; Willard, 2012). Leiomyosarcomas express vimentin, like almost all mesenchymal tumors, as well as desmin and smooth muscle actin (α-SMA) (Hayes et al., 2013; Pellegrino et al., 2018).

*Tyrosine kinases Receptors (TKRs) as therapeutic targets*

TKRs are known to be involved in the regulation of critical cellular processes, such as proliferation and differentiation, cell survival and metabolism, cell migration, and cell cycle control (Blume-Jensen and Hunter, 2001; Ullrich and Schlessinger, 1990).

Tyrosine kinases are often abnormally activated in malignant tumors and genetic mutations of TKRs produce aberrant proteins that are constitutively active or deregulated, capable of altering intracellular signal transduction, disrupting normal cell function, and inducing uncontrolled cell proliferation and survival (Esteban-Villarrubia et al., 2020).

The tyrosine kinase activity is activated by its ligand, a growth factor known as Stem Cell Factor. Upon receptor-ligand binding, the receptor undergoes autophosphorylation and

phosphorylates a downstream signaling pathway involved in cell differentiation and proliferation (Del Alcazar et al., 2021).

The c-Kit receptor and the platelet-derived growth factor receptor (PDGFR) belong to class III of the receptor tyrosine kinase family. In canine gastrointestinal mesenchymal neoplasms, these receptors may present alterations (Esteban-Villarrubia et al., 2020; Marech et al., 2014).

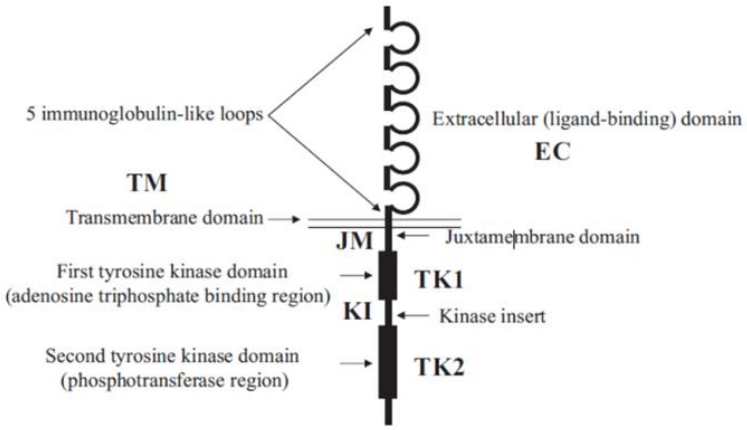


**Figure 5.6**: Type III receptor tyrosine kinases structure (Lasota and Miettinen, 2006).

**Platelet-Derived Growth Factors (PDGFs)** are a group of polypeptide growth factors (named A, B, C, and D) involved in the recruitment of perivascular cells during the process of angiogenesis and implicated in the increased growth of muscle cells, glial cells, and fibroblasts. PDGF receptor is PDGFR, and it is expressed in two distinct isoforms, referred to as α and β (Rossi et al., 2005). Their binding induces receptor homodimerization and the phosphorylation of specific tyrosine residues, as well as the activation of a cascade of intracellular signaling pathways, which are essential for regulating the growth of different cell lineages. Aberrant reactivation of these signaling pathways, due to PDGFR mutation, is involved in the carcinogenesis of several neoplasms, including canine GISTs (Lasota and Miettinen, 2006), where PDGFR contributes to the autocrine stimulation of neoplastic cells

and to the stimulation of angiogenesis, thereby promoting the growth of intratumoral blood vessels and supporting neoplastic growth (Esteban-Villarrubia et al., 2020; London, 2009).

In particular, mutations can occur in the *PDGFRA* gene (platelet-derived growth factor receptor A), which encodes the tyrosine kinase protein PDGFRα.

Also PDGFRα is a receptor activated by the stem cell factor, and mutations in this gene can affect the extracellular domain of Kit encoded by exon 9 (Takanosu et al., 2016; Treggiari et al., 2020). As mentioned before, its activating ligand is the stem cell factor; ligand binding induces the dimerization of two c-Kit receptors and their autophosphorylation, initiating downstream signaling involved in the regulation of intracellular processes, including mast cell proliferation and degranulation (Esteban-Villarrubia et al., 2020; Lasota and Miettinen, 2006).

In human and canine GISTs, mutations have been identified in c-Kit and PDGFRα (Gregory-Bryson et al., 2010; Morini et al., 2022), whereas the expression of PDGFRβ plays an important role in human leiomyosarcomas (Gaumann et al., 2014). For this reason, these TKRs have potential as therapeutic targets for specific tyrosine kinase inhibition (Esteban-Villarrubia et al., 2020; Marech et al., 2014).

The TKIs used in targeted therapies disrupt the cellular pathways that regulate the growth of neoplastic cells. They are classified as either small molecules or macromolecules and act on signaling pathways involving TKRs and intracellular kinases that control cell proliferation and tumor angiogenesis (Shyam Sunder et al., 2023).

In veterinary literature, several studies have reported the efficacy of treatment with TKIs such as toceranib phosphate and imatinib mesylate in dogs with unresectable or metastatic GISTs (Del Alcazar et al., 2021; Irie et al., 2015; Kobayashi et al., 2013); therefore, targeting

c-Kit can be considered a rational approach in the adjuvant treatment of canine GISTs (Gregory-Bryson et al., 2010).

The **aim** of this study was to evaluate the immunohistochemical expression of PDGFRβ in canine intestinal leiomyosarcomas and to assess the association between PDGFRβ expression and the expression of the nuclear marker Ki-67, in order to investigate a possible correlation between tumor proliferation and the expression of the receptor, to determine whether this receptor may represent a potential therapeutic target.

**Materials & Methods**

The cases included in this study were selected from the histological archives of the Department of Veterinary Medicine of the University of Bologna and from the University of Milan.

Following confirmation of the diagnosis of leiomyosarcoma based on histomorphology and a smooth muscle immunophenotype (α-SMA positivity with c-KIT negativity) (Pellegrino et al., 2018), FFPE samples were subjected to immunohistochemistry for PDGFRβ and Ki-67. Sections cut at 3 µm thickness were incubated in an oven at 60 °C for 30 minutes. Subsequently, the sections were subjected to deparaffinization with X-Free solvent and rehydration in descending alcohol series. Endogenous peroxidase activity was then blocked using a 3% $H_2O_2$ solution in methanol for 30 minutes.

The antigen retrieval, primary and secondary antibody incubation were performed according to the protocols outlined in the Table 5.7.

**Table 5.7:** Antigen retrieval, primary and secondary antibody incubation for Ki-67 and PDGFRβ.

| | **Ki-67** | **PDGFRβ** |
|---|---|---|
| **Antigen retrieval** | citrate buffer (pH 6) in microwave 750 W for 20 minutes | EDTA buffer (pH 8) in microwave 750 W for 10 minutes |
| **Primary antibody** | MIB-1, Dako, 1:1500 overnight | PDGFRβ(D-6):sc-374573, Santa Cruz Biotech, 1:600, overnight |
| **Secondary antibody** | Goat Anti-mouse cod. BA9200, Vector Laboratories, Newark, CA 94560, USA. 1:200 in blocking solution, room temperature, 30 minutes | |

The reaction was amplified by the avidin-biotin method (Vectastain® Elite ABC-HRP kit, Vector, Burlingame, CA, USA) and visualized with 0.04% 3,3-diaminobenzidine (Code: 10-0048, Histoline Milano, IT) and then signal contrasted with Harris Hematoxylin staining. Finally, the sections underwent a dehydration process, which included 2-minute immersions in distilled water followed by increasing concentrations of ethanol (70%, 90%, 100%), concluding with two immersions in X-Free solvent for clarification.

The digitized immunohistochemical sections for Ki-67 were obtained using the Grundium Ocus®20 scanner (MGU-00004) and analyzed with QuPath software (versions 0.5.1 and 0.6.0). Representative areas of varying size were selected to cover the tumor, focusing on regions with the highest proliferation, using the 'rectangle', 'ellipse', or 'polygon' tools. For each section, manual cell counting was performed in the selected areas using the 'point tool', counting both Ki-67 positive cells (DAB-stained) and negative cells, with a minimum of 1,000 total cells counted per case (Figure 5.7). Manual cell counting has been applied rather than automatic system, to better simulate the diagnostic setting. For each image, the percentage of positive cells over the total number of cells in the selected fields was calculated.

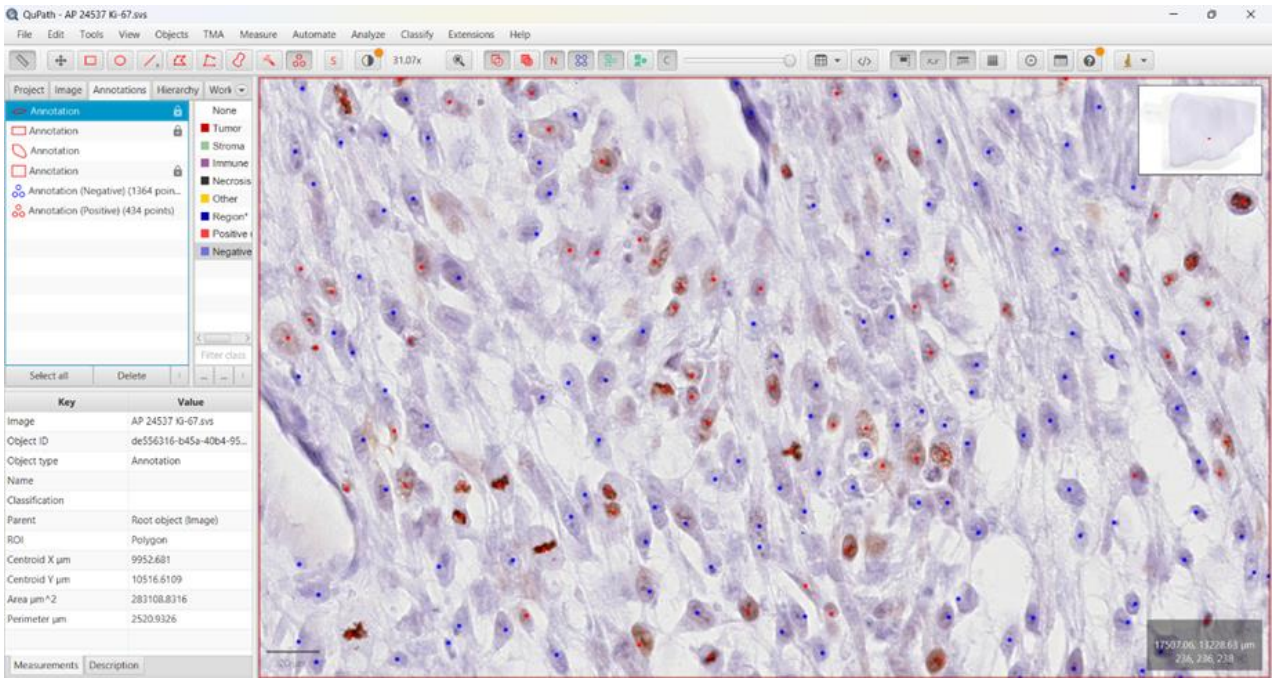


**Figure 5.7:** Example of Ki-67 positive cell detection in a tumor area of an intestinal leiomyosarcoma using QuPath software.

The sections subjected to immunohistochemistry for PDGFRβ were examined performing a semi-quantitative assessment of PDGFRβ expression according to a scoring system previously applied to other canine STS (Avallone et al., 2017, 2015), evaluating the number of negative cases (Figure 5.8) and positive cases (Figure 5.9), as well as the percentage of positive cells.

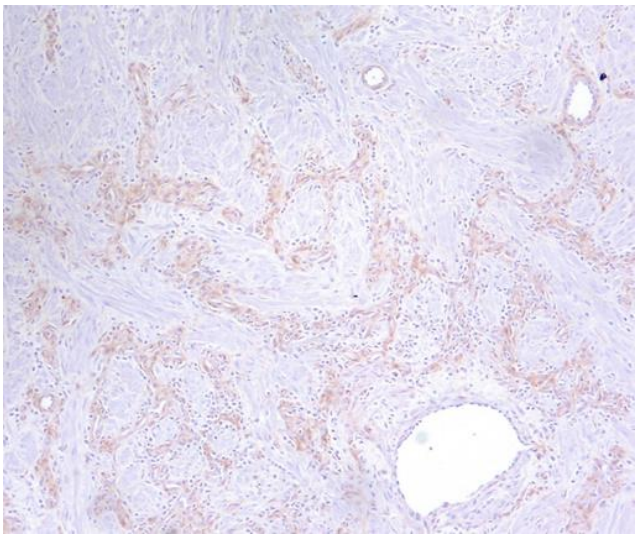

**Figure 5.8:** Example of a PDGFRβ-negative intestinal leiomyosarcoma case in a dog, with internal positive control (pericytes).

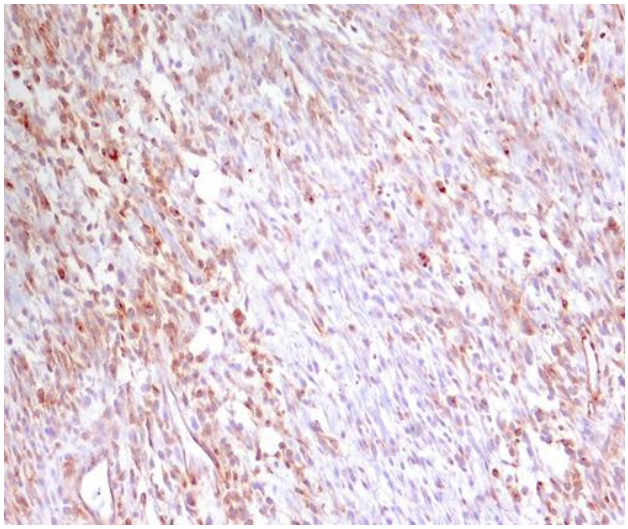

**Figure 5.9:** Example of PDGFRβ-positive neoplastic cells in a canine intestinal leiomyosarcoma.

Statistical analysis was performed using Jamovi software, version 2.4. Descriptive statistics included mean, median, standard deviation, and range (minimum, maximum). The association between PDGFRβ expression and Ki-67 values was assessed using a one-way ANOVA (non-parametric) Kruskal-Wallis test.

**Results**

In 25 canine intestinal leiomyosarcomas selected, two groups were compared, PDGFRβ-negative (22) and PDGFRβ-positive (3), with respect to the values obtained for the cell proliferation marker Ki-67, including mean, median, standard deviation, and range (minimum, maximum). The mean Ki-67 value for the positive group was 14.1, nearly double that of the negative group, which had a mean of 7.72. The standard deviation was similar between the two groups (group 0 = 9.41; group 1 = 8.86) (Table 5.8).

**Table 5.8:** Descriptive statistical data showing the number of PDGFRβ-positive and -negative cases, along with the corresponding Ki-67 values, including mean, median, standard

| | **PDGFRβ** | **Ki-67** |
|---|---|---|
| **Mean** | negative | 7.72 |
| | positive | 14.1 |
| **Median** | negative | 3.8 |
| | positive | 10.5 |
| **Standard deviation** | negative | 9.41 |
| | positive | 8.86 |
| **Minimum** | negative | 0.00 |
| | positive | 7.52 |
| **Maximum** | negative | 39.3 |
| | positive | 24.1 |

The analysis is graphically represented using a box plot (Figure 5.10). Ki-67 values were higher in the PDGFRβ-positive group compared to the PDGFRβ-negative group. The

median of the positive group was also noticeably higher (median = 10.5, range 7.52-24.1) than that of the negative group (median = 3.82, range 0.00-39.3) (Figure 5.10). Additionally, although the standard deviation was similar between the two groups, the negative group exhibited a wider range of values, with the presence of outliers.

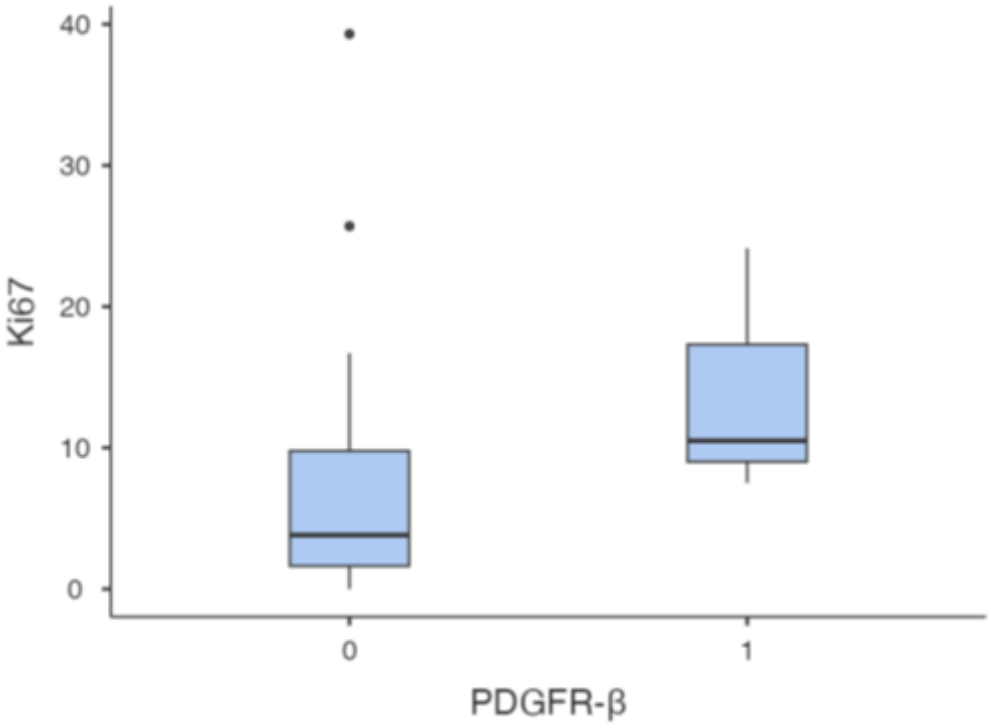


**Figure 5.10:** Box plot showing Ki-67 values in canine intestinal leiomyosarcomas stratified by PDGFRβ expression, 0 = negative, 1 = positive.

To evaluate the association between PDGFRβ expression and Ki-67 levels, a one-way (non-parametric) Kruskal-Wallis ANOVA test was used, which was not statistically significant (p= 0.118).

**Discussion**

The distinction between canine GISTs and intestinal leiomyosarcomas is fundamental due to the different therapeutic approaches, as GISTs can respond to targeted molecular therapy

with tyrosine kinase inhibitors (Brady et al., 2022; Del Alcazar et al., 2021). PDGFR plays an important role at the tumor level, promoting the growth of intratumoral blood vessels by stimulating angiogenesis and contributing to autocrine stimulation of neoplastic cells, thereby facilitating tumor growth (Esteban-Villarrubia et al., 2020; London, 2009). Since PDGFRβ expression plays an important role in leiomyosarcomas, this tyrosine kinase receptor has potential as a therapeutic target for TKIs (Gaumann et al., 2014). However, to our knowledge, no study has yet investigated its significance in dogs.

In this study, the expression of PDGFRβ in canine intestinal leiomyosarcomas was evaluated using immunohistochemistry and the expression of the nuclear proliferation marker Ki-67 was assessed in the cases under study using QuPath software on digitized slides, with the aim of providing reliable data on the potential association between tumor proliferation and PDGFRβ expression, and to explore whether this receptor could represent a potential therapeutic target for TKIs.

Based on the findings of this study, only a minority of canine intestinal leiomyosarcomas showed PDGFRβ expression. However, this observation should not be interpreted just as a numerical limitation, but rather as preliminary evidence of biological heterogeneity within these tumors, in line with the recognized heterogeneity observed inter- and intra-histotype.

In fact, the identification of PDGFRβ-positive leiomyosarcomas suggests the existence of a biologically distinct subset in which PDGFR-mediated signaling pathways could contribute to tumor growth and progression.

Interestingly, the three positive cases tended to display higher Ki-67 indices compared to the 23 negative cases, as suggested by the box plot analysis.

This result is particularly relevant in canine intestinal leiomyosarcomas, a rare neoplasm for which treatment options beyond surgical management are limited. The possibility of

identifying tumors with actionable molecular features, even in a small proportion of cases, represents a meaningful step toward more personalized therapeutic approaches.

However, the rarity of this neoplasm in dogs, the limited sample size, and the low frequency of PDGFRβ expression represent important limitations. Consequently, the current evidence is insufficient to establish whether TKIs could represent an effective therapeutic option for this tumor type in dogs. Future studies including a larger number of cases assessed immunohistochemically for PDGFRβ, together with investigations into alternative potential TKI targets in canine intestinal leiomyosarcomas, may provide valuable insights and new research directions.

Meanwhile, these findings suggest that PDGFRβ expression may identify a subset of canine intestinal leiomyosarcomas in which TKIs could represent a potential therapeutic option, warranting immunohistochemical assessment for appropriate patient selection.

**References**

Avallone G, Pellegrino V, Roccabianca P, et al. Tyrosine Kinase Receptor Expression in Canine Liposarcoma. Vet Pathol 2017;54:212–7.

Avallone G, Stefanello D, Boracchi P, et al. Growth Factors and COX2 Expression in Canine Perivascular Wall Tumors. Vet Pathol 2015;52:1034–40.

Avallone G, Pellegrino V, Muscatello LV, et al. Canine smooth muscle tumors: A clinicopathological study. Vet Pathol 2022;59:244–55.

Blume-Jensen P, Hunter T. Oncogenic kinase signalling. Nature 2001;411:355–65.

Brady RV, Rebhun RB, Skorupski KA, et al. Retrospective immunohistochemical investigation of suspected non-visceral leiomyosarcoma in dogs. J VET Diagn Invest 2022;34:465–73.

Del Alcazar CM, Mahoney JA, Dittrich K, et al. Outcome, prognostic factors and histological characterization of canine gastrointestinal sarcomas. Vet Comparative Oncology 2021;19:578–86.

Esteban-Villarrubia J, Soto-Castillo JJ, Pozas J, et al. Tyrosine Kinase Receptors in Oncology. Int J Mol Sci 2020;21:8529.

Gaumann AKA, Drexler HCA, Lang SA, et al. The inhibition of tyrosine kinase receptor signalling in leiomyosarcoma cells using the small molecule kinase inhibitor PTK787/ZK222584 (Vatalanib®). International Journal of Oncology 2014;45:2267–77.

Gillespie V, Baer K, Farrelly J, et al. Canine Gastrointestinal Stromal Tumors: Immunohistochemical Expression of CD34 and Examination of Prognostic Indicators Including Proliferation Markers Ki67 and AgNOR. Vet Pathol 2011;48:283–91.

Gregory-Bryson E, Bartlett E, Kiupel M, et al. Canine and human gastrointestinal stromal tumors display similar mutations in c-KIT exon 11. BMC Cancer 2010;10:559.

Hayes S, Yuzbasiyan-Gurkan V, Gregory-Bryson E, et al. Classification of Canine Nonangiogenic, Nonlymphogenic, Gastrointestinal Sarcomas Based on Microscopic, Immunohistochemical, and Molecular Characteristics. Vet Pathol 2013;50:779–88.

Irie M, Takeuchi Y, Ohtake Y, et al. Imatinib mesylate treatment in a dog with gastrointestinal stromal tumors with a c-kit mutation. J Vet Med Sci 2015;77:1535–9.

Kobayashi S, Canepa HM, Bailey AS, et al. Compound EGFR Mutations and Response to EGFR Tyrosine Kinase Inhibitors. Journal of Thoracic Oncology 2013;8:118–22.

Lasota J, Miettinen M. KIT and PDGFRA mutations in gastrointestinal stromal tumors (GISTs). Seminars in Diagnostic Pathology 2006;23:91–102.

London CA. Tyrosine Kinase Inhibitors in Veterinary Medicine. Topics in Companion Animal Medicine 2009;24:106–12.

Marech I, Patruno R, Zizzo N, et al. Masitinib (AB1010), from canine tumor model to human clinical development: Where we are? Critical Reviews in Oncology/Hematology 2014;91:98–111.

Miettinen M, Fetsch JF. Evaluation of biological potential of smooth muscle tumours. Histopathology 2006;48:97–105.

Morini M, Gentilini F, Turba ME, et al. Mutational Analysis of c-KIT and PDGFRA in Canine Gastrointestinal Stromal Tumors (GISTs). Veterinary Sciences 2022;9:376.

Pellegrino V, Muscatello LV, Sarli G, et al. Canine Gastrointestinal Spindle Cell Tumors Efficiently Diagnosed by Tissue Microarray-Based Immunohistochemistry. Vet Pathol 2018;55:678–81.

Rossi G, Cavazza A, Marchioni A, et al. Role of Chemotherapy and the Receptor Tyrosine Kinases KIT, PDGFRα, PDGFRβ, and Met in Large-Cell Neuroendocrine Carcinoma of the Lung. JCO 2005;23:8774–85.

Shyam Sunder S, Sharma UC, Pokharel S. Adverse effects of tyrosine kinase inhibitors in cancer therapy: pathophysiology, mechanisms and clinical management. Sig Transduct Target Ther 2023;8:262.

Takanosu M, Amano S, Kagawa Y. Analysis of c-KIT exon 11 mutations in canine gastrointestinal stromal tumours. The Veterinary Journal 2016;207:118–23.

Ullrich A, Schlessinger J. Signal transduction by receptors with tyrosine kinase activity. Cell 1990;61:203–12.

Willard MD. Alimentary Neoplasia in Geriatric Dogs and Cats. Veterinary Clinics of North America: Small Animal Practice 2012;42:693–706.